SOLUTIONS OF ESHELBY-TYPE INCLUSION PROBLEMS AND A RELATED HOMOGENIZATION METHOD BASED ON A SIMPLIFIED STRAIN GRADIENT ELASTICITY THEORY

A Dissertation

by

HEMEI MA

Submitted to the Office of Graduate Studies of
Texas A&M University
in partial fulfillment of the requirements for the degree of

DOCTOR OF PHILOSOPHY

May 2010

Major Subject: Mechanical Engineering

SOLUTIONS OF ESHELBY-TYPE INCLUSION PROBLEMS AND A RELATED HOMOGENIZATION METHOD BASED ON A SIMPLIFIED STRAIN GRADIENT ELASTICITY THEORY

A Dissertation

by

HEMEI MA

Submitted to the Office of Graduate Studies of
Texas A&M University
in partial fulfillment of the requirements for the degree of

DOCTOR OF PHILOSOPHY

Approved by:

Chair of Committee,	Xin-Lin Gao
Committee Members,	Anastasia Muliana
	J. N. Reddy
	Jay Walton
Head of Department,	Dennis O'Neal

May 2010

Major Subject: Mechanical Engineering

ABSTRACT

Solutions of Eshelby-Type Inclusion Problems and a Related Homogenization Method Based on a Simplified Strain Gradient Elasticity Theory. (May 2010)

Hemei Ma, B.Sc., Tongji University, Shanghai, China;

M.Sc., Tongji University, Shanghai, China

Chair of Advisory Committee: Dr. Xin-Lin Gao

Eshelby-type inclusion problems of an *infinite* or a *finite* homogeneous isotropic elastic body containing an arbitrary-shape inclusion prescribed with an eigenstrain and an eigenstrain gradient are analytically solved. The solutions are based on a simplified strain gradient elasticity theory (SSGET) that includes one material length scale parameter in addition to two classical elastic constants.

For the infinite-domain inclusion problem, the Eshelby tensor is derived in a general form by using the Green's function in the SSGET. This Eshelby tensor captures the inclusion size effect and recovers the classical Eshelby tensor when the strain gradient effect is ignored. By applying the general form, the explicit expressions of the Eshelby tensor for the special cases of a spherical inclusion, a cylindrical inclusion of infinite length and an ellipsoidal inclusion are obtained. Also, the volume average of the new Eshelby tensor over the inclusion in each case is analytically derived. It is quantitatively shown that the new Eshelby tensor and its average can explain the inclusion size effect, unlike its counterpart based on classical elasticity.

To solve the finite-domain inclusion problem, an extended Betti's reciprocal

theorem and an extended Somigliana's identity based on the SSGET are proposed and utilized. The solution for the disturbed displacement field incorporates the boundary effect and recovers that for the infinite-domain inclusion problem. The problem of a spherical inclusion embedded concentrically in a finite spherical body is analytically solved by applying the general solution, with the Eshelby tensor and its volume average obtained in closed forms. It is demonstrated through numerical results that the newly obtained Eshelby tensor can capture the inclusion size and boundary effects, unlike existing ones.

Finally, a homogenization method is developed to predict the effective elastic properties of a heterogeneous material using the SSGET. An effective elastic stiffness tensor is analytically derived for the heterogeneous material by applying the Mori-Tanaka and Eshelby's equivalent inclusion methods. This tensor depends on the inhomogeneity size, unlike what is predicted by existing homogenization methods based on classical elasticity. Numerical results for a two-phase composite reveal that the composite becomes stiffer when the inhomogeneities get smaller.

ACKNOWLEDGEMENTS

I would like to gratefully thank my advisor, Professor Xin-Lin Gao, for his support, guidance, patience and encouragement during my graduate studies at Texas A&M University. He has demonstrated to me what makes a great researcher: dedication, diligence, persistence, commitment to excellence, and honor. Without him, this dissertation work would not have been possible.

I am very thankful to my other committee members, Professor J.N. Reddy, Professor Jay Walton, Professor Anastasia Muliana and Professor Steve Suh, for their time and help. I have benefitted greatly from their comments and advice. I also thank everyone in Professor Gao's research group for helping me over the years.

Especially, I am eternally grateful to my parents, my husband and my sister for their unconditional and selfless love. I am so blessed to have their full support during my graduate studies and in my daily life.

Finally, I thank my Lord, Jesus Christ, who helps me to overcome all frustrations. He gives me hope, faith, love and compassion.

TABLE OF CONTENTS

CHAPTER Page

Page

LIST OF FIGURES

FIGURE Page

CHAPTER I

INTRODUCION

1.1. Background

Composites with complex microstructures are finding important applications in many engineering designs and products. For example, polymer matrix composites reinforced by various hard particles and short fibers (schematically shown in Fig. 1.1) are now widely used in the aerospace and automobile industries. These composites can be regarded as an assemblage of "pure" phases, which have significantly different physical properties and remain separate and distinct on a macroscopic level within the finished structure. For example, a polymer-based composite material reinforced with metal particles consists of two distinct phases, namely, the polymer matrix and the metal particles. To effectively analyze the macroscopic behavior of a composite, a heterogeneous material model including all individual phases in the composite is not practically favorable because of computational difficulties involved in the simulation process. For instance, an extremely fine mesh may have to be used in order to incorporate microscopic details of the composite, which could be prohibitively expensive in computation. In addition, the exact spatial distribution of the individual phases is far from ascertained due to the high randomness in the fabrication of the composite. Hence, an equivalent material model with homogenized or effective properties is desirable in the macroscopic analysis of the overall response of the composite, which has motivated the development of Micromechanics. Micromechanics is a branch of solid mechanics that aims to predict the macroscopic mechanical behavior of

---

This dissertation follows the style of *Journal of the Mechanics and Physics of Solids*.

materials based on the understanding of their microstructures (e.g., Mura, 1987; Qu and Cherkaoui, 2006; Nemat-Nasser and Hori, 1999; Li and Wang, 2008). It studies composites or heterogeneous materials by incorporating microstructures of individual phases that constitute these materials, and uses suitable homogenization methods to determine the effective properties that can be applied directly in the macroscale analysis.

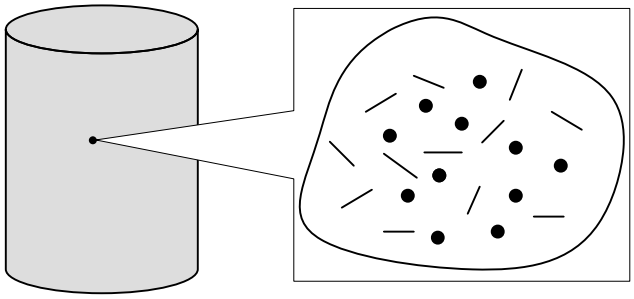

Fig.1.1. Macroscopic composite material and its microscopic structures.

The beginning of micromechanics may be traced back to Eshelby's seminal study in the 1950s (Eshelby, 1957, 1959). On the microscopic scale, the problem of *inhomogeneities*, whose material properties are different from their surrounding matrix, is encountered. This problem was not analytically solved until Eshelby proposed an eigenstrain method for an inclusion problem, which can be used to simulate the inhomogeneity problem. According to Eshelby's original work, an *inclusion* is defined as a subdomain Ω_I in an infinite domain Ω_∞, where a stress-free eigenstrain $\boldsymbol{\varepsilon}^*$ is prescribed in the inclusion Ω_I and vanishes outside (see Fig. 1.2a). The material property, denoted by $\mathbf{C}^M$ in Fig. 1.2a, is the same in Ω_I and $\Omega_\infty - \Omega_I$. In a similar way, an *inhomogeneity* is defined as a subdomain Ω_H in an infinite domain Ω_∞ (see Fig.1.2b), where the material properties in Ω_H and in $\Omega_\infty - \Omega_H$, denoted respectively by $\mathbf{C}^F$ and $\mathbf{C}^M$ in Fig.1.2b, are different. From the above definitions, it is clear

that in an *inclusion* problem, an eigenstrain is distributed in a *homogeneous* material, while in an *inhomogeneity* problem, a different material is embedded in a homogeneous matrix, leading to a *heterogeneous* (composite) material. The strain and stress fields will be disturbed due to the existence of the eigenstrain or the inhomogeneity.

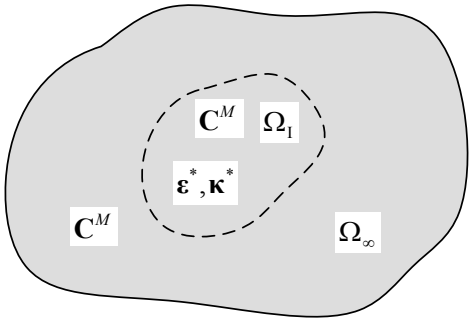

Fig.1.2a. Inclusion Problem.

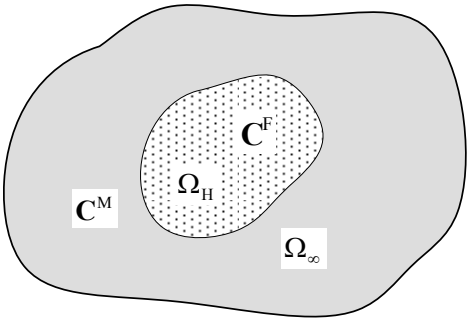

Fig. 1.2b. Inhomogeneity problem.

Eshelby showed that if a uniform eigenstrain $\boldsymbol{\varepsilon}^*$ is prescribed inside an ellipsoidal inclusion, then the disturbed strain $\boldsymbol{\varepsilon}^d$ is related to $\boldsymbol{\varepsilon}^*$ by (Eshelby, 1957)

$$\varepsilon_{ij}^{d} = S_{ijkl}\varepsilon_{kl}^{*}, \tag{1.1}$$

where S_{ijkl} is a fourth-order tensor now known as the Eshelby tensor, which provides a direct link between the disturbed strain in Ω_∞ and the stress-free uniform transformation strain (eigenstrain) in Ω_I. The analytical expressions of S_{ijkl} for an ellipsoidal inclusion have been provided in Eshelby (1957, 1959) and subsequent studies (e.g., Mura, 1987; Ju and Sun, 1999; Li and Wang, 2008). By adjusting the value of $\boldsymbol{\varepsilon}^*$, the stress and the strain fields in the inclusion and in the inhomogeneity can be made equivalent. As a result, the inhomogeneity problem, encountered in the composite analysis, can be solved once the Eshelby tensor for the inclusion problem is obtained. This is known as the Eshelby's equivalent eigenstrain method. With the knowledge of the mechanical field within each

constituent of the heterogeneous material, it is now possible to determine the overall or effective mechanical properties based on some averaging theorems. Clearly, the Eshelby tensor S_{ijkl} plays a key role in such homogenization analysis, and the development of new homogenization methods will hinge on the availability of new expressions of S_{ijkl}.

1.2. Motivation

Despite the significance of the Eshelby tensor S_{ijkl} in Micromechanics, it is deduced by Eshelby and most subsequent researchers based on classical elasticity and depends only on the elastic constants and the inclusion shape (e.g., the aspect ratios for an ellipsoidal inclusion). As a result, the Eshelby tensor and the subsequent homogenization methods cannot capture the size effect exhibited by particle-matrix composites at the micro- or nano-scale (e.g., Vollenberg and Heikens, 1989; Vollenberg, et al., 1989; Lloyd, 1994; Kouzeli and Mortensen, 2002). This has motivated the studies on Eshelby-type inclusion problems using higher-order elasticity theories, which, unlike classical elasticity, contain microstructure-dependent material length scale parameters and are therefore capable of explaining the size effect.

The higher-order elasticity theories that have been used in studying the Eshelby inclusion problems include a micropolar theory (Cheng and He, 1995, 1997; Ma and Hu, 2006), a microstretch theory (Kiris and Inan, 2006; Ma and Hu, 2007), a modified couple stress theory (Zheng and Zhao, 2004), and a strain gradient elasticity theory (Zhang and Sharma, 2005). However, most of the higher-order elasticity theories used in these studies involve at least four elastic constants, with two or more being the material length scale parameters. Due to the difficulties in determining these microstructure-dependent length scale parameters (e.g., Lakes, 1995; Lam et al., 2003; Maranganti and Sharma, 2007) and in

dealing with the fourth-order Eshelby tensor, it is very desirable to study the Eshelby inclusion problem using a higher-order elasticity theory containing only one material length scale parameter in addition to the two classical elastic constants. Among the afore-mentioned works, the one reported in Zheng and Zhao (2004) appears to be the only study that involves just one additional length scale parameter, which is based on a couple stress theory modified from the classical couple stress theory (Koiter, 1964) that contains four elastic constants in the constitutive equations but three in the displacement-equations of equilibrium. There is still a lack of studies on the Eshelby-type inclusion problems based on strain gradient elasticity theories involving only one additional elastic constant. The objective of this dissertation is therefore to provide a systematic study of various Eshelby-type inclusion problems involving a spherical, cylindrical or ellipsoidal inclusion embedded in an *infinite* or a *finite* homogeneous isotropic elastic body, applying a simpler one-length-scale-parameter strain gradient theory. It will be based on a simplified strain gradient theory (SSGET) elaborated by Gao and Park (2007), which involves only one material length parameter in addition to two classical elastic constants. The resulting non-classical Eshelby tensors based on the SSGET will then be utilized to develop new homogenization methods for analyzing heterogeneous composites.

1.3. Organization

The rest of this dissertation is organized as follows.

In Chapter II, the Green's function in the SSGET is first obtained in terms of elementary functions by applying Fourier transforms, which reduces to the Green's function in classical elasticity when the strain gradient effect is not considered. The Eshelby tensor is then derived in a general form for an inclusion of arbitrary shape, which consists of a

classical part and a gradient part. The former depends on two classical elastic constants only, while the latter depends on the length scale parameter additionally, thereby enabling the interpretation of the size effect.

In Chapter III and Chapter IV, the explicit expressions of the Eshelby tensors for a spherical and for a cylindrical inclusion are obtained, respectively, by applying the general form of the Eshelby tenor derived in Chapter II. Both of the non-classical Eshelby tensors varies with positions even inside the inclusions and captures the inclusion-size dependence, unlike the classical Eshelby tensors. The volume averages of these newly derived Eshelby tensors over the spherical and the cylindrical inclusions are obtained in closed forms, to facilitate the further homogenization analyses of particle-reinforced and fiber-reinforced composites.

In Chaper 5, the problem of an ellipsoidal inclusion (with three distinct semi-axes) in an infinite homogeneous isotropic elastic material is analytically solved by using the general form of the Eshelby tensor in the SSGET. Analytical expressions for the Eshelby tensor are derived for both the interior and exterior cases in terms of two line integrals with an unbounded upper limit and two surface integrals over a unit sphere. The Eshelby tensors for the spherical and cylindrical inclusion problems based on the SSGET are included in the current Eshelby tensor as two limiting cases. The volume average of the new Eshelby tensor over the ellipsoidal inclusion needed in homogenization analyses is also analytically obtained in this chapter.

In Chapter VI, a solution for the Eshelby-type inclusion problem of a finite homogeneous isotropic elastic body containing an inclusion prescribed with a uniform eigenstrain and a uniform eigenstrain gradient is derived in a general form using the SSGET. An extended Betti's reciprocal theorem and an extended Somigliana's identity based on the

SSGET are proposed and utilized to solve the finite-domain inclusion problem. The solution for the disturbed displacement field is expressed in terms of the Green's function for an infinite three-dimensional elastic body in the SSGET. It contains a volume integral term and a surface integral term. The former is the same as that for the infinite-domain inclusion problem based on the SSGET, while the latter represents the boundary effect. The solution reduces to that of the infinite-domain inclusion problem when the boundary effect is not considered. The problem of a spherical inclusion embedded concentrically in a finite spherical elastic body is analytically solved by applying the general solution, with the Eshelby tensor and its volume average obtained in closed forms.

A homogenization method is developed in Chapter VII to predict the effective elastic properties of a heterogeneous material in the framework of the SSGET. At the macroscopic scale, the heterogeneous material is modeled as a homogeneous strain-gradient medium whose behavior can be characterized by the constitutive relations in the SSGET. The effective elastic properties of the heterogeneous material are found to be dependent not only on the volume fractions and shapes of the inhomogeneities but also on the inhomogeneity sizes, unlike what is predicted by the homogenization method based on classical elasticity. The effective elastic stiffness tensor is analytically obtained by using the Mori-Tanaka method and Eshelby's equivalent inclusion method.

CHAPTER II

GREEN'S FUNCTION AND ESHELBY TENSOR BASED ON A SIMPLIFIED STRAIN GRADIENT ELASTICITY THEORY

2.1. Introduction

In this chapter, a simplified strain gradient elasticity theory (SSGET) involving only one additional material length scale parameter (Altan and Aifantis, 1997; Gao and Park, 2007) is used to analytically solve the Eshelby-type problem of an infinite homogeneous isotropic elastic medium containing an inclusion of arbitrary shape. A variationally consistent formulation of the SSGET was provided in Gao and Park (2007). This simplified strain gradient elasticity theory has been applied to solve a number of problems (e.g., Lazopoulos, 2004; Li et al., 2004; Gao and Park, 2007; Gao et al., 2009).

The rest of this chapter is organized as follows. In Section 2.2, the simplified strain gradient elasticity theory (SSGET) is fist reviewed. It is followed by Section 2.3 where a three-dimensional (3-D) Green's function in the SSGET is obtained from directly solving the governing equations using Fourier transforms. Based on this Green's function obtained, the Eshelby tensor is derived in Section 2.4 in a general form for a 3-D inclusion of arbitrary shape, which consists of a classical part and a gradient part. The former contains only one classical elastic constant (Poisson's ratio), while the latter includes the length scale parameter additionally. This chapter concludes with a summary in Section 2.5.

2.2. Simplified Strain Gradient Elasticity Theory (SSGET)

As reviewed in Gao and Ma (2010a), the SSGET is the simplest strain gradient elasticity theory evolving from Mindlin's pioneering work (Mindlin, 1964, 1965; Mindlin and Eshel, 1968). It is also known as the first gradient elasticity theory of Helmholtz type (e.g., Lazar et al., 2005) and the dipolar gradient elasticity theory (e.g., Georgiadis et al., 2004). The SSGET has been well studied and successfully used to solve a number of important problems on dislocations (e.g., Lazar and Maugin, 2005), cracking (e.g., Altan and Aifantis, 1992; Gourgiotis and Georgiadis, 2009), wave dispersion (e.g., Georgiadis et al., 2004), inclusions (Gao and Ma, 2009, 2010a, 2010b; Ma and Gao, 2009), beams (e.g., Giannakopoulos and Stamoulis, 2007), plates (e.g., Lazopoulos, 2004), and thick-walled shells (Gao and Park, 2007; Gao et al., 2009).

However, for a better understanding of this relatively recent SSGET, further elaborations on the aspects of the theory interpretation and length scale parameter determination are still warranted. There has been a slow embracement of strain gradient elasticity and plasticity theories, as indicated earlier by Fleck and Hutchinson (1997) for strain gradient elasticity theories and very recently by Evans and Hutchinson (2009) for strain gradient plasticity theories. One reason for this slow embracement is the lack of clarity in the theory interpretation, and another is the ambiguity in determining length scale parameters through curve fitting (Evans and Hutchinson, 2009). These apply to the SSGET and therefore will be discussed further below.

As stated in Gao and Park (2007), elements of the SSGET were first suggested by Altan and Aifantis (1992, 1997) by simplifying Mindlin's first strain gradient theory in linear elasticity (Mindlin and Eshel, 1968) without derivations. The strain energy density function, w, employed by Mindlin and Eshel (1968) for an isotropic linearly elastic material

has the general form:

$$\begin{aligned} w &= w(\varepsilon_{ij}, \varepsilon_{ij,k}) \\ &= \frac{1}{2}\lambda\varepsilon_{ii}\varepsilon_{jj} + \mu\varepsilon_{ij}\varepsilon_{ij} + c_1\varepsilon_{ij,j}\varepsilon_{ik,k} + c_2\varepsilon_{ii,k}\varepsilon_{kj,j} + c_3\varepsilon_{ii,k}\varepsilon_{jj,k} + c_4\varepsilon_{ij,k}\varepsilon_{ij,k} + c_5\varepsilon_{ij,k}\varepsilon_{kj,i}, \end{aligned} \tag{2.1}$$

where ε_{ij} is the infinitesimal strain, λ and μ are the Lamé constants in classical elasticity, and c_1–c_5 are the five additional material constants (called strain gradient coefficients) having the dimension of force. By taking

$$c_1 = c_2 = c_5 = 0,\ \ c_3 = \frac{1}{2}c\lambda,\ \ c_4 = c\mu, \tag{2.2}$$

Eq. (2.1) becomes

$$w = w(\varepsilon_{ij}, \varepsilon_{ij,k}) = \frac{1}{2}\lambda\varepsilon_{ii}\varepsilon_{jj} + \mu\varepsilon_{ij}\varepsilon_{ij} + c\left(\frac{1}{2}\lambda\varepsilon_{ii,k}\varepsilon_{jj,k} + \mu\varepsilon_{ij,k}\varepsilon_{ij,k}\right), \tag{2.3}$$

where c, as the only remaining strain gradient coefficient, has the dimension of length squared. Eq. (2.3) can also be written as (Gao and Park, 2007)

$$w = w(\varepsilon_{ij}, \varepsilon_{ij,k}) = \frac{1}{2}\left(\tau_{ij}\varepsilon_{ij} + \mu_{ijk}\kappa_{ijk}\right), \tag{2.4}$$

where the Cauchy stress τ_{ij} (energetically conjugated to ε_{ij}), the double stress μ_{ijk} (energetically conjugated to κ_{ijk}), the infinitesimal strain ε_{ij}, and the strain gradient κ_{ijk} are, respectively, defined by

$$\tau_{ij} = C_{ijkl}\varepsilon_{kl} = \lambda\varepsilon_{ll}\delta_{ij} + 2\mu\varepsilon_{ij}, \quad \mu_{ijk} = L^2 C_{ijmn}\kappa_{mnk} = L^2(\lambda\kappa_{llk}\delta_{ij} + 2\mu\kappa_{ijk}),$$

$$\varepsilon_{ij} = \frac{1}{2}\left(u_{i,j} + u_{j,i}\right), \quad \kappa_{ijk} \equiv \varepsilon_{ij,k} = \frac{1}{2}\left(u_{i,jk} + u_{j,ik}\right), \tag{2.5a–d}$$

where u_i is the displacement and δ_{ij} is the Kronecker delta. In Eqs. (2.5a,b), L is the material length scale parameter (with $L^2 = c$, c being the strain gradient coefficient introduced in Eq. (2.3)) and C_{ijkl} is the elastic stiffness tensor for isotropic elastic materials given by

$$C_{ijkl} = \lambda \delta_{ij} \delta_{kl} + \mu (\delta_{ik} \delta_{jl} + \delta_{il} \delta_{jk}) . \tag{2.6}$$

The simplified strain energy density function in Eq. (2.3) was first suggested in Altan and Aifantis (1997) without reasoning. Following Lazar and Maugin (2005), it can now be understood that this simplified strain energy density function is physical and exhibits the symmetry both in τ_{ij} and ε_{ij} and in μ_{ijk} and κ_{ijk} for the linearly elastic material, as shown in Eq. (2.4). Based on Eq. (2.3), a variationally consistent formulation of the SSGET has been provided in Gao and Park (2007), leading to the simultaneous determination of the governing equations and the complete boundary conditions. However, the form of the strain energy density function *w* given in Eq. (2.3) or Eq. (2.1) can be discussed further next.

Physically, for linearly elastic materials, the dependence of *w* on $\nabla \boldsymbol{\varepsilon} = \varepsilon_{ij,k} \mathbf{e}_i \otimes \mathbf{e}_j \otimes \mathbf{e}_k$ included in Eq. (2.1) arises from the non-local nature of atomic forces, which was first studied by Kröner (1963), where the connection between the lattice curvature and the double stress was explored and the necessity of including the strain gradient effect for some elastic materials was demonstrated. This was pointed out earlier by Nix and Gao (1998). The mathematical framework that led to Mindlin's strain energy density function in Eq. (2.1) was established by Toupin (1962) and Green and Rivlin (1964a, b).

For plastically deformable materials, the strain gradient effect as reflected in Eq. (2.1) is associated with geometrically necessary dislocations, which is in addition to the homogeneous plastic strain arising from statistically stored dislocations (e.g., Ashby, 1970; Fleck et al., 1994; Nix and Gao, 1998; Gao et al., 1999). As a result, the strain energy density function given in Eq. (2.1) was adopted by Fleck and Hutchinson (1997) in

developing their strain gradient plasticity theory for incompressible materials, where $\varepsilon_{ii} = 0$ and the first, fourth and fifth terms in Eq. (2.1) vanish, thereby leaving only three additional constants c_1, c_4 and c_5 in the expression of w for the general case. These three constants can be determined from fitting experimental data obtained in micro-torsion, micro-bending and micro-indentation tests (e.g., Fleck and Hutchinson, 1997; Shi et al., 2000; Lam et al., 2003).

The determination of the only material length scale parameter L involved in the SSGET, which is introduced in Eq. (2.3) through $c = L^2$, has been discussed in a number of publications. The most recent one is that by Gourgiotis and Georgiadis (2009), where it was stated that the coefficient c (and thus L) can be estimated from comparing the dispersion curves of Rayleigh waves obtained using the strain gradient theory based on Eq. (2.3) and those from lattice dynamics calculations, as was done in Georgiadis et al. (2004). This approach was also used earlier by Altan and Aifantis (1992). Similar to that in the strain gradient plasticity theory of Fleck and Hutchinson (1997) for determining c_1, c_4 and c_5 mentioned above, the parameter L can also be estimated by fitting experimental data from small-scale tests. This has been demonstrated by Giannakopoulos and Stamoulis (2007) by fitting the strain gradient elasticity based analytical results for the normalized stiffness of a cantilever beam to the experimental data obtained by Kakunai et al. (1985) using heterodyne holographic interferometry. Efforts have also been made to estimate L by fitting the measured data from bending and torsion tests of microstructured solids (including bones and polymeric foams) that are elastically deformed (Aifantis, 1999, 2003). These reported methods for determining the material length scale parameter L in the SSGET have been elaborated by Lakes (1995) together with other methods in a broader context.

As shown in Gao and Park (2007), in the SSGET the equilibrium equations have the

form:

$$\sigma_{ij,j} + f_i = 0\,, \tag{2.7}$$

where f_i is the body force, and σ_{ij} is the total stress, which is related to the Cauchy stress through

$$\sigma_{ij} \equiv \tau_{ij} - \mu_{ijk,k}\,, \tag{2.8}$$

with the Cauchy stress τ_{ij} and the double stress μ_{ijk} given in Eqs. (2.5a–d) in terms of the displacement u_i.

Substituting Eqs. (2.5a–d) and (2.8) into Eq. (2.7) yields the Navier-like displacement equations of equilibrium in the SSGET as

$$(\lambda+\mu)u_{i,ij} + \mu u_{j,kk} - L^2\left[(\lambda+\mu)u_{i,ij} + \mu u_{j,kk}\right]_{,mm} + f_j = 0\,. \tag{2.9}$$

Clearly, Eq. (2.9) reduces to the Navier equations in classical elasticity when $L = 0$ (i.e., when the strain gradient effect is not considered). Note that the standard index notation, together with the Einstein summation convention, is used in Eqs. (2.1)–(2.9) and throughout this dissertation, with each Latin index (subscript) ranging from 1 to 3 and each Greek index (subscript) ranging from 1 to 2, unless otherwise stated.

2.3. Green's Function Based on SSGET

The solution of Eq. (2.9) subject to the boundary conditions of u_i and their derivatives vanishing at infinity, provides the fundamental solution and Green's function in the SSGET, as will be shown next.

The 3-D Fourier transform of a sufficiently smooth function $F(\mathbf{x})$ and its inverse can be defined as

$$\hat{F}(\boldsymbol{\xi}) = \iiint_{-\infty}^{+\infty} F(\mathbf{x}) e^{-i\boldsymbol{\xi}\cdot\mathbf{x}} d\mathbf{x}, \tag{2.10a}$$

$$F(\mathbf{x}) = \frac{1}{(2\pi)^3} \iiint_{-\infty}^{+\infty} \hat{F}(\boldsymbol{\xi}) e^{i\boldsymbol{\xi}\cdot\mathbf{x}} d\boldsymbol{\xi}, \tag{2.10b}$$

where $\mathbf{x}$ is the position vector of a point in the 3-D physical space, $\boldsymbol{\xi}$ is the position vector of the same point in the Fourier (transformed) space, i is the usual imaginary number with $i^2 = -1$, and $\hat{F}(\boldsymbol{\xi})$ is the Fourier transform of $F(\mathbf{x})$.

Suppose that u_i are sufficiently differentiable and that u_i and their derivatives vanish at $|\mathbf{x}| \to \infty$. Then, applying Eq. (2.10a), the product rule and the divergence theorem gives

$$\hat{u}_i(\boldsymbol{\xi}) = \iiint_{-\infty}^{+\infty} u_i(\mathbf{x}) e^{-i\boldsymbol{\xi}\cdot\mathbf{x}} d\mathbf{x}, \quad \hat{u}_{k,ij}(\boldsymbol{\xi}) = -\xi_i \xi_j \hat{u}_k(\boldsymbol{\xi}), \quad \hat{u}_{k,ijll}(\boldsymbol{\xi}) = \xi_i \xi_j \xi_l \xi_l \hat{u}_k(\boldsymbol{\xi}). \tag{2.11}$$

Taking Fourier transforms on Eq. (2.9) and using Eqs. (2.10a) and (2.11) will lead to

$$\xi^2 (1 + L^2 \xi^2) \left[(\lambda + 2\mu) \xi_i^0 \xi_j^0 + \mu (\delta_{ij} - \xi_i^0 \xi_j^0) \right] \hat{u}_i = \hat{f}_j, \tag{2.12}$$

where $\xi \equiv |\boldsymbol{\xi}| = (\xi_k \xi_k)^{1/2}$, and $\xi_i^0 = \xi_i / \xi$ are the components of the unit vector $\boldsymbol{\xi}^0 = \boldsymbol{\xi} / \xi$. Eq. (2.12) gives a system of three algebraic equations to solve for the three unknowns $\hat{u}_i$. This equation system can be readily solved to obtain

$$\hat{u}_i(\boldsymbol{\xi}) = \hat{G}_{ij}(\boldsymbol{\xi}) \hat{f}_j(\boldsymbol{\xi}), \tag{2.13a}$$

where $\hat{G}_{ij}(\boldsymbol{\xi})$ is the inverse of the coefficient matrix of $\hat{u}_i(\boldsymbol{\xi})$ in Eq. (2.12) given by (see Appendix A)

$$\hat{G}_{ij}(\boldsymbol{\xi}) = \frac{1}{\xi^2 (1 + L^2 \xi^2)} \left[\frac{1}{\mu} \left(\delta_{ij} - \xi_i^0 \xi_j^0 \right) + \frac{1}{\lambda + 2\mu} \xi_i^0 \xi_j^0 \right]. \tag{2.13b}$$

Taking inverse Fourier transforms on both sides of Eq. (2.13a) then yields, with the help of the convolution theorem, the solution of Eq. (2.9) as

$$u_i(\mathbf{x}) = \iiint_{-\infty}^{+\infty} G_{ij}(\mathbf{x} - \mathbf{y}) f_j(\mathbf{y}) d\mathbf{y}, \tag{2.14}$$

where G_{ij} (**x**), as the inverse Fourier transform of $\hat{G}_{ij}(\boldsymbol{\xi})$ listed in Eq. (2.13b), is (see Eq. (2.10b))

$$G_{ij}(\mathbf{x}) = \frac{1}{8\pi^3}\iiint_{-\infty}^{+\infty} \hat{G}_{ij}(\boldsymbol{\xi}) e^{\mathrm{i}\boldsymbol{\xi}\cdot\mathbf{x}} d\boldsymbol{\xi}. \tag{2.15}$$

Eq. (2.14) gives the fundamental solution in the SSGET in terms of the Green's function G_{ij} (**x**) defined in Eq. (2.15). Note that the Green's function $\mathbf{G}(\mathbf{x}-\mathbf{y})$ is a second-order tensor. From Eq. (2.14), it is clear that its component $G_{ij}(\mathbf{x}-\mathbf{y})$ represents the displacement component u_i at point **x** in a 3-D infinite elastic body due to a unit concentrated body force applied at point **y** in the body in the *j*th direction.

To evaluate the definite integral in Eq. (2.15), a convenient spherical coordinate system (ξ, θ, φ) in the transformed space is chosen such that the angle between **x** and $\boldsymbol{\xi}$ is θ, with the direction of **x** being the axis where $\theta = 0$. Then, it follows that $\boldsymbol{\xi}\cdot\mathbf{x} = \xi_k x_k = \xi x\cos\theta$, with $x \equiv |\,\mathbf{x}\,| = (x_k x_k)^{1/2}$, and the volume element $d\boldsymbol{\xi} = \xi^2 \sin\theta\, d\xi\, d\theta\, d\varphi$. Substituting Eq. (2.13b) into Eq. (2.15) yields

$$\begin{aligned} G_{ij}(\mathbf{x}) &= \frac{1}{8\pi^3}\int_0^{2\pi}\left\langle \int_0^{\pi}\left\{ \int_0^{\infty} \frac{1}{1+L^2\xi^2}\left[\frac{1}{\mu}\left(\delta_{ij} - \xi_i^0\xi_j^0\right) + \frac{1}{\lambda+2\mu}\xi_i^0\xi_j^0\right] e^{\mathrm{i}\xi x\cos\theta} d\xi \right\} \sin\theta d\theta \right\rangle d\varphi \\ &= \frac{1}{8\pi^3}\int_0^{\pi}\left\langle \left\{ \int_0^{2\pi}\left[\frac{1}{\mu}\left(\delta_{ij} - \xi_i^0\xi_j^0\right) + \frac{1}{\lambda+2\mu}\xi_i^0\xi_j^0\right] d\phi \right\} \left(\int_0^{\infty} \frac{1}{1+L^2\xi^2} e^{\mathrm{i}\xi x\cos\theta} d\xi \right) \right\rangle \sin\theta d\theta. \end{aligned} \tag{2.16}$$

From Eq. (2.13b) it is seen that $\hat{G}_{ij}(\boldsymbol{\xi})$ is an even function of $\boldsymbol{\xi}$ with $\hat{G}_{ij}(-\boldsymbol{\xi}) = \hat{G}_{ij}(\boldsymbol{\xi})$, and from Eq. (2.15) it then follows that $G_{ij}(\mathbf{x})$ is also an even function of **x** with $G_{ij}(-\mathbf{x}) = G_{ij}(\mathbf{x})$. Using this fact and the expression of $G_{ij}(\mathbf{x})$ in Eq. (2.16) gives

$$\int_0^{\infty} \frac{1}{1+L^2\xi^2} e^{\mathrm{i}\xi x\cos\theta} d\xi = \frac{1}{2}\int_{-\infty}^{\infty} \frac{1}{1+L^2\xi^2} e^{\mathrm{i}\xi x\cos\theta} d\xi = \frac{\pi}{2L} e^{-|x\cos\theta|/L}, \tag{2.17}$$

where the second equality follows from the Euler formula, integration properties of even and odd functions, and a known integration result in calculus. Also, it can be shown that (see Appendix B)

$$\int_0^{2\pi} \xi_i^0 \xi_j^0 d\varphi = \pi\left[\delta_{ij} \sin^2\theta - x_i^0 x_j^0 (1 - 3\cos^2\theta)\right], \tag{2.18}$$

where $x_i^0 = x_i / x$ are the components of the unit vector $\mathbf{x}^0 = \mathbf{x}/x$. Substituting Eqs. (2.17) and (2.18) into Eq. (2.16) then yields

$$G_{ij}(\mathbf{x}) = \frac{1}{16\pi L}\int_{-1}^{1}\left\{\left[\frac{2}{\mu} + \left(\frac{1}{\lambda+2\mu} - \frac{1}{\mu}\right)(1-t^2)\right]\delta_{ij} - \left(\frac{1}{\lambda+2\mu} - \frac{1}{\mu}\right)x_i^0 x_j^0 (1-3t^2)\right\} e^{-|xt|/L} dt, \tag{2.19}$$

where use has been made of $t = -\cos\theta$ to facilitate the integration.

Evaluating the integral in Eq. (2.19) finally gives the Green's function as

$$G_{ij}(\mathbf{x}) = \frac{1}{32\pi\mu(1-\nu)}\left[\Psi(x)\delta_{ij} + \mathrm{X}(x) x_i^0 x_j^0\right], \tag{2.20}$$

where ν is Poisson's ratio, and

$$\Psi(x) = \frac{2}{x}\left\{(3-4\nu)\left(1 - e^{-\frac{x}{L}}\right) + \frac{1}{x^2}\left[2L^2 - (x^2 + 2Lx + 2L^2)e^{-\frac{x}{L}}\right]\right\}, \tag{2.21a}$$

$$\mathrm{X}(x) = \frac{2}{x}\left[\left(1 - \frac{6L^2}{x^2}\right) + \left(2 + \frac{6L}{x} + \frac{6L^2}{x^2}\right)e^{-\frac{x}{L}}\right] \tag{2.21b}$$

are two convenient functions. Note that in reaching Eq. (2.20) use has also been made of the identities (e.g., Timoshenko and Goodier, 1970):

$$\lambda = \frac{E\nu}{(1+\nu)(1-2\nu)}, \quad \mu = \frac{E}{2(1+\nu)}, \tag{2.22}$$

where E is the Young's modulus.

The Green's function derived here in Eqs. (2.20) and (2.21a,b) can be shown to be the same as that obtained by Polyzos et al. (Polyzos et al. 2003) using a different approach

based on the use of the Helmholtz decomposition and potential functions. This Green's function can also be reduced to the Green's function in classical elasticity when the strain gradient effect is ignored. That is, by setting $L = 0$, Eqs. (2.20) and (2.21a,b) become

$$G_{ij}(x) = \frac{1}{16\pi\mu(1-\nu)x}\left[(3-4\nu)\delta_{ij} + x_i^0 x_j^0\right], \tag{2.23}$$

which is the Green's function for 3-D problems in classical elasticity (e.g., Mura, 1987; Li and Wang, 2008).

To facilitate the differentiation of the Green's function needed for determining Eshelby tensor, the expressions given in Eqs. (2.20) and (2.21a,b) can be rewritten as follows. Note that $x_{,i} = x_i / x = x_i^0$ and $x_{i,j} = \partial x_i / \partial x_j = \delta_{ij}$. It then follows that

$$x_{,ij} = \frac{1}{x}\left(\delta_{ij} - x_i^0 x_j^0\right) \Rightarrow\ x_i^0 x_j^0 = \delta_{ij} - x x_{,ij}. \tag{2.24}$$

Inserting Eq. (2.24) into Eq. (2.20) then gives

$$G_{ij}(\mathbf{x}) = \frac{1}{32\pi\mu(1-\nu)}\{[\Psi(x) + \mathrm{X}(x)]\delta_{ij} - \mathrm{X}(x)x x_{,ij}\}. \tag{2.25}$$

Next, using Eq. (2.21b) and the following two identities:

$$\frac{1}{x^2}x_{,ij} = \frac{2}{3x^3}\delta_{ij} - \frac{1}{3}\left(\frac{1}{x}\right)_{,ij}, \tag{2.26a}$$

$$\left(1 + \frac{3L^2}{x^2} + \frac{3L}{x}\right)e^{-\frac{x}{L}}x_{,ij} = \left(\frac{1}{x} + \frac{2L}{x^2} + \frac{2L^2}{x^3}\right)e^{-\frac{x}{L}}\delta_{ij} - L^2\left(\frac{1}{x}e^{-\frac{x}{L}}\right)_{,ij} \tag{2.26b}$$

leads to

$$\mathrm{X}(x)x x_{,ij} = 2\left\{\left[-\frac{4L^2}{x^3} + 2\left(\frac{1}{x} + \frac{2L}{x^2} + \frac{2L^2}{x^3}\right)e^{-\frac{x}{L}}\right]\delta_{ij} + \left(x + \frac{2L^2}{x} - \frac{2L^2}{x}e^{-\frac{x}{L}}\right)_{,ij}\right\}. \tag{2.27}$$

Substituting Eqs. (2.21a,b) and (2.27) into Eq. (2.25) finally yields

$$G_{ij}(\mathbf{x}) = \frac{1}{16\pi\mu(1-\nu)}\left[A(x)\delta_{ij} - B(x)_{,ij}\right], \tag{2.28}$$

where

$$A(x) \equiv 4(1-\nu)\frac{1}{x}\left(1-e^{-\frac{x}{L}}\right),\ B(x) \equiv x+\frac{2L^2}{x}-\frac{2L^2}{x}e^{-\frac{x}{L}}. \tag{2.29}$$

It can be readily shown that when $L = 0$, Eqs. (2.28) and (2.29) reduce to Eq. (2.23), the Green's function in classical elasticity.

Eqs. (2.28) and (2.29) give the final form of the strain gradient Green's function for 3-D elastic deformations in terms of elementary functions, which is different from the form obtained in Eqs. (2.20) and (2.21a,b) that involves $x_i^0 (= x_i / x)$ and $x_j^0 (= x_j / x)$ and is not convenient for differentiation. Eqs. (2.28) and (2.29) will be directly used in Section 2.4 to derive the general expressions of the Eshelby tensor based on the SSGET.

2.4. Eshelby Tensor and Eshelby-Like Tensor

Consider an infinite homogenous isotropic elastic body containing an inclusion in 3-D space. An eigenstrain $\boldsymbol{\varepsilon}^*$ and an eigenstrain gradient $\boldsymbol{\kappa}^*$ are prescribed in the inclusion, while no body force or any other external force is present in the elastic body. $\boldsymbol{\varepsilon}^*$ and $\boldsymbol{\kappa}^*$ may have been induced by inelastic deformations such as thermal expansion, phase transformation, residual stress, and plastic flow (e.g., Qu and Cherkaoui, 2006). For the case of plastic flow induced deformations, $\boldsymbol{\varepsilon}^*$ may be a plastic strain arising from statistically stored dislocations, and $\boldsymbol{\kappa}^*$ may be a plastic strain gradient resulting from local storage of geometrically necessary dislocations (e.g., Ashby, 1970; Fleck et al., 1994; Gao et al., 1999) that can be prescribed independently of $\boldsymbol{\varepsilon}^*$. Besides $\boldsymbol{\varepsilon}^*$ and $\boldsymbol{\kappa}^*$, there is no body force or surface force acting in the elastic infinite body containing the inclusion. Hence, the displacement, strain and stress fields induced by the presence of $\boldsymbol{\varepsilon}^*$ and $\boldsymbol{\kappa}^*$ here are disturbed fields, which may be superposed to those caused by applied body and/or surface

forces.

From Eqs. (2.7) and (2.8), the stress-equations of equilibrium in the absence of body forces are

$$\tau_{ij,j} - \mu_{ijp,pj} = 0, \tag{2.30}$$

where the Cauchy stress τ_{ij} is related to the elastic strain $\varepsilon_{ij}^{e} = \varepsilon_{ij} - \varepsilon_{ij}^{*}$ through the generalized Hooke's law:

$$\tau_{ij} = C_{ijkl}(\varepsilon_{kl} - \varepsilon_{kl}^{*}), \tag{2.31a}$$

and the double stress μ_{ijk} is obtained from Eq. (2.5b) as

$$\mu_{ijp} = L^2 C_{ijkl}(\kappa_{klp} - \kappa_{klp}^{*}), \tag{2.31b}$$

with C_{ijkl} being the components of the stiffness tensor of the isotropic elastic body given by Eq. 2.6.

Substituting Eqs. (2.31a,b) into Eq. (2.30) then yields the displacement-equations of equilibrium as

$$C_{ijkl}(\varepsilon_{kl} - L^2\kappa_{klp,p})_{,j} - C_{ijkl}(\varepsilon_{kl,j}^{*} - L^2\kappa_{klp,pj}^{*}) = 0, \tag{2.32}$$

where C_{ijkl} are given in Eq. (2.6). A comparison of Eq. (2.32) with Eq. (2.9) shows that Eq. (2.32) will be the same as that of Eq. (2.9) if the body force components f_j there are now replaced by $-C_{ijkl}(\varepsilon_{kl,j}^{*} - L^2\kappa_{klp,pj}^{*})$ and Eqs. (2.5c,d) are used. As a result, the solution of Eq. (2.32) can be readily obtained from Eq. (2.14) as

$$u_i(\mathbf{x}) = -\iiint_{-\infty}^{+\infty} G_{ij}(\mathbf{x}-\mathbf{y})\, C_{jklm}\varepsilon_{lm,k}^{*}\, d\mathbf{y} + \iiint_{-\infty}^{+\infty} G_{ij}(\mathbf{x}-\mathbf{y})\left[L^2(C_{jklm}\kappa_{lmp,pk}^{*})\right] d\mathbf{y}. \tag{2.33}$$

The use of the product rule, the divergence theorem and the fact that $\varepsilon_{lm}^{*} = 0$, $\kappa_{lmp}^{*} = 0$ outside the inclusion (and thus at infinity) in Eq. (2.33), together with C_{ijkl} = constants,

gives

$$u_i(\mathbf{x}) = \iiint_{-\infty}^{+\infty} G_{ij,k}(\mathbf{x}-\mathbf{y})\, C_{jklm}\varepsilon^*_{lm}\, d\mathbf{y} + \iiint_{-\infty}^{+\infty} G_{ij,kp}(\mathbf{x}-\mathbf{y})[L^2(C_{jklm}\kappa^*_{lmp})]d\mathbf{y}\,. \qquad (2.34)$$

Eq. (2.34) is valid for any (uniform or non-uniform) ε^*_{lm} and κ^*_{lmp}. For the Eshelby problem with ε^*_{lm} and κ^*_{lmp} being uniform in the inclusion and vanishing outside the inclusion and the elastic body being homogeneous (with C_{ijkl} = constants), Eq. (2.34) can be rewritten as

$$u_i(\mathbf{x}) = C_{jklm}\varepsilon^*_{lm}\iiint_{\Omega} G_{ij,k}(\mathbf{x}-\mathbf{y})d\mathbf{y} + L^2 C_{jklm}\kappa^*_{lmp}\iiint_{\Omega} G_{ij,kp}(\mathbf{x}-\mathbf{y})d\mathbf{y}\,, \qquad (2.35)$$

where Ω denotes the region occupied by the inclusion.

It should be mentioned that all the derivatives in the integrals introduced so far are with respect to **y**, which is the integration variable. However, it can be easily proved that

$$\frac{\partial G_{ij}(\mathbf{x}-\mathbf{y})}{\partial y_k} = -\frac{\partial G_{ij}(\mathbf{x}-\mathbf{y})}{\partial x_k}\,. \qquad (2.36)$$

Using Eq. (2.36) in Eq. (2.35) then gives the displacement as

$$u_i(\mathbf{x}) = -C_{jklm}\varepsilon^*_{lm}\frac{\partial}{\partial x_k}\left[\iiint_{\Omega} G_{ij}(\mathbf{x}-\mathbf{y})d\mathbf{y}\right] + L^2 C_{jklm}\kappa^*_{lmp}\frac{\partial}{\partial x_k \partial x_p}\left[\iiint_{\Omega} G_{ij}(\mathbf{x}-\mathbf{y})d\mathbf{y}\right]. \qquad (2.37)$$

Let

$$\langle F\rangle \equiv \iiint_{\Omega} F(\mathbf{y})d\mathbf{y} \qquad (2.38)$$

be the volume integral of a sufficiently smooth function $F(\mathbf{y})$ over the inclusion occupying region Ω. Then, Eq. (2.37) can be written as

$$u_i(\mathbf{x}) = -C_{jklm}\varepsilon^*_{lm}\langle G_{ij}\rangle_{,k} + L^2 C_{jklm}\kappa^*_{lmp}\langle G_{ij}\rangle_{,kp}\,, \qquad (2.39)$$

where $\langle G_{ij}\rangle$ is the volume integral of the Green's function $G_{ij}(\mathbf{x}–\mathbf{y})$ defined according to Eq. (2.38), and the derivatives indicated are now with respect to **x**. Inserting Eq. (2.39) into Eq. (2.5c) then yields

$$\begin{aligned}\varepsilon_{ij} &= -\frac{1}{2}\left(\left\langle G_{iq}\right\rangle_{,kj}+\left\langle G_{jq}\right\rangle_{,ki}\right)C_{qklm}\varepsilon^{*}_{lm}+\frac{L^2}{2}\left(\left\langle G_{iq}\right\rangle_{,kpj}+\left\langle G_{jq}\right\rangle_{,kpi}\right)C_{qklm}\kappa^{*}_{lmp} \\ &\equiv S_{ijlm}\varepsilon^{*}_{lm}+T_{ijlmp}\kappa^{*}_{lmp}\end{aligned} \tag{2.40}$$

as the actual (disturbance) strain, ε_{ij}, induced by the presence of the eigenstrain, ε^{*}_{lm}, and the eigenstrain gradient, κ^{*}_{lmp}, where

$$S_{ijlm} \equiv -\frac{1}{2}\left(\left\langle G_{iq}\right\rangle_{,kj}+\left\langle G_{jq}\right\rangle_{,ki}\right)C_{qklm}, \quad T_{ijlmp} \equiv \frac{L^2}{2}\left(\left\langle G_{iq}\right\rangle_{,kpj}+\left\langle G_{jq}\right\rangle_{,kpi}\right)C_{qklm}. \tag{2.41a,b}$$

Clearly, Eq. (2.40) shows that ε_{ij} is solely related to ε^{*}_{lm} in the absence of κ^{*}_{lmp}, and ε_{ij} is linked to only κ^{*}_{lmp} if $\varepsilon^{*}_{lm} = 0$.

The fourth-order tensor S_{ijlm} defined in Eqs. (2.40) and (2.41a) is known as the Eshelby tensor. Since ε_{ij} and ε^{*}_{ij} are both symmetric, S_{ijlm} satisfies $S_{ijlm} = S_{ijml} = S_{jilm}$ (a minor symmetry rather than the major symmetry that requires $S_{ijmn} = S_{mnij}$ additionally) and therefore has 36 independent components. From Eqs. (2.28), (2.29), (2.38) and (2.41a) it then follows that

$$\begin{aligned}S_{ijlm} &= -\frac{1}{8\pi\mu}\left[\Lambda_{,kj}\delta_{iq}+\Lambda_{,ki}\delta_{jq}-\frac{1}{2(1-\nu)}\Phi_{,ijkq}\right]C_{qklm} \\ &\quad +\frac{1}{8\pi\mu(1-\nu)}\left[(1-\nu)(\Gamma_{,kj}\delta_{iq}+\Gamma_{,ki}\delta_{jq})+L^2(\Lambda-\Gamma)_{,ijkq}\right]C_{qklm},\end{aligned} \tag{2.42}$$

where

$$\Phi(\mathbf{x}) \equiv \left\langle |\mathbf{x}-\mathbf{y}| \right\rangle, \qquad \Lambda(\mathbf{x}) \equiv \left\langle \frac{1}{|\mathbf{x}-\mathbf{y}|} \right\rangle, \qquad \Gamma(\mathbf{x}) \equiv \left\langle \frac{e^{-\frac{|\mathbf{x}-\mathbf{y}|}{L}}}{|\mathbf{x}-\mathbf{y}|} \right\rangle \tag{2.43a–c}$$

are three scalar-valued functions that can be obtained analytically or numerically by evaluating the volume integrals. Clearly, among these three functions only $\Gamma(\mathbf{x})$ depends on the length scale parameter L. As a result, the Eshelby tensor given in Eq. (2.42) can be

separated into the classical part, S^C_{ijlm}, which is independent of the material length scale parameter L, and the gradient part, S^G_{ijlm}, which depends on L, thereby being microstructure-dependent. Accordingly, the general form of the Eshelby tensor in the SSGET derived in Eq. (2.42) for an inclusion of arbitrary shape can be rewritten as

$$\begin{aligned} S_{ijlm} &= S^C_{ijlm} + S^G_{ijlm}, \\ S^C_{ijlm} &= -\frac{1}{8\pi\mu}\left[\Lambda_{,kj}\delta_{iq} + \Lambda_{,ki}\delta_{jq} - \frac{1}{2(1-\nu)}\Phi_{,ijkq}\right]C_{qklm}, \\ S^G_{ijlm} &= \frac{1}{8\pi\mu(1-\nu)}\left[(1-\nu)(\Gamma_{,kj}\delta_{iq} + \Gamma_{,ki}\delta_{jq}) + L^2(\Lambda-\Gamma)_{,ijkq}\right]C_{qklm}, \end{aligned} \tag{2.44a–c}$$

where the scalar-valued functions $\Lambda(\mathbf{x})$, $\Phi(\mathbf{x})$ and $\Gamma(\mathbf{x})$ are defined in Eq. (2.43) along with Eq. (2.38). Clearly, when $L = 0$ (i.e., when the strain gradient effect is ignored), Eqs. (2.43) and (2.44a–c) show that $S^G_{ijlm} = 0$ and $S_{ijlm} = S^C_{ijlm}$. That is, the Eshelby tensor obtained in Eqs. (2.44a–c) using the SSGET reduces to that based on classical elasticity.

The fifth-order Eshelby-like tensor T_{ijlmp} defined in Eqs. (2.40) and (2.41b) links the eigenstrain gradient, κ^*_{lmp}, to the actual (induced) strain, ε_{ij}. Since ε_{ij} is symmetric and $\kappa^*_{lmp} = \kappa^*_{mlp}$, T_{ijlmp} satisfies $T_{ijlmp} = T_{ijmlp} = T_{jilmp}$ and therefore has 108 independent components (as opposed to $3^5 = 243$ such components). From Eqs. (2.28), (2.29), (2.38) and (2.41b) it follows that

$$T_{ijlmp} = \frac{L^2}{32\pi\mu(1-\nu)}\left\{4(1-\nu)\left[(\Lambda-\Gamma)_{,kpj}\delta_{iq} + (\Lambda-\Gamma)_{,kpi}\delta_{jq}\right] - 2\left[\Phi + 2L^2(\Lambda-\Gamma)\right]_{,ijkpq}\right\}C_{qklm} \tag{2.45}$$

as the expression of the fifth-order tensor, with the scalar-valued functions $\Lambda(\mathbf{x})$, $\Phi(\mathbf{x})$ and $\Gamma(\mathbf{x})$ defined in Eq. (2.43) along with Eq. (2.38). Clearly, T_{ijlmp} has only the gradient part and vanishes when $L = 0$ (i.e., when the strain gradient effect is not considered). In fact, in this special case without the microstructural effect (i.e., $L = 0$), both S^G_{ijlm} and T_{ijlmp} vanish,

and Eq. (2.40) simply becomes $\varepsilon_{ij} = S^C_{ijlm}\varepsilon^*_{ij}$, the defining relation for the Eshelby tensor based on classical elasticity (Eshelby, 1957), as expected.

It can be shown that $\Lambda(\mathbf{x})$, $\Phi(\mathbf{x})$ and $\Gamma(\mathbf{x})$ defined in Eqs. (2.43a–c) satisfy the following relations (see Appendix C):

$$\Phi_{,ijkk} = 2\Lambda_{,ij}, \quad \Gamma_{,ijkk} = \frac{1}{L^2}\Gamma_{,ij}, \quad \nabla^2\Lambda(\mathbf{x}) = \begin{cases} -4\pi, & \mathbf{x} \in \Omega, \\ 0, & \mathbf{x} \notin \Omega, \end{cases} \tag{2.46a–c}$$

By using Eqs. (2.46a–c) and (2.26), the Eshelby tensor in Eqs. (2.44b,c) can be further simplified as

$$S^C_{ijlm} = -\frac{1}{8\pi(1-2\nu)(1-\nu)}\left[2\nu(1-2\nu)\Lambda_{,ij}\delta_{lm} + (1-\nu)(1-2\nu)(\Lambda_{,mj}\delta_{il} + \Lambda_{,lj}\delta_{im} + \Lambda_{,mi}\delta_{jl} + \Lambda_{,li}\delta_{jm}) - (1-2\nu)\Phi_{,ijlm}\right], \tag{2.47a}$$

$$S^G_{ijlm} = \frac{1}{8\pi(1-\nu)}\left[2\nu\Gamma_{,ij}\delta_{lm} + (1-\nu)(\Gamma_{,jm}\delta_{il} + \Gamma_{,im}\delta_{jl} + \Gamma_{,jl}\delta_{im} + \Gamma_{,il}\delta_{jm}) - 2L^2\Gamma_{,ijlm} + 2L^2\Lambda_{,ijlm}\right]. \tag{2.47b}$$

and the Eshelby-like tensor in Eq. (2.45) can be simplified as

$$T_{ijlmp} = \frac{L^2}{8\pi(1-\nu)}\left[2\nu\Psi_{,ijp}\delta_{lm} + (1-\nu)(\Psi_{,mpj}\delta_{il} + \Psi_{,mpi}\delta_{jl} + \Psi_{,lpj}\delta_{im} + \Psi_{,lpi}\delta_{jm}) - \Pi_{,ijlmp}\right], \tag{2.48}$$

where

$$\Psi(\mathbf{x}) \equiv \Lambda - \Gamma, \quad \Pi(\mathbf{x}) \equiv \Phi + 2L^2(\Lambda - \Gamma). \tag{2.49}$$

Note that in Eqs. (2.47a,b) and (2.48), ν is the Poisson's ratio, which is related to the Lamé constants λ and μ through (e.g., Timoshenko and Goodier, 1970)

$$\lambda = \frac{E\nu}{(1+\nu)(1-2\nu)}, \quad \mu = \frac{E}{2(1+\nu)}, \tag{2.50}$$

where E is Young's modulus.

2.5. Conclusion

The Eshelby-type inclusion problem is solved analytically by using the SSGET. This is accomplished by first deriving the Green's function in the SSGET in terms of

elementary functions using Fourier transforms. The resulting Green's function reduces to that in classical elasticity when the strain gradient effect is ignored. The Eshelby tensor is then obtained in a general form for an inclusion of arbitrary shape using the Green's function method. The newly derived Eshelby tensor consists of two parts: a classical part depending only on Poisson's ratio and the shape of the inclusion, and a gradient part involving the length scale parameter and depending on the size of the inclusion additionally. The classical part is identical to the Eshelby tensor based the classical elasticity theory; while the gradient part vanishes when the strain gradient effect is not considered.

CHAPTER III

ESHELBY TENSOR FOR A SPHERICAL INCLUSION

3.1. Introduction

The Eshelby inclusion problem of a spherical inclusion embedded in an infinite homogeneous isotropic elastic medium is of great importance due to its direct relation to particle-reinforced composites (e.g., Weng, 1984; Gao, 2008). Therefore, in this chapter, the Eshelby tensor for the spherical inclusion problem based on the simplified strain gradient elasticity theory (SSGET) will be derived by directly applying the general formulas obtained in Chapter II.

The rest of this chapter is organized as follows. In Section 3.2, the explicit expressions of the Eshelby tensor are obtained for the spherical inclusion problem by directly applying the general form of the Eshelby tensor derived in Chapter II. This specific Eshelby tensor is found to be position-dependent even inside the inclusion, unlike its counterpart based on classical elasticity. For homogenization applications, the volume average of this Eshelby tensor over the spherical inclusion is analytically determined. Sample numerical results are provided in Section 3.3 to illustrate the newly developed Eshelby tensor for the spherical inclusion problem. This chapter concludes in Section 3.4.

3.2. Eshelby Tensor for a Spherical Inclusion

Consider a spherical inclusion of radius R and centered at the origin of the Cartesian coordinate system (x_1, x_2, x_3) in the physical space. In this case, the three volume integrals defined in Eq. (2.43) along with Eq. (2.38) can be exactly evaluated to obtain the following

closed-form expressions:

$$\Phi(x)=\begin{cases}-\dfrac{\pi}{15}x^4+\dfrac{2\pi}{3}R^2x^2+\pi R^4, & \mathbf{x}\in\Omega,\\ \dfrac{4\pi}{15}\dfrac{R^5}{x}+\dfrac{4\pi}{3}R^3x, & \mathbf{x}\notin\Omega;\end{cases} \tag{3.1a,b}$$

$$\Lambda(x)=\begin{cases}-\dfrac{2\pi}{3}x^2+2\pi R^2, & \mathbf{x}\in\Omega,\\ \dfrac{4\pi}{3}\dfrac{R^3}{x}, & \mathbf{x}\notin\Omega;\end{cases} \tag{3.1c,d}$$

$$\Gamma(x)=\begin{cases}4\pi L^2-4\pi L^2(L+R)e^{-\frac{R}{L}}\dfrac{1}{x}\sinh\left(\dfrac{x}{L}\right), & \mathbf{x}\in\Omega,\\ \dfrac{-4\pi L^3}{x}\left[\sinh\left(\dfrac{R}{L}\right)-\dfrac{R}{L}\cosh\left(\dfrac{R}{L}\right)\right]e^{-\frac{x}{L}}, & \mathbf{x}\notin\Omega.\end{cases} \tag{3.1e,f}$$

Note that in Eqs. (3.1a–f), $x\equiv|\mathbf{x}|=(x_k x_k)^{1/2}$, as defined earlier in Section 2.3. Note that $\Phi(x)$, $\Lambda(x)$ and $\Gamma(x)$ in Eqs. (3.1a–f) are independent on the direction of position vector $\mathbf{x}$ due to the spherical symmetry of the inclusion. These expressions can be readily shown to be equivalent to those provided by Cheng and He (1995) and Zheng and Zhao (2004), where different definitions and notation were used for the three scalar-valued functions. Clearly, $\Phi(x)$, $\Lambda(x)$ or $\Gamma(x)$ given in Eqs. (3.1a–f) are infinitely differentiable at any $x\neq 0$.

The general forms of the Eshelby tensor $\mathbf{S}$ and the Eshelby gradient tensor $\mathbf{T}$, given in Eqs. (2.44a-c) and Eq. (2.45), respectively, are expressed in terms of the derivatives of $\Phi(x)$, $\Lambda(x)$ and $\Gamma(x)$ with respect to x_i. To facilitate the differentiation of these three functions, the following differential relations are given for a sufficiently smooth function $F(x)$.

$$
\begin{aligned}
&F_{,i} = x_i D_1 F,\\
&F_{,ij} = x_i x_j D_2 F + \delta_{ij} D_1 F,\\
&F_{,ijk} = x_i x_j x_k D_3 F + \left\langle \delta_{ij} x_k \right\rangle_3 D_2 F,\\
&F_{,ijkl} = x_i x_j x_k x_l D_4 F + \left\langle \delta_{ij} x_k x_l \right\rangle_6 D_3 F + \left\langle \delta_{ij} \delta_{kl} \right\rangle_3 D_2 F,\\
&F_{,ijmm} = x^2 x_i x_j D_4 F + \left(x^2 \delta_{ij} + 7 x_i x_j\right) D_3 F + 5\delta_{ij} D_2 F,\\
&F_{,ijklm} = x_i x_j x_k x_l x_m D_5 F + \left\langle \delta_{ij} x_k x_l x_m \right\rangle_{10} D_4 F + \left\langle \delta_{ij} \delta_{kl} x_m \right\rangle_{15} D_3 F,\\
&F_{,ijkkm} = x_i x_j x_m x^2 D_5 F + \left(x^2 \left\langle \delta_{ij} x_m \right\rangle_3 + 9 x_i x_j x_m\right) D_4 F + 7 \left\langle \delta_{ij} x_m \right\rangle_3 D_3 F,
\end{aligned}
\tag{3.2}
$$

where

$$
\left.
\begin{gathered}
D_1 F = \frac{F'}{x}, \quad D_2 F = \frac{1}{x^2}\left(F'' - \frac{F'}{x}\right), \quad D_3 F = \frac{1}{x^3}\left(F''' - \frac{3F''}{x} + \frac{3F'}{x^2}\right),\\
D_4 F = \frac{1}{x^4}\left[F^{(4)} - \frac{6F'''}{x} + \frac{15F''}{x^2} - \frac{15F'}{x^3}\right],\\
D_5 F = \frac{1}{x^5}\left[F^{(5)} - \frac{10F^{(4)}}{x} + \frac{45F^{(3)}}{x^2} - \frac{105F''}{x^3} + \frac{105F'}{x^4}\right],\\
\left\langle \delta_{ij} x_k \right\rangle_3 \equiv \delta_{ij} x_k + \delta_{kj} x_i + \delta_{ik} x_j,\\
\left\langle \delta_{ij} x_k x_l \right\rangle_6 \equiv \delta_{ij} x_k x_l + \delta_{kl} x_i x_j + \delta_{jl} x_i x_k + \delta_{jk} x_i x_l + \delta_{il} x_j x_k + \delta_{ik} x_j x_l,\\
\left\langle \delta_{ij} x_k x_l x_m \right\rangle_{10} \equiv \delta_{ij} x_k x_l x_m + \delta_{ik} x_j x_l x_m + \delta_{il} x_k x_j x_m + \delta_{im} x_k x_l x_j + \delta_{jk} x_i x_l x_m + \delta_{jl} x_k x_i x_m\\
+ \delta_{jm} x_k x_l x_i + \delta_{kl} x_i x_j x_m + \delta_{km} x_i x_l x_j + \delta_{lm} x_k x_i x_j,\\
\left\langle \delta_{ij} \delta_{kl} x_m \right\rangle_{15} \equiv (\delta_{ij}\delta_{kl} + \delta_{ik}\delta_{jl} + \delta_{il}\delta_{jk}) x_m + (\delta_{ij}\delta_{lm} + \delta_{im}\delta_{jl} + \delta_{il}\delta_{jm}) x_k + (\delta_{ij}\delta_{km} + \delta_{ik}\delta_{jm} + \delta_{im}\delta_{jk}) x_l\\
+ (\delta_{jm}\delta_{kl} + \delta_{jk}\delta_{ml} + \delta_{jl}\delta_{mk}) x_i + (\delta_{im}\delta_{kl} + \delta_{ik}\delta_{ml} + \delta_{il}\delta_{mk}) x_j,\\
\left\langle \delta_{ij} \delta_{kl} \right\rangle_3 \equiv \delta_{ij}\delta_{kl} + \delta_{ik}\delta_{jl} + \delta_{il}\delta_{jk}.
\end{gathered}
\right\}
\tag{3.3}
$$

In Eq. (3.3) $F' = \mathrm{d}F/\mathrm{d}x$, $F'' = \mathrm{d}^2F/\mathrm{d}x^2$, $F''' = \mathrm{d}^3F/\mathrm{d}x^3$, $F^{(4)} = \mathrm{d}^4F/\mathrm{d}x^4$, and $F^{(5)} = \mathrm{d}^5F/\mathrm{d}x^5$, as usual. Also, in Eqs. (3.2) and (3.3) F can be replaced by $\Phi(x)$, $\Lambda(x)$ or $\Gamma(x)$ involved in Eqs. (2.44a–c) and Eq. (2.45).

Using Eqs. (2.6), (3.2) and (3.3) in Eq. (2.44b) leads to

$$
\begin{aligned}
S^C_{ijlm} = {} & K^C_1(x)\,\delta_{ij}\delta_{lm} + K^C_2(x)\,(\delta_{il}\delta_{jm} + \delta_{im}\delta_{jl}) + K^C_3(x)\delta_{lm}x^0_i x^0_j + K^C_4(x)\delta_{ij}x^0_l x^0_m\\
& + K^C_5(x)(\delta_{il}x^0_j x^0_m + \delta_{im}x^0_j x^0_l + \delta_{jl}x^0_i x^0_m + \delta_{jm}x^0_i x^0_l) + K^C_6(x)(x^0_i x^0_j x^0_l x^0_m),
\end{aligned}
\tag{3.4}
$$

where

$$
K^C_1(x) = \frac{1}{8\pi(1-\nu)(1-2\nu)}\left[-4\nu(1-\nu)D_1\Lambda + \nu x^2 D_3\Phi + (1+3\nu)D_2\Phi\right],
\tag{3.5a}
$$

$$K_2^C(x) = \frac{1}{8\pi(1-\nu)}\left[-2(1-\nu)\, D_1\Lambda + D_2\Phi\right], \tag{3.5b}$$

$$K_3^C = \frac{x^2}{8\pi(1-\nu)(1-2\nu)}\left[-4\nu(1-\nu)D_2\Lambda + \nu x^2 D_4\Phi + (1+5\nu)D_3\Phi\right], \tag{3.5c}$$

$$K_4^C = \frac{x^2}{8\pi(1-\nu)} D_3\Phi, \tag{3.5d}$$

$$K_5^C = \frac{x^2}{8\pi(1-\nu)}\left[-(1-\nu)D_2\Lambda + D_3\Phi\right], \tag{3.5e}$$

$$K_6^C = \frac{x^4}{8\pi(1-\nu)} D_4\Phi. \tag{3.5f}$$

It is seen from Eqs. (3.4) and (3.5a–f) that S_{ijlm}^C depends only on one material constant (i.e., Poisson's ratio ν) even for this spherical inclusion. Similarly, applying Eqs. (2.6), (3.2) and (3.3) to Eq. (2.44c) results in

$$\begin{aligned} S_{ijlm}^G = {} & K_1^G(x)\,\delta_{ij}\delta_{lm} + K_2^G(x)(\delta_{il}\delta_{jm} + \delta_{im}\delta_{jl}) + K_3^G(x)\delta_{lm}x_i^0x_j^0 + K_4^G(x)\delta_{ij}x_l^0x_m^0 \\ & + K_5^G(x)(\delta_{il}x_j^0x_m^0 + \delta_{im}x_j^0x_l^0 + \delta_{jl}x_i^0x_m^0 + \delta_{jm}x_i^0x_l^0) + K_6^G(x)(x_i^0x_j^0x_l^0x_m^0), \end{aligned} \tag{3.6}$$

where

$$K_1^G = \frac{1}{4\pi(1-\nu)}\left[\frac{2\nu(1-\nu)}{1-2\nu} D_1\Gamma - \frac{\nu}{1-2\nu} L^2x^2 D_3(\Gamma-\Lambda) - \frac{1+3\nu}{1-2\nu} L^2 D_2(\Gamma-\Lambda)\right], \tag{3.7a}$$

$$K_2^G = \frac{1}{4\pi(1-\nu)}\left[(1-\nu)\, D_1\Gamma - L^2 D_2(\Gamma-\Lambda)\right], \tag{3.7b}$$

$$K_3^G = \frac{x^2}{4\pi(1-\nu)}\left[\frac{2\nu(1-\nu)}{1-2\nu} D_2\Gamma - \frac{\nu}{1-2\nu} L^2x^2 D_4(\Gamma-\Lambda) - \frac{1+5\nu}{1-2\nu} L^2 D_3(\Gamma-\Lambda)\right], \tag{3.7c}$$

$$K_4^G = -\frac{L^2x^2}{4\pi(1-\nu)} D_3(\Gamma-\Lambda), \tag{3.7d}$$

$$K_5^G = \frac{x^2}{8\pi(1-\nu)}\left[(1-\nu)D_2\Gamma - 2\, L^2 D_3(\Gamma-\Lambda)\right], \tag{3.7e}$$

$$K_6^G = -\frac{L^2x^4}{4\pi(1-\nu)} D_4(\Gamma-\Lambda). \tag{3.7f}$$

Clearly, Eqs. (3.6) and (3.7a–f) show that S_{ijlm}^G depends not only on Poisson's ratio ν but also on the material length scale parameter L, unlike S_{ijlm}^C given in Eqs. (3.4) and (3.5a–f). Finally, the use of Eqs. (2.6), (3.2) and (3.3) in Eq. (2.45) yields

$$
\begin{aligned}
T_{ijlmp} = \frac{L^2}{8\pi(1-\nu)}\Bigg\{ & -\frac{4\nu(1-\nu)}{1-2\nu}\delta_{lm}\Big[x_i x_j x_p D_3(\Gamma-\Lambda) + \langle x_p\delta_{ij}\rangle_3 D_2(\Gamma-\Lambda)\Big] \\
& -(1-\nu)(x_i x_m x_p \delta_{jl} + x_j x_m x_p \delta_{il} + x_i x_l x_p \delta_{jm} + x_j x_l x_p \delta_{im}) D_3(\Gamma-\Lambda) \\
& -(1-\nu)(\langle x_i\delta_{mp}\rangle_3 \delta_{jl} + \langle x_j\delta_{mp}\rangle_3 \delta_{il} + \langle x_i\delta_{lp}\rangle_3 \delta_{jm} + \langle x_j\delta_{lp}\rangle_3 \delta_{im}) D_2(\Gamma-\Lambda) \\
& +\frac{2\nu L^2}{1-2\nu}\delta_{lm}\Big[x_i x_j x_p x^2 D_5(\Gamma-\Lambda-\frac{\Phi}{2L^2}) + (x^2\langle x_p\delta_{ij}\rangle_3 + 9x_i x_j x_p) D_4(\Gamma-\Lambda-\frac{\Phi}{2L^2}) \\
& +7\langle x_p\delta_{ij}\rangle_3 D_3(\Gamma-\Lambda-\frac{\Phi}{2L^2})\Big] + 2L^2\Big[x_i x_j x_l x_m x_p D_5(\Gamma-\Lambda-\frac{\Phi}{2L^2}) \\
& +\langle \delta_{ij} x_l x_m x_p\rangle_{10} D_4(\Gamma-\Lambda-\frac{\Phi}{2L^2}) + \langle \delta_{ij}\delta_{lm} x_p\rangle_{15} D_3(\Gamma-\Lambda-\frac{\Phi}{2L^2})\Big]\Bigg\}.
\end{aligned}
\tag{3.8}
$$

Then, it follows from Eqs. (3.1a,c,e), (3.3), (3.4) and (3.5a–f) that the classical part of the Eshelby tensor for the interior case with **x** locating inside the spherical inclusion (i.e., **x** $\in$ Ω or $x < R$) is

$$
S^C_{ijlm} = \frac{5\nu-1}{15(1-\nu)}\delta_{ij}\delta_{lm} + \frac{4-5\nu}{15(1-\nu)}(\delta_{il}\delta_{jm} + \delta_{im}\delta_{jl}). \tag{3.9}
$$

Next, using Eqs. (3.1a,c,e) and (3.3) leads to

$$
\begin{aligned}
& D_1\Lambda = -\frac{4}{3}\pi, \quad D_2\Lambda = D_3\Lambda = D_4\Lambda = 0, \\
& D_1\Phi = \frac{4}{15}\pi(-x^2+5R^2), \quad D_2\Phi = -\frac{8}{15}\pi, \quad D_3\Phi = D_4\Phi = 0, \\
& D_1\Gamma = -\frac{4\pi L(L+R)e^{-\frac{R}{L}}}{x^3}\left[x\cosh\left(\frac{x}{L}\right) - L\sinh\left(\frac{x}{L}\right)\right], \\
& D_2\Gamma = -\frac{4\pi(L+R)e^{-\frac{R}{L}}}{x^5}\left[-3Lx\cosh\left(\frac{x}{L}\right) + (x^2+3L^2)\sinh\left(\frac{x}{L}\right)\right], \\
& D_3\Gamma = -\frac{4\pi(L+R)e^{-\frac{R}{L}}}{Lx^7}\left[x(x^2+15L^2)\cosh\left(\frac{x}{L}\right) - 3L(2x^2+5L^2)\sinh\left(\frac{x}{L}\right)\right], \\
& D_4\Gamma = -\frac{4\pi(L+R)e^{-\frac{R}{L}}}{L^2x^9}\left[-5Lx(2x^2+21L^2)\cosh\left(\frac{x}{L}\right) + (x^4+45L^2x^2+105L^4)\sinh\left(\frac{x}{L}\right)\right], \\
& D_5\Gamma = -\frac{4\pi(L+R)e^{-\frac{R}{L}}}{L^3x^{11}}\left[(x^5+105L^2x^3+945L^4x)\cosh\left(\frac{x}{L}\right) - 15L(x^4+28L^2x^2+63L^4)\sinh\left(\frac{x}{L}\right)\right]
\end{aligned}
\tag{3.10}
$$

for any interior point **x** $\in$ Ω (or $x < R$). Substituting Eq. (3.10) into Eqs. (3.6) and (3.7a–f) will then give the closed-form expression of the gradient part of the Eshelby tensor for the

interior case with **x** locating inside the spherical inclusion. Similarly, the use of Eq. (3.10) in Eq. (3.8) will yield the explicit formula for determining T_{ijlmp} at any **x** inside the spherical inclusion (i.e., $\mathbf{x} \in \Omega$ or $x < R$).

Note that Eq. (3.9) clearly shows that for the spherical inclusion considered here the classical part of the Eshelby tensor, S^C_{ijlm}, is uniform inside the inclusion, independent of L, R and x. In fact, S^C_{ijlm} listed in Eq. (3.9) is identical to that based on classical elasticity (see, e.g., Equation (3.123) in Li and Wang, (2008)). In contrast, the gradient part, S^G_{ijlm}, given in Eqs. (3.6), (3.7a–f) and (3.10) depends on L, R and x in a complicated manner, and is therefore non-uniform inside the spherical inclusion and differs for different materials (with distinct values of L) and inclusion sizes (with distinct values of R). However, if the strain gradient effect is ignored, then $L = 0$ and Eqs. (3.6), (3.7a–f) and (3.10) give $S^G_{ijlm} = 0$. It thus follows from Eq. (2.44a) that $S_{ijlm} = S^C_{ijlm}$. That is, the Eshelby tensor for the spherical inclusion derived here using the SSGET reduces to that based on classical elasticity when $L = 0$.

Considering that S^G_{ijlm} is position-dependent inside the spherical inclusion, its volume average over the spherical region occupied by the inclusion is examined next. This averaged Eshelby tensor is needed for predicting the effective elastic properties of a heterogeneous composite containing spherical inclusions. The volume average of a sufficiently smooth function $F(\mathbf{x})$ over the spherical inclusion occupying region Ω is defined by

$$\langle F \rangle_{\mathrm{V}} = \frac{1}{\mathrm{Vol}(\Omega)} \iiint_{\Omega} F dV = \frac{1}{4\pi R^3/3} \int_0^R \int_0^{2\pi} \int_0^{\pi} F x^2 \sin\theta d\theta d\varphi dx, \tag{3.11}$$

where use has been made of the volume element $dV = x^2 \sin\theta \, d\theta \, d\varphi \, dx$ in a spherical

coordinate system. Letting S^G_{ijlm} given in Eqs. (3.6) and (3.7a–f) be $F(\mathbf{x})$ in Eq. (3.11) will lead to $\langle S^G_{ijlm}\rangle_{\mathrm{V}}$.

Note that in the spherical coordinate system adopted here,

$$x^0_1 = \sin\theta\cos\varphi, \qquad x^0_2 = \sin\theta\sin\varphi, \qquad x^0_3 = \cos\theta. \tag{3.12}$$

It then follows from Eq. (3.12) that

$$\begin{aligned}
&\int_0^{2\pi}\int_0^{\pi} x^0_i x^0_j \sin\theta\, d\theta\, d\varphi = \frac{4}{3}\pi\,\delta_{ij},\\
&\int_0^{2\pi}\int_0^{\pi} (\delta_{il}x^0_j x^0_m + \delta_{im}x^0_j x^0_l + \delta_{jl}x^0_i x^0_m + \delta_{jm}x^0_i x^0_l)\sin\theta\, d\theta\, d\varphi = \frac{8}{3}\pi\,(\delta_{il}\delta_{jm} + \delta_{im}\delta_{jl}),\\
&\int_0^{2\pi}\int_0^{\pi} (x^0_i x^0_j x^0_l x^0_m)\sin\theta\, d\theta\, d\varphi = \frac{4}{15}\pi\,(\delta_{ij}\delta_{lm} + \delta_{il}\delta_{jm} + \delta_{im}\delta_{jl}).
\end{aligned} \tag{3.13}$$

Using Eqs. (3.13) and (3.6) in Eq. (3.11) then gives

$$\langle S^G_{ijlm}\rangle_{\mathrm{V}} = \frac{1}{R^3}\left[\left(3\overline{K^G_1} + \overline{K^G_3} + \overline{K^G_4} + \frac{1}{5}\overline{K^G_6}\right)\delta_{ij}\delta_{lm} + \left(3\overline{K^G_2} + 2\overline{K^G_5} + \frac{1}{5}\overline{K^G_6}\right)(\delta_{il}\delta_{jm} + \delta_{im}\delta_{jl})\right], \tag{3.14}$$

where

$$\overline{K^G_n} \equiv \int_0^R x^2 K^G_n(x)\, dx, \tag{3.15}$$

with K^G_n (n = 1, 2, …, 6) to be substituted from Eqs. (3.7a–f) and (3.10). The six integrals in Eq. (3.15) can be exactly evaluated, and Eq. (3.14) becomes

$$\langle S^G_{ijlm}\rangle_{\mathrm{V}} = \frac{1}{10(1-\nu)}\left(\frac{L}{R}\right)^3\left[1-\left(\frac{R}{L}\right)^2 - \left(1+\frac{R}{L}\right)^2 e^{-\frac{2R}{L}}\right]\left[(5\nu-1)\delta_{ij}\delta_{lm} + (4-5\nu)(\delta_{il}\delta_{jm} + \delta_{im}\delta_{jl})\right], \tag{3.16}$$

which gives

$$\langle S^G_{1111}\rangle_{\mathrm{V}} = \frac{7-5\nu}{10(1-\nu)}\left(\frac{L}{R}\right)^3\left[1-\left(\frac{R}{L}\right)^2 - \left(1+\frac{R}{L}\right)^2 e^{-\frac{2R}{L}}\right] = \langle S^G_{2222}\rangle_{\mathrm{V}} = \langle S^G_{3333}\rangle_{\mathrm{V}},$$

$$\langle S^G_{1122}\rangle_{\mathrm{V}} = \frac{5\nu-1}{10(1-\nu)}\left(\frac{L}{R}\right)^3\left[1-\left(\frac{R}{L}\right)^2 - \left(1+\frac{R}{L}\right)^2 e^{-\frac{2R}{L}}\right] = \langle S^G_{1133}\rangle_{\mathrm{V}} = \langle S^G_{2233}\rangle_{\mathrm{V}} = \langle S^G_{2211}\rangle_{\mathrm{V}} = \langle S^G_{3311}\rangle_{\mathrm{V}} = \langle S^G_{3322}\rangle_{\mathrm{V}},$$

$$\left\langle S^G_{1212}\right\rangle_{\mathrm{V}} = \frac{4-5\nu}{10(1-\nu)}\left(\frac{L}{R}\right)^3\left[1-\left(\frac{R}{L}\right)^2-\left(1+\frac{R}{L}\right)^2 e^{-\frac{2R}{L}}\right] = \left\langle S^G_{2323}\right\rangle_{\mathrm{V}} = \left\langle S^G_{3131}\right\rangle_{\mathrm{V}} \qquad (3.17\text{a–c})$$

as the 12 non-vanishing, volume-averaged components of the gradient part of the Eshelby tensor inside the inclusion. Clearly, these components are constants, but they depend on the inclusion size, R, the length scale parameter, L, and Poisson's ratio, ν, of the material. This differs from the components of the classical part of the Eshelby tensor inside the inclusion, which, as given in Eq. (3.9), are constants depending only on ν. However, when $L = 0$ (or $R/L \to \infty$), Eq. (3.17a–c) shows that all non-zero components of $\left\langle S^G_{ijlm}\right\rangle_{\mathrm{V}}$ will vanish, as will be further illustrated in the next section.

By following the same procedure, the volume average of the classical part of the Eshelby tensor inside the inclusion, $\left\langle S^C_{ijlm}\right\rangle_{\mathrm{V}}$, can also be obtained using Eqs. (3.9) and (3.11). Since S^C_{ijlm} is uniform inside the inclusion, there will be $\left\langle S^C_{ijlm}\right\rangle_{\mathrm{V}} = S^C_{ijlm}$. It then follows from Eqs. (2.6), (3.11), (3.9) and (3.16) that

$$\left\langle S_{ijlm}\right\rangle_{\mathrm{V}} = \frac{1}{15(1-\nu)}\left\{1+\frac{3}{2}\left(\frac{L}{R}\right)^3\left[1-\left(\frac{R}{L}\right)^2-\left(1+\frac{R}{L}\right)^2 e^{-\frac{2R}{L}}\right]\right\}\left[(5\nu-1)\delta_{ij}\delta_{lm}+(4-5\nu)(\delta_{il}\delta_{jm}+\delta_{im}\delta_{jl})\right] \qquad (3.18)$$

as the volume average of the Eshelby tensor inside the spherical inclusion based on the SSGET. Clearly, when $L = 0$ (or $R/L \to \infty$), Eq. (3.18) reduces to $\left\langle S^C_{ijlm}\right\rangle_{\mathrm{V}} = S^C_{ijlm}$ given in Eq. (3.9).

The volume average of T_{ijlmp} for $\mathbf{x}$ locating inside the spherical inclusion (i.e., $\mathbf{x} \in \Omega$ or $x < R$) can be readily shown to vanish, i.e.,

$$\left\langle T_{ijlmp}\right\rangle_{\mathrm{V}} = \frac{1}{\mathrm{Vol}(\Omega)}\iiint_{\Omega} T_{ijlmp}\,dV = \frac{1}{4\,\pi\,R^3/3}\int_0^R\int_0^{2\pi}\int_0^{\pi} T_{ijlmp}\,x^2\sin\theta\,d\theta\,d\varphi\,dx \equiv 0. \qquad (3.19)$$

The reason for this is that T_{ijlmp} involved in Eq. (3.19) and to be substituted from Eqs. (3.8)

and (3.10) is odd in x_i^0, which makes the integration of T_{ijlmp} over any spherical surface vanish (e.g., Li et al. 2007).

Similarly, the Eshelby tensor for the exterior case with **x** locating outside the spherical inclusion (i.e., $\mathbf{x} \notin \Omega$ or $x > R$) can be determined by using Eqs. (3.1b,d,f) in the general formulas derived in Section 2.4 for an inclusion of arbitrary shape. Specifically, from Eqs. (3.3) and Eqs. (3.1b,d,f) it follows that

$$
\begin{aligned}
&D_1\Lambda = -\frac{4\pi}{3}\frac{R^3}{x^3}, \quad D_2\Lambda = \frac{4\pi R^3}{x^5}, \quad D_3\Lambda = -\frac{20\pi R^3}{x^7}, \quad D_4\Lambda = \frac{140\pi R^3}{x^9},\\
&D_1\Phi = -\frac{4\pi}{15}\frac{R^3}{x^3}(R^2 - 5x^2), \quad D_2\Phi = -\frac{4\pi}{15}\frac{R^3}{x^5}(-3R^2 + 5x^2),\\
&D_3\Phi = -\frac{4\pi R^3}{x^7}(R^2 - x^2), \quad D_4\Phi = -\frac{4\pi R^3}{x^9}(-7R^2 + 5x^2),\\
&D_1\Gamma = \frac{4\pi L^2\left[\sinh\left(\frac{R}{L}\right) - \frac{R}{L}\cosh\left(\frac{R}{L}\right)\right]}{x^3}\left(x + L\right)e^{-\frac{x}{L}},\\
&D_2\Gamma = -\frac{4\pi L\left[\sinh\left(\frac{R}{L}\right) - \frac{R}{L}\cosh\left(\frac{R}{L}\right)\right]}{x^5}\left(x^2 + 3Lx + 3L^2\right)e^{-\frac{x}{L}},\\
&D_3\Gamma = \frac{4\pi\left[\sinh\left(\frac{R}{L}\right) - \frac{R}{L}\cosh\left(\frac{R}{L}\right)\right]}{x^7}\left(x^3 + 6Lx^2 + 15L^2x + 15L^3\right)e^{-\frac{x}{L}},\\
&D_4\Gamma = -\frac{4\pi\left[\sinh\left(\frac{R}{L}\right) - \frac{R}{L}\cosh\left(\frac{R}{L}\right)\right]}{Lx^9}\left(x^4 + 10Lx^3 + 45L^2x^2 + 105L^3x + 105L^4\right)e^{-\frac{x}{L}},\\
&D_5\Gamma = \frac{4\pi\left[\sinh\left(\frac{R}{L}\right) - \frac{R}{L}\cosh\left(\frac{R}{L}\right)\right]}{L^2x^{11}}\left(x^5 + 15Lx^4 + 105L^2x^3 + 420L^3x^2 + 945L^4x + 945L^5\right)e^{-\frac{x}{L}}
\end{aligned}
\tag{3.20}
$$

for any exterior point $\mathbf{x} \notin \Omega$ (or $x > R$). Note that the functions listed in Eq. (3.20) for the exterior case with $\mathbf{x} \notin \Omega$ (or $x > R$) are clearly different from those defined in Eq. (3.10) for the interior case with $\mathbf{x} \in \Omega$ (or $x < R$). From Eqs. (3.20), (3.4) and (3.5a–f) the classical part of the Eshelby tensor for any **x** outside the spherical inclusion (i.e., $\mathbf{x} \in \Omega$ or $x < R$) is then obtained as

$$S^{C}_{ijlm} = \frac{R^3}{x^5(1-\nu)}\left\{\frac{1}{30}\left[-5(1-2\nu)x^2+3R^2\right]\delta_{ij}\delta_{lm}+\frac{1}{30}\left[5(1-2\nu)x^2+3R^2\right](\delta_{il}\delta_{jm}+\delta_{im}\delta_{jl})\right.$$
$$+\frac{1}{2}\left[(1-2\nu)x^2-R^2\right]\delta_{lm}x^0_i x^0_j-\frac{1}{2}\left(R^2-x^2\right)\delta_{ij}x^0_l x^0_m$$
$$\left.-\frac{1}{2}\left(R^2-\nu x^2\right)(\delta_{il}x^0_j x^0_m+\delta_{im}x^0_j x^0_l+\delta_{jl}x^0_i x^0_m+\delta_{jm}x^0_i x^0_l)-\frac{1}{2}\left(5x^2-7R^2\right)x^0_i x^0_j x^0_l x^0_m\right. . \tag{3.21}$$

It can be readily shown that the expression given in Eq. (3.21) is the same as that based on classical elasticity (e.g., Cheng and He, 1995). Clearly, a comparison of Eq. (3.21) with Eq. (3.9) shows that S^{C}_{ijlm} is not uniform outside the spherical inclusion, although it is uniform inside the same spherical inclusion.

Finally, using Eq. (3.20) in Eqs. (3.6) and (3.7a–f) will result in the explicit formula for determining S^{G}_{ijlm} at any exterior point $\mathbf{x} \notin \Omega$ (or $x > R$), and the substitution of Eq. (3.20) into Eq. (3.8) will lead to the closed-form expression for T_{ijlmp} at any point $\mathbf{x}$ locating outside the spherical inclusion.

3.3. Numerical Results

By using the closed-form expressions of the Eshelby tensor for the spherical inclusion derived in the preceding section, some numerical results are obtained and presented here to quantitatively illustrate how the components of the newly obtained Eshelby tensor vary with position and inclusion size.

From Eqs. (3.6), (3.7a–f) and (3.10), the components of the gradient part of the Eshelby tensor at any $\mathbf{x}$ inside the spherical inclusion along the x_1 axis (with $x_2 = 0 = x_3$) can be obtained as

$$S^{G}_{1111} = \frac{L+R}{x^5(1-\nu)}e^{-\frac{R}{L}}\left\{\left[-(1-\nu)x^4+2(\nu+4)x^2L^2+24L^4\right]\sinh\left(\frac{x}{L}\right)-2xL(\nu x^2+12L^2)\cosh\left(\frac{x}{L}\right)\right\},$$

$$S^G_{1122} = S^G_{1133} = \frac{L+R}{x^5(1-\nu)} e^{-\frac{R}{L}} \left\{ -\left[\nu x^4 + (2\nu+5)x^2L^2 + 12L^4\right]\sinh\left(\frac{x}{L}\right) + xL(x^2 + 2\nu x^2 + 12L^2)\cosh\left(\frac{x}{L}\right)\right\},$$

$$S^G_{1212} = S^G_{1313} = \frac{L+R}{2x^5(1-\nu)} e^{-\frac{R}{L}} \left\{ -\left[(1-\nu)x^4 + (11-\nu)x^2L^2 + 24L^4\right]\sinh\left(\frac{x}{L}\right) + xL\left[(3-\nu)x^2 + 24L^2\right]\cosh\left(\frac{x}{L}\right)\right\},$$

$$S^G_{2211} = S^G_{3311} = \frac{L(L+R)}{x^5(1-\nu)} e^{-\frac{R}{L}} \left\{ -L\left[(5-\nu)x^2 + 12L^2)\right]\sinh\left(\frac{x}{L}\right) + x\left[(1-\nu)x^2 + 12L^2)\right]\cosh\left(\frac{x}{L}\right)\right\},$$

$$S^G_{2222} = S^G_{3333} = -\frac{L(L+R)}{x^5(1-\nu)} e^{-\frac{R}{L}} \left\{ -L\left[(5-\nu)x^2 + 9L^2\right]\sinh\left(\frac{x}{L}\right) + x\left[(2-\nu)x^2 + 9L^2\right]\cosh\left(\frac{x}{L}\right)\right\},$$

$$S^G_{2233} = S^G_{3322} = \frac{L(L+R)}{x^5(1-\nu)} e^{-\frac{R}{L}} \left\{ L\left[(1+\nu)x^2 + 3L^2)\right]\sinh\left(\frac{x}{L}\right) - x(\nu x^2 + 3L^2)\cosh\left(\frac{x}{L}\right)\right]\right\},$$

$$S^G_{2323} = \frac{L(L+R)}{x^5(1-\nu)} e^{-\frac{R}{L}} \left\{ L\left[(2-\nu)x^2 + 3L^2\right]\sinh\left(\frac{x}{L}\right) - x\left[(1-\nu)x^2 + 3L^2)\right]\cosh\left(\frac{x}{L}\right)\right\}. \quad \text{(3.22a–g)}$$

Note that in this special case (with $x = x_1$, $x_2 = 0 = x_3$) there are only 12 non-zero components among the 36 independent components of S^G_{ijlm}.

In the numerical analysis, the Poisson's ratio ν is taken to be 0.3, and the material length scale parameter L to be 17.6 μm. Figure. 3.1 shows the distribution of $S_{1111} = S^C_{1111} + S^G_{1111}$ along the x_1 axis (or a radial direction of the inclusion due to the spherical symmetry) for five different values of the inclusion radius, where the values of S^C_{1111} and S^G_{1111} are, respectively, obtained from Eqs. (3.9) and (3.22a).

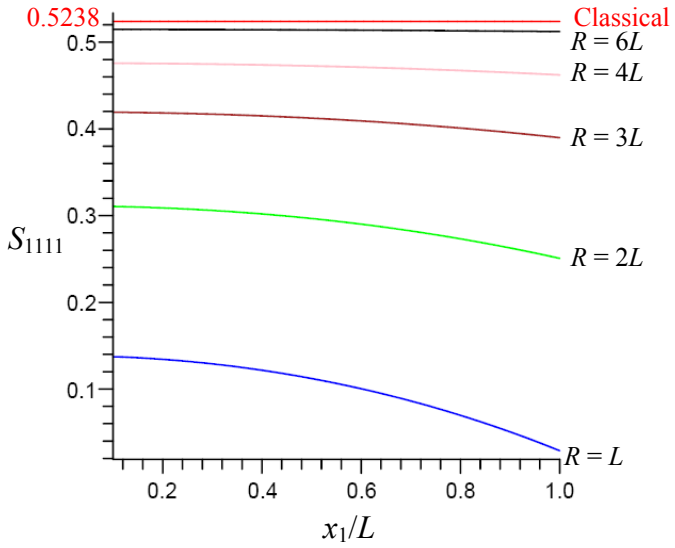

Fig. 3.1. S_{1111} along a radial direction of the spherical inclusion.

It is seen from Fig. 3.1 that S_{1111} varies with x (the position) and depends on R (the inclusion size), unlike the classical part S^C_{1111} which is a constant (i.e., $S^C_{1111} = 0.5238$ from Eq. (3.9), as shown) independent of both x and R. When R is small (comparable to the length scale parameter L = 17.6 μm here), S_{1111} is much smaller than S^C_{1111}, which indicates that the magnitude of $S^G_{1111} (= S_{1111} - S^C_{1111})$ is very large and the strain gradient effect is significant. However, when R is much greater than L (e.g., $R = 6L$ = 105.6 μm shown here), S_{1111} is seen to be quite uniform and its value approaches from below S^C_{1111} (= 0.5238), indicating that the magnitude of S^G_{1111} is very small and the strain gradient effect become insignificant and can therefore be ignored.

Similar trends are observed from Figs. 3.2 and 3.3, where the values of S_{1212} and S_{2222} varying with x and R are displayed together with those of their classical parts that are horizontal lines independent of both x and R. The values of S^G_{1212} and S^G_{2222} included in $S_{1212} (= S^C_{1212} + S^G_{1212})$ and $S_{2222} (= S^C_{2222} + S^G_{2222})$ that are illustrated in Figs. 3.2 and 3.3 are,

respectively, obtained from Eqs. (3.22c) and (3.22e), while those of S^C_{1212} and S^C_{2222} are both calculated using Eq. (3.9).

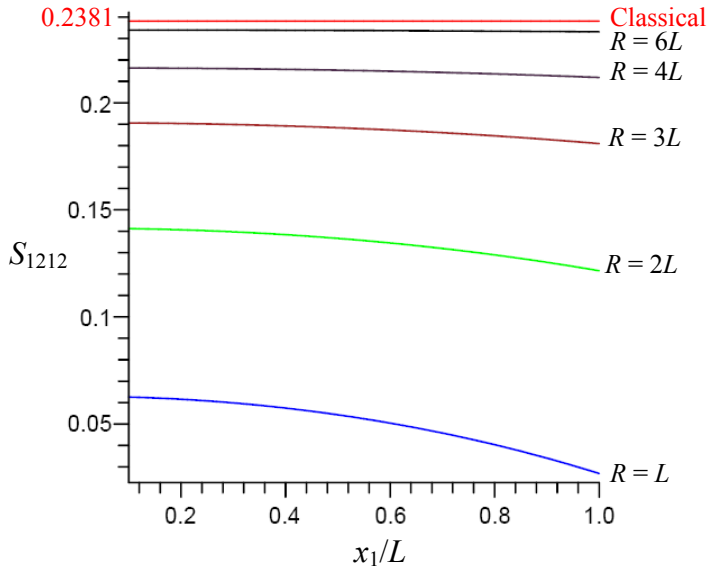

Fig. 3.2. S_{1212} along a radial direction of the spherical inclusion.

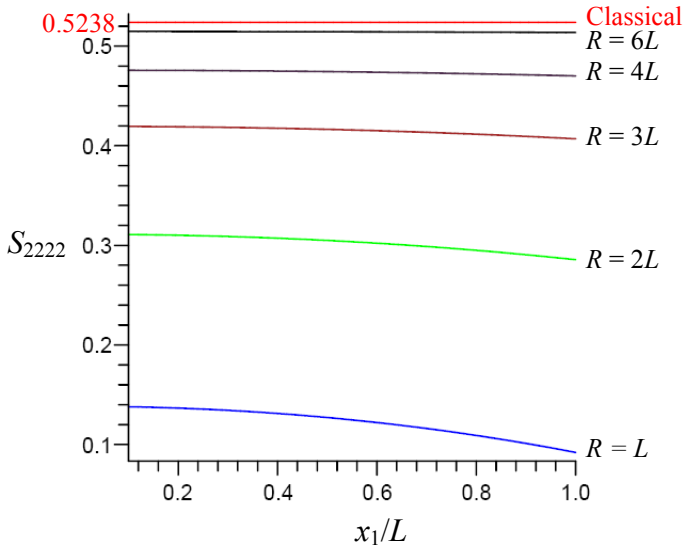

Fig. 3.3. S_{2222} along a radial direction of the spherical inclusion.

The variation of the component of the averaged Eshelby tensor inside the spherical inclusion, $\langle S_{1111} \rangle_V$, with the inclusion size (i.e., radius R) is shown in Fig. 3.4, where its

counterpart in classical elasticity, $\langle S^C_{1111} \rangle_V$, is also displayed for comparison. Note that $\langle S_{1111} \rangle_V$ is obtained from Eq. (3.18), while $\langle S^C_{1111} \rangle_V$ ($= S^C_{1111} = 0.5238$) is from Eq. (3.9). The material properties used here are $\nu = 0.3$ and $L = 17.6$ μm, which are the same as those used in generating the results shown in Figs. 3.1–3.3. It is observed from Fig. 3.4 that $\langle S_{1111} \rangle_V$ is indeed varying with R: the smaller R, the smaller $\langle S_{1111} \rangle_V$, while $\langle S^C_{1111} \rangle_V$ is a constant independent of R. Moreover, the difference between $\langle S_{1111} \rangle_V$ and $\langle S^C_{1111} \rangle_V$, which is $\langle S^G_{1111} \rangle_V$ ($= \langle S_{1111} \rangle_V - \langle S^C_{1111} \rangle_V$), is seen to be significantly large only when the inclusion is small (with $R/L < 25$ or $R < 440$ μm here). As the inclusion size increases, $\langle S_{1111} \rangle_V$ approaches from below the corresponding value of S^C_{1111} (= 0.5238) based on classical elasticity. The same is true for all the other non-vanishing components of $\langle S_{1111} \rangle_V$, as seen from Eqs. (3.18) and (3.9). These observations, once again, indicate that the strain gradient effect is insignificant for large inclusions and may be neglected.

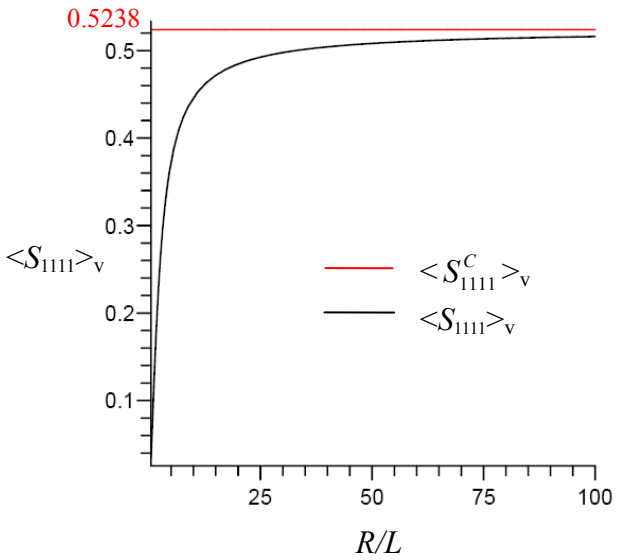

Fig. 3.4. $\langle S_{1111} \rangle_V$ varying with the inclusion radius.

Clearly, the numerical results presented above quantitatively show that the newly obtained Eshelby tensor captures the size effect at the micron scale, unlike that based on classical elasticity.

3.4. Summary

The Eshelby tensor for the spherical inclusion problem is explicitly obtained by employing the general form of the non-classical Eshelby tensor derived in Chapter II using the SSGET. To further illustrate this Eshelby tensor, sample numerical results are provided, which reveal that the components of the new Eshelby tensor vary with both the position and the inclusion size, thereby capturing the size effect at the micron scale.

In addition, the volume average of this new Eshelby tensor over the spherical inclusion is derived in a closed form, which is needed in homogenization analyses. The components of the averaged Eshelby tensor are found to decrease as the inclusion radius decreases, and these components are observed to approach from below the values of the corresponding components of the Eshelby tensor based on classical elasticity when the inclusion size is large enough.

CHAPTER IV

ESHELBY TENSOR FOR A PLANE STRAIN CYLINDRICAL INCLUSION

4.1. Introduction

The current chapter aims to apply the general formulas for a 3-D inclusion of arbitrary shape obtained in Chapter II to solve the Eshelby cylindrical inclusion problem, which is closely related to the fiber-reinforced composites (e.g., Luo and Weng, 1989) and hence of great importance. The solution is derived in a closed form, and the Eshelby tensors for the two regions inside and outside the cylindrical inclusion are obtained in explicit expressions for the first time using a higher-order elasticity theory.

The rest of this chapter is organized as follows. In Section 4.2, the closed-form expressions of the Eshelby tensor and the Eshelby-like tensor for a plane strain cylindrical inclusion embedded in an infinite homogeneous isotropic elastic material are presented, which have 15 and 30 independent components, respectively. The non-classical Eshelby tensor is derived for the two regions inside and outside the inclusion, and the volume average of the new Eshelby tensor over the cylindrical inclusion is exactly determined. Numerical results are provided in Section 4.3 to quantitatively illustrate the position dependence and the inclusion size dependence of the newly obtained Eshelby tensor for the cylindrical inclusion. The chapter concludes in Section 4.4.

4.2. Eshelby Tensor for a Cylindrical Inclusion

A closed-form expression of the Eshelby tensor for a plane strain cylindrical

inclusion of infinite length embedded in an infinite homogeneous isotropic elastic body is derived here by using the general formulas obtained in Chapter II.

Consider an infinitely long cylindrical inclusion of radius a whose symmetry axis (central line) passes through the origin of the cylindrical coordinate system (r, θ, x_3) in the physical space. In this case, $\Lambda(\mathbf{x})$, $\Phi(\mathbf{x})$ defined in Eqs. (2.43a,b) can be obtained from their derivatives given in Mura (1987) for both interior points (i.e., $\mathbf{x} \in \Omega$ or $x < a$) and exterior points (i.e., $\mathbf{x} \notin \Omega$ or $x > a$) as

$$\Lambda(x) = \begin{cases} -\pi x^2 + C_1, & \mathbf{x} \in \Omega, \\ -2\pi R^2 \ln x + C_2, & \mathbf{x} \notin \Omega, \end{cases} \tag{4.1a,b}$$

$$\Phi(x) = \begin{cases} -\dfrac{1}{8}\pi x^4 + Mx^2 + C_3, & \mathbf{x} \in \Omega, \\ -\dfrac{1}{2}\pi R^4 \ln x - \pi R^2 x^2 \ln x + Nx^2 + C_4, & \mathbf{x} \notin \Omega, \end{cases} \tag{4.2a,b}$$

where $x = |\mathbf{x}| = \sqrt{x_1^2 + x_2^2}$ (unlike in the arbitrary 3-D case), and C_1~C_4 , M and N are constants whose values are of no interest here since only the second-order derivatives of Λ and fourth-order derivatives of Φ are involved in the expressions of $\mathbf{S}$ and $\mathbf{T}$ given in Eqs. (2.44a–c) and (2.45), respectively. Also, $\Gamma(\mathbf{x})$ defined in Eq. (2.43c) can be evaluated to obtain the following closed-form expressions (see Appendix D):

$$\Gamma(x) = \begin{cases} 4\pi L\left[L - aI_0\left(\dfrac{x}{L}\right)K_1\left(\dfrac{a}{L}\right)\right], & \mathbf{x} \in \Omega, \\ 4\pi L a I_1\left(\dfrac{a}{L}\right)K_0\left(\dfrac{x}{L}\right), & \mathbf{x} \notin \Omega, \end{cases} \tag{4.3a,b}$$

where $I_n(\cdot)$ and $K_n(\cdot)$ (n = 0, 1) are, respectively, the modified Bessel functions of the first and second kinds of the nth order, which satisfy the following asymptotic relations (e.g., Arfken and Weber, 2005):

$$I_n(z)\sim\frac{1}{\sqrt{2\pi z}}e^{z},\quad K_n(z)\sim\sqrt{\frac{\pi}{2z}}e^{-z}\quad as\ \ z\to\infty. \tag{4.4}$$

Note that Λ, Φ and Γ in Eqs. (4.1a,b)–(4.3a,b) are independent on the direction of the position vector **x** due to the circular symmetry of the inclusion. Clearly, $\Lambda(x)$, $\Phi(x)$ and $\Gamma(x)$ are infinitely differentiable at any $x \neq 0$.

Note that for this case, the inclusion is infinitely long and can be treated as in a plane strain state, $x=|\mathbf{x}|=\left(x_1^2+x_2^2\right)^{1/2}$ and the derivatives of $\Phi(x)$, $\Lambda(x)$ and $\Gamma(x)$, defined in Eq. (2.43a–c), with respect to x_3 should vanish. Accordingly, the fourth-order Eshelby tensor, **S**, and the fifth-order Eshelby-like tensor, **T**, will have expressions different from those for the spherical inclusion, listed in Eqs. (3.4), (3.6) and (3.8), as will be seen below.

Using the expression of $\Lambda(x)$, $\Phi(x)$ and $\Gamma(x)$, given in Eqs. (4.1)–(4.3) into the general forms of **S** and **T**, given in Eqs. (2.44a–c) and (2.45), obtains the special expressions of **S** and **T** for the plane strain cylindrical inclusion. Considering that the general forms of **S** and **T** are expressed in terms of the derivatives of $\Lambda(x)$, $\Phi(x)$ and $\Gamma(x)$ with respect to x_i, it is convenient to first give the following differential equations for a sufficiently smooth function $F(x)$ (with $x=\left(x_1^2+x_2^2\right)^{1/2}$).

$$\left.\begin{aligned}
&F_{,\alpha}=x_\alpha D_1F,\quad F_{,\alpha\beta}=x_\alpha x_\beta D_2F+\delta_{\alpha\beta}D_1F,\\
&F_{,\alpha\beta\gamma}=x_\alpha x_\beta x_\gamma D_3F+\left\langle\delta_{\alpha\beta}x_\gamma\right\rangle_3 D_2F,\\
&F_{,\alpha\beta\gamma\gamma}=x^2x_\alpha x_\beta D_4F+\left(x^2\delta_{\alpha\beta}+6x_\alpha x_\beta\right)D_3F+4\delta_{\alpha\beta}D_2F,\\
&F_{,\alpha\beta\gamma\chi}=x_\alpha x_\beta x_\gamma x_\chi D_4F+\left\langle\delta_{\alpha\beta}x_\gamma x_\chi\right\rangle_6 D_3F+\left\langle\delta_{\alpha\beta}\delta_{\gamma\chi}\right\rangle_3 D_2F,\\
&F_{,\alpha\beta\gamma\theta\chi}=x_\alpha x_\beta x_\gamma x_\chi x_\theta D_5F+\left\langle\delta_{\alpha\beta}x_\gamma x_\chi x_\theta\right\rangle_{10} D_4F+\left\langle\delta_{\alpha\beta}\delta_{\gamma\theta}x_\chi\right\rangle_{15} D_3F,\\
&F_{,\alpha\beta\gamma\theta\theta}=x_\alpha x_\beta x_\gamma x^2D_5F+\left(x^2\left\langle\delta_{\alpha\beta}x_\gamma\right\rangle_3+8x_\alpha x_\beta x_\gamma\right)D_4F+6\left\langle\delta_{\alpha\beta}x_\gamma\right\rangle_3 D_3F,
\end{aligned}\right\} \tag{4.5}$$

where use has been made of the results $\delta_{\alpha\alpha}=2$ and

$$
\left.
\begin{aligned}
D_1F=\frac{F'}{x},\quad D_2F=\frac{1}{x^2}\left(F''-\frac{F'}{x}\right),\quad D_3F=\frac{1}{x^3}\left(F'''-\frac{3F''}{x}+\frac{3F'}{x^2}\right),\\
D_4F=\frac{1}{x^4}\left[F^{(4)}-\frac{6F'''}{x}+\frac{15F''}{x^2}-\frac{15F'}{x^3}\right],\\
D_5F=\frac{1}{x^5}\left[F^{(5)}-\frac{10F^{(4)}}{x}+\frac{45F'''}{x^2}-\frac{105F''}{x^3}+\frac{105F'}{x^4}\right],\\
\left\langle\delta_{\alpha\beta}x_\chi x_\gamma\right\rangle_6\equiv\delta_{\alpha\beta}x_\chi x_\gamma+\delta_{\chi\gamma}x_\alpha x_\beta+\delta_{\alpha\gamma}x_\chi x_\beta+\delta_{\alpha\chi}x_\gamma x_\beta+\delta_{\beta\gamma}x_\chi x_\alpha+\delta_{\beta\chi}x_\alpha x_\gamma,\\
\left\langle\delta_{\alpha\beta}\delta_{\gamma\chi}\right\rangle_3\equiv\delta_{\alpha\beta}\delta_{\gamma\chi}+\delta_{\alpha\gamma}\delta_{\beta\chi}+\delta_{\alpha\chi}\delta_{\beta\gamma},\qquad \left\langle\delta_{\alpha\beta}x_\gamma\right\rangle_3\equiv\delta_{\alpha\beta}x_\gamma+\delta_{\alpha\gamma}x_\beta+\delta_{\beta\gamma}x_\alpha,\\
\left\langle\delta_{\alpha\beta}x_\theta x_\gamma x_\chi\right\rangle_{10}\equiv\delta_{\alpha\beta}x_\theta x_\gamma x_\chi+\delta_{\alpha\theta}x_\beta x_\gamma x_\chi+\delta_{\alpha\gamma}x_\theta x_\beta x_\chi+\delta_{\alpha\chi}x_\theta x_\gamma x_\beta+\delta_{\beta\theta}x_\alpha x_\gamma x_\chi\\
+\delta_{\beta\gamma}x_\theta x_\alpha x_\chi+\delta_{\beta\chi}x_\theta x_\gamma x_\alpha+\delta_{\theta\gamma}x_\alpha x_\beta x_\chi+\delta_{\theta\chi}x_\alpha x_\beta x_\gamma+\delta_{\gamma\chi}x_\alpha x_\beta x_\theta,\\
\left\langle\delta_{\alpha\beta}\delta_{\gamma\theta}x_\chi\right\rangle_{15}\equiv(\delta_{\beta\gamma}\delta_{\theta\chi}+\delta_{\beta\theta}\delta_{\gamma\chi}+\delta_{\beta\chi}\delta_{\theta\gamma})x_\alpha+(\delta_{\alpha\gamma}\delta_{\theta\chi}+\delta_{\alpha\theta}\delta_{\gamma\chi}+\delta_{\alpha\chi}\delta_{\theta\gamma})x_\beta+(\delta_{\beta\alpha}\delta_{\theta\chi}+\delta_{\beta\theta}\delta_{\alpha\chi}+\delta_{\beta\chi}\delta_{\theta\alpha})x_\gamma\\
+(\delta_{\beta\gamma}\delta_{\alpha\chi}+\delta_{\beta\alpha}\delta_{\gamma\chi}+\delta_{\beta\chi}\delta_{\alpha\gamma})x_\theta+(\delta_{\beta\gamma}\delta_{\theta\alpha}+\delta_{\beta\theta}\delta_{\gamma\alpha}+\delta_{\beta\alpha}\delta_{\theta\gamma})x_\chi.
\end{aligned}
\right\}
\tag{4.6}
$$

In Eq. (4.6), $F'=\mathrm{d}F/\mathrm{d}x$, $F''=\mathrm{d}^2F/\mathrm{d}x^2$, $F'''=\mathrm{d}^3F/\mathrm{d}x^3$, $F^{(4)}=\mathrm{d}^4F/\mathrm{d}x^4$, and $F^{(5)}=\mathrm{d}^5F/\mathrm{d}x^5$. Also, in Eqs. (4.5) and (4.6) F can be replaced by $\Phi(x)$, $\Lambda(x)$ or $\Gamma(x)$ involved in the general form of the Eshelby tensor in Eqs. (2.44b,c) and the general form of the Eshelby-like tensor in Eq.(2.45). Note that each Greek index ranges from 1 to 2 in Eqs. (4.5) and (4.6) and throughout this dissertation unless otherwise stated.

After using Eqs. (4.5) and (4.6) in Eqs. (2.44b,c), the components of the Eshelby tensor, with each index ranging from 1 to 2, for a plane strain cylindrical inclusion can be obtained in the form of

$$
\begin{aligned}
S^{\bullet}_{\alpha\beta\gamma\theta}=J^{\bullet}_1(x)\,\delta_{\alpha\beta}\delta_{\gamma\theta}+J^{\bullet}_2(x)\,(\delta_{\alpha\gamma}\delta_{\beta\theta}+\delta_{\alpha\theta}\delta_{\beta\gamma})+J^{\bullet}_3(x)\delta_{\gamma\theta}x^0_\alpha x^0_\beta+J^{\bullet}_4(x)\delta_{\alpha\beta}x^0_\gamma x^0_\theta\\
+J^{\bullet}_5(x)(\delta_{\alpha\gamma}x^0_\beta x^0_\theta+\delta_{\alpha\theta}x^0_\beta x^0_\gamma+\delta_{\beta\gamma}x^0_\alpha x^0_\theta+\delta_{\beta\theta}x^0_\alpha x^0_\gamma)+J^{\bullet}_6(x)(x^0_\alpha x^0_\beta x^0_\gamma x^0_\theta),
\end{aligned}
\tag{4.7}
$$

where $x^0_\alpha=x_\alpha/x$ is the component of the unit vector $\mathbf{x}^0=\mathbf{x}/x$, and $J^{\bullet}_1(x)\sim J^{\bullet}_6(x)$ are scalar-valued functions in terms of $\Lambda(x)$, $\Gamma(x)$, $\Phi(x)$ and ν, which are different for each case and will be individually given below. The superscript "•" in Eq. (4.7) can be replaced by "*C*" or "*G*" to represent the classical or the gradient part of the Eshelby tensor, respectively.

Clearly, $S^{\bullet}_{\alpha\beta\gamma\theta}$ has 9 independent components (rather than $2^4 = 16$ ones) due to the minor symmetry (i.e., $S^{\bullet}_{\alpha\beta\gamma\theta} = S^{\bullet}_{\beta\alpha\gamma\theta} = S^{\bullet}_{\alpha\beta\theta\gamma}$) exhibited by the Eshelby tensor.

For the classical part of the Eshelby tensor (i.e., $S^{C}_{\alpha\beta\gamma\theta}$), $J^{C}_{1}(x) \sim J^{C}_{6}(x)$ are obtained as

$$
\begin{aligned}
J^{C}_{1} &= \frac{1}{8\pi(1-\nu)(1-2\nu)}\left[-4\nu(1-\nu)D_1\Lambda + \nu x^2 D_3\Phi + (1+2\nu)D_2\Phi\right], \\
J^{C}_{2} &= \frac{1}{8\pi(1-\nu)}\left[-2(1-\nu)\,D_1\Lambda + D_2\Phi\right], \\
J^{C}_{3} &= \frac{x^2}{8\pi(1-\nu)(1-2\nu)}\left[-4\nu(1-\nu)D_2\Lambda + \nu x^2 D_4\Phi + (1+4\nu)D_3\Phi\right], \\
J^{C}_{4} &= \frac{x^2}{8\pi(1-\nu)} D_3\Phi, \\
J^{C}_{5} &= \frac{x^2}{8\pi(1-\nu)}\left[-(1-\nu)D_2\Lambda + D_3\Phi\right], \\
J^{C}_{6} &= \frac{x^4}{8\pi(1-\nu)} D_4\Phi.
\end{aligned}
\tag{4.8a–f}
$$

Using Eqs. (4.8a–f) in Eq. (4.7) will yield the expression of $S^{C}_{\alpha\beta\gamma\theta}$, which has 9 independent components.

From Eqs. (2.44b) and (4.5), the other non-vanishing components of $\mathbf{S}^{C}$ for a plane strain cylindrical inclusion can be readily obtained as

$$
S^{C}_{\alpha 3\beta 3} = -\frac{1}{8\pi}\left(x^0_\alpha x^0_\beta x^2 D_2\Lambda + \delta_{\alpha\beta} D_1\Lambda\right), \tag{4.9a}
$$

$$
\begin{aligned}
S^{C}_{\alpha\beta 33} = -\frac{\nu}{8\pi(1-\nu)(1-2\nu)} &\left\{4(1-\nu)\left(x^0_\alpha x^0_\beta x^2 D_2\Lambda + \delta_{\alpha\beta} D_1\Lambda\right)\right. \\
&\left. -\left[x^0_\alpha x^0_\beta x^4 D_4\Phi + x^2\left(\delta_{\alpha\beta} + 6x^0_\alpha x^0_\beta\right)D_3\Phi + 4\delta_{\alpha\beta} D_2\Phi\right]\right\},
\end{aligned}
\tag{4.9b}
$$

where use has been made of the fact that the derivatives of $\Lambda(x)$ and $\Phi(x)$ with respect to x_3 involved in Eq. (2.44b) vanish. It is clear that $S^{C}_{\alpha 3\beta 3}$ has 3 independent components and $S^{C}_{\alpha\beta 33}$ has 3 independent components.

For the gradient part of the Eshelby tensor (i.e., $S^G_{\alpha\beta\gamma\theta}$), $J^G_1(x) \sim J^G_6(x)$ are found to be

$$
\begin{aligned}
J^G_1 &= \frac{1}{4\pi(1-\nu)(1-2\nu)}\left[2\nu(1-\nu)D_1\Gamma - \nu L^2x^2D_3(\Gamma-\Lambda) - (1+2\nu)L^2D_2(\Gamma-\Lambda)\right],\\
J^G_2 &= \frac{1}{4\pi(1-\nu)}\left[(1-\nu)D_1\Gamma - L^2D_2(\Gamma-\Lambda)\right],\\
J^G_3 &= \frac{x^2}{4\pi(1-\nu)(1-2\nu)}\left[2\nu(1-\nu)D_2\Gamma - \nu L^2x^2D_4(\Gamma-\Lambda) - (1+4\nu)L^2D_3(\Gamma-\Lambda)\right],\\
J^G_4 &= -\frac{L^2x^2}{4\pi(1-\nu)}D_3(\Gamma-\Lambda),\\
J^G_5 &= \frac{x^2}{8\pi(1-\nu)}\left[(1-\nu)D_2\Gamma - 2L^2D_3(\Gamma-\Lambda)\right],\\
J^G_6 &= -\frac{L^2x^4}{4\pi(1-\nu)}D_4(\Gamma-\Lambda).
\end{aligned}
\tag{4.10a–f}
$$

Substituting Eqs. (4.10a–f) into Eq. (4.7) will give the expression for $S^G_{\alpha\beta\gamma\theta}$, which has 9 independent components. The other non-vanishing components of $\mathbf{S}^G$ are obtained from Eqs. (2.24c) and (4.5) as

$$
S^G_{3\alpha3\beta} = \frac{1}{8\pi}\left(x^0_\alpha x^0_\beta x^2 D_2\Gamma + \delta_{\alpha\beta}D_1\Gamma\right), \tag{4.11a}
$$

$$
\begin{aligned}
S^G_{\alpha\beta33} = \frac{\nu}{4\pi(1-\nu)(1-2\nu)}\{&\delta_{\alpha\beta}\left[2(1-\nu)D_1\Gamma - L^2x^2D_3(\Gamma-\Lambda) - 4L^2D_2(\Gamma-\Lambda)\right]\\
&+ x^0_\alpha x^0_\beta x^2\left[2(1-\nu)D_2\Gamma - L^2x^2D_4(\Gamma-\Lambda) - 6L^2D_3(\Gamma-\Lambda)\right]\},
\end{aligned}
\tag{4.11b}
$$

where use has been made of the fact that the derivatives of $\Lambda(x)$, $\Phi(x)$ and $\Gamma(x)$ with respect to x_3 involved in Eq. (2.44c) vanish. Clearly, $S^G_{\alpha3\beta3}$ has 3 independent components, and $S^G_{\alpha\beta33}$ has 3 independent components.

By using Eq. (4.5) in Eq. (2.45), the components of the fifth-order Eshelby-like tensor **T**, with each index ranging from 1 to 2, for a plane strain cylindrical inclusion can be determined as

$$
\begin{aligned}
T_{\alpha\beta\gamma\phi\theta} = \frac{L^2}{8\pi(1-\nu)}\Bigg\{ & \frac{4\nu(1-\nu)}{1-2\nu}\delta_{\gamma\phi}\left[x^0_\alpha x^0_\beta x^0_\theta x^3 D_3\mathrm{P} + \left\langle x^0_\theta \delta_{\alpha\beta}\right\rangle_3 x D_2\mathrm{P}\right] \\
& + (1-\nu)(x^0_\alpha x^0_\phi x^0_\theta \delta_{\beta\gamma} + x^0_\beta x^0_\phi x^0_\theta \delta_{\alpha\gamma} + x^0_\alpha x^0_\gamma x^0_\theta \delta_{\beta\phi} + x^0_\beta x^0_\gamma x^0_\theta \delta_{\alpha\phi}) x^3 D_3\mathrm{P} \\
& + (1-\nu)\left[\left\langle x^0_\alpha \delta_{\phi\theta}\right\rangle_3 \delta_{\beta\gamma} + \left\langle x^0_\beta \delta_{\phi\theta}\right\rangle_3 \delta_{\alpha\gamma} + \left\langle x^0_\alpha \delta_{\gamma\theta}\right\rangle_3 \delta_{\beta\phi} + \left\langle x^0_\beta \delta_{\gamma\theta}\right\rangle_3 \delta_{\alpha\phi}\right] x D_2\mathrm{P} \\
& - \frac{\nu}{1-2\nu}\delta_{\gamma\phi}\left[x^0_\alpha x^0_\beta x^0_\theta x^5 D_5\mathrm{G} + (\left\langle x^0_\theta \delta_{\alpha\beta}\right\rangle_3 + 8x^0_\alpha x^0_\beta x^0_\theta) x^3 D_4\mathrm{G} + 6\left\langle x^0_\theta \delta_{\alpha\beta}\right\rangle_3 x D_3\mathrm{G}\right] \\
& - \left[x^0_\alpha x^0_\beta x^0_\gamma x^0_\phi x^0_\theta x^5 D_5\mathrm{G} + \left\langle \delta_{\alpha\beta} x^0_\gamma x^0_\phi x^0_\theta\right\rangle_{10} x^3 D_4\mathrm{G} + \left\langle \delta_{\alpha\beta}\delta_{\gamma\phi} x^0_\theta\right\rangle_{15} x D_3\mathrm{G}\right]\Bigg\},
\end{aligned}
\tag{4.12}
$$

which includes 18 independent components. The other non-vanishing components of **T** are obtained from Eqs. (2.45) and (4.5) as

$$
T_{\alpha 3\beta 3\theta} = \frac{L^2}{8\pi}\left[x^3 x^0_\alpha x^0_\beta x^0_\theta D_3\mathrm{P} + x\left\langle \delta_{\alpha\beta} x^0_\theta\right\rangle_3 D_2\mathrm{P}\right], \tag{4.13a}
$$

which includes 6 independent components, and

$$
\begin{aligned}
T_{\alpha\beta 33\theta} = \frac{\nu L^2}{8\pi(1-\nu)(1-2\nu)}\Big\{ & 4(1-\nu)\left[x^3 x^0_\alpha x^0_\beta x^0_\theta D_3\mathrm{P} + x\left\langle \delta_{\alpha\beta} x^0_\theta\right\rangle_3 D_2\mathrm{P}\right] \\
& - \left[x^5 x^0_\alpha x^0_\beta x^0_\theta D_5\mathrm{G} + x^3\left(\left\langle \delta_{\alpha\beta} x^0_\theta\right\rangle_3 + 8x^0_\alpha x^0_\beta x^0_\theta\right) D_4\mathrm{G} + 6x\left\langle \delta_{\alpha\beta} x^0_\theta\right\rangle_3 D_3\mathrm{G}\right]\Big\},
\end{aligned}
\tag{4.13b}
$$

which contains 6 independent components. The functions P(x) and G(x) involved in Eqs. (4.12) and (4.13a,b) are defined in terms of $\Lambda(x)$, $\Gamma(x)$ and $\Phi(x)$ as

$$
\mathrm{P}(x) \equiv \Lambda - \Gamma, \quad \mathrm{G}(x) \equiv \Phi + 2L^2(\Lambda - \Gamma). \tag{4.14}
$$

Eqs. (4.7)–(4.13a,b) give the expressions for the components of the fourth-order Eshelby tensor, **S**, and the fifth-order Eshelby-like tensor, **T**, based on the simplified strain gradient theory for a plane strain cylindrical inclusion and with an infinite length in the x_3 direction. As indicated earlier, for this plane strain inclusion problem, **S** has 15 independent components and **T** has 30 independent components, which are in contrast to 36 and 108, the numbers of independent components of **S** and **T**, respectively, in the general case of a 3-D inclusion of arbitrary shape (see Eqs. (2.47a,b) and (2.48)). In addition, these expressions for the components of **S** and **T** are in terms of the three scalar-valued functions $\Lambda(x)$, $\Phi(x)$ and $\Gamma(x)$, which are independent of x_3 (with $x = |\mathbf{x}| = \left(x_1^2 + x_2^2\right)^{1/2}$).

Using Eqs. (4.1a) and (4.2a) along with Eqs. (4.6) and (4.8a–f) in the expression of $\mathbf{S}^{C}$ given in Eqs. (4.7) and (4.9a,b) leads to the non-zero components of the classical part of the Eshelby tensor at any $\mathbf{x}$ inside the cylindrical inclusion (i.e., $\mathbf{x} \in \Omega$ or $x < a$) as

$$S^{C}_{\alpha\beta\gamma\theta} = \frac{4\nu-1}{8(1-\nu)}\,\delta_{\alpha\beta}\delta_{\gamma\theta} + \frac{3-4\nu}{8(1-\nu)}(\delta_{\alpha\gamma}\delta_{\beta\theta} + \delta_{\alpha\theta}\delta_{\beta\gamma}),\;\; S^{C}_{\alpha 3\beta 3} = \frac{1}{4}\delta_{\alpha\beta},\;\; S^{C}_{\alpha\beta 33} = \frac{\nu}{2(1-\nu)}\delta_{\alpha\beta}, \quad (4.15a\text{–}c)$$

which are identical to those based on classical elasticity (e.g., Mura, 1987). Note that Eqs. (4.15a–c) list all 15 independent components of $\mathbf{S}^{C}$.

The use of Eqs. (4.1a), (4.2a) and (4.3a) in Eqs. (4.7), (4.10a–f) and (4.11a,b) gives the expressions of the non-zero components of the gradient part of the Eshelby tensor $\mathbf{S}^{G}$ for points inside the inclusion (i.e., $\mathbf{x} \in \Omega$ or $x < a$) as

$$\begin{aligned} S^{G}_{\alpha\beta\gamma\theta} &= J^{G}_{1}(x)\,\delta_{\alpha\beta}\delta_{\gamma\theta} + J^{G}_{2}(x)\,(\delta_{\alpha\gamma}\delta_{\beta\theta} + \delta_{\alpha\theta}\delta_{\beta\gamma}) + J^{G}_{3}(x)\delta_{\gamma\theta}x^{0}_{\alpha}x^{0}_{\beta} + J^{G}_{4}(x)\delta_{\alpha\beta}x^{0}_{\gamma}x^{0}_{\theta} \\ &\quad + J^{G}_{5}(x)(\delta_{\alpha\gamma}x^{0}_{\beta}x^{0}_{\theta} + \delta_{\alpha\theta}x^{0}_{\beta}x^{0}_{\gamma} + \delta_{\beta\gamma}x^{0}_{\alpha}x^{0}_{\theta} + \delta_{\beta\theta}x^{0}_{\alpha}x^{0}_{\gamma}) + J^{G}_{6}(x)(x^{0}_{\alpha}x^{0}_{\beta}x^{0}_{\gamma}x^{0}_{\theta}), \end{aligned} \quad (4.16)$$

where

$$\begin{aligned} J^{G}_{1} &= \frac{aK_{1}}{(1-\nu)x^{3}}\left[LxI_{0} - (\nu x^{2} + 2L^{2})I_{1}\right], \\ J^{G}_{2} &= \frac{aK_{1}}{(1-\nu)x^{3}}\left[LxI_{0} + (-x^{2} + \nu x^{2} - 2L^{2})I_{1}\right], \\ J^{G}_{3} &= \frac{aK_{1}}{(1-\nu)x^{3}L}\left[-x(\nu x^{2} + 4L^{2})I_{0} + L(x^{2} + 2\nu x^{2} + 8L^{2})I_{1}\right], \\ J^{G}_{4} &= \frac{aK_{1}}{(1-\nu)x^{3}}\left[-4LxI_{0} + (x^{2} + 8L^{2})I_{1}\right], \\ J^{G}_{5} &= \frac{aK_{1}}{2(1-\nu)x^{3}L}\left[-x(x^{2} - \nu x^{2} + 8L^{2})I_{0} + 2L(2x^{2} - \nu x^{2} + 8L^{2})I_{1}\right], \\ J^{G}_{6} &= \frac{aK_{1}}{(1-\nu)x^{3}L}\left[x(x^{2} + 24L^{2})I_{0} - 8L(x^{2} + 6L^{2})I_{1}\right], \end{aligned} \quad (4.17a\text{–}f)$$

and

$$S^{G}_{3\alpha 3\beta} = \frac{a}{2xL}K_{1}\left[x^{0}_{\alpha}x^{0}_{\beta}(-xI_{0} + 2LI_{1}) - \delta_{\alpha\beta}LI_{1}\right], \quad (4.18a)$$

$$S^{G}_{\alpha\beta 33} = -\frac{\nu}{1-\nu}\frac{aK_{1}}{xL}\left[\delta_{\alpha\beta}LI_{1} + x^{0}_{\alpha}x^{0}_{\beta}(xI_{0} - 2LI_{1})\right]. \quad (4.18b)$$

In Eqs. (4.17a–f) and (4.18a,b), $I_0 = I_0(\frac{x}{L})$, $I_1 = I_1(\frac{x}{L})$ and $K_1 = K_1(\frac{a}{L})$ are modified Bessel functions of the indicated arguments, with $x < a$. Eqs. (4.16)–(4.18a,b) provide the explicit expressions of all 15 independent components of $\mathbf{S}^G$.

It is clearly seen from Eqs. (4.15a–c) that the classical part of the Eshelby tensor, $\mathbf{S}^C$, is independent of x, a and L and is therefore uniform inside the cylindrical inclusion. In contrast, the gradient part, $\mathbf{S}^G$, given by Eqs. (4.16)–(4.18a,b) depends on x, a and L in a complicated manner. That is, $\mathbf{S}^G$ is non-uniform inside the cylindrical inclusion and differs for materials with different values of a (the inclusion size) and/or L (the material length scale parameter). However, if the strain gradient effect is not considered, then $L = 0$ (so that $x/L \to \infty$, $a/L \to \infty$) and Eqs. (4.4), (4.16)–(4.18a,b) give $S^G_{ijlm} = 0$. It thus follows from Eq. (2.44a) that $\mathbf{S} = \mathbf{S}^C$. That is, the Eshelby tensor for the cylindrical inclusion derived here using the simplified strain gradient elasticity theory reduces to that based on classical elasticity when $L = 0$.

Considering that $\mathbf{S}^G$ is position-dependent inside the inclusion, the volume average of $\mathbf{S}^G$ over the cylindrical inclusion will be needed in calculating the volume average of $\mathbf{S}$ (= $\mathbf{S}^C$ + $\mathbf{S}^G$) to be used for predicting the effective properties of a heterogeneous fiber-reinforced composite. Hence, the volume average of $\mathbf{S}^G$ is evaluated next.

Note that the volume average of a sufficiently smooth function $F(x)$ (with $x = |\mathbf{x}| = \sqrt{x_1^2 + x_2^2}$) over the domain Ω_u occupied by the cylindrical inclusion of a unit length is defined by

$$\langle F \rangle_V \equiv \frac{1}{\mathrm{Vol}(\Omega_u)} \iiint_{\Omega_u} F dV = \frac{1}{\pi a^2} \int_0^a \int_0^{2\pi} F\, x\, d\theta\, dx \ , \tag{4.19}$$

where use has been made of the volume element $dV = x\, d\theta\, dx\, dx_3$ in the cylindrical

coordinate system (r, θ, x_3) (with $r = x = \left(x_1^2 + x_2^2\right)^{1/2}$) and the fact that $F = F(x)$ is independent of x_3. In Eq. (4.19) and throughout this chapter, the volume average over the inclusion domain Ω_u is denoted by the symbol $\langle\ \rangle_V$.

Consider the transformation from the Cartesian to the cylindrical coordinate system:

$$x_1^0 = \cos\theta, \qquad x_2^0 = \sin\theta. \tag{4.20}$$

It follows from Eq. (4.20) that

$$\int_0^{2\pi} x_\alpha^0 x_\beta^0 \, d\theta = \pi\delta_{\alpha\beta}, \qquad \int_0^{2\pi} x_\alpha^0 x_\beta^0 x_\gamma^0 x_\theta^0 \, d\theta = \frac{\pi}{4}(\delta_{\alpha\beta}\delta_{\gamma\theta} + \delta_{\alpha\gamma}\delta_{\beta\theta} + \delta_{\alpha\theta}\delta_{\beta\gamma}). \tag{4.21a,b}$$

Applying Eqs. (4.19) and (4.21a,b) to Eqs. (4.7), (4.10a–f) and (4.11a,b) leads to the volume average of the gradient part of the Eshelby tensor, $\langle \mathbf{S}^G \rangle_V$, as

$$\langle S^G_{\alpha\beta\gamma\theta} \rangle_V = \frac{1}{a^2}\left[\left(2\overline{J_1^G} + \overline{J_3^G} + \overline{J_4^G} + \frac{1}{4}\overline{J_6^G}\right)\delta_{\alpha\beta}\delta_{\gamma\theta} + \left(2\overline{J_2^G} + 2\overline{J_5^G} + \frac{1}{4}\overline{J_6^G}\right)(\delta_{\alpha\gamma}\delta_{\beta\theta} + \delta_{\alpha\theta}\delta_{\beta\gamma})\right], \tag{4.22}$$

$$\langle S^G_{3\alpha3\beta} \rangle_V = \frac{\delta_{\alpha\beta}}{8\pi a^2}\int_0^a \left(x^2 D_2\Gamma + 2D_1\Gamma\right)x\,dx, \tag{4.23}$$

$$\begin{aligned}\langle S^G_{\alpha\beta33} \rangle_V = \frac{\nu\delta_{\alpha\beta}}{4\pi(1-\nu)(1-2\nu)a^2}\int_0^a \{&2(1-\nu)\left(x^2 D_2\Gamma + 2D_1\Gamma\right) \\ &- L^2\left[8D_2(\Gamma-\Lambda) + 8x^2 D_3(\Gamma-\Lambda) + x^4 D_4(\Gamma-\Lambda)\right]\}x\,dx,\end{aligned} \tag{4.24}$$

where

$$\overline{J_n^G} \equiv \textstyle\int_0^a x\, J_n^G(x)\, dx \quad (n = 1, 2, ..., 6), \tag{4.25}$$

with J_n^G (n = 1, 2, ..., 6) to be substituted from Eqs. (4.10a–f). The six integrals for $\overline{J_1^G} \sim \overline{J_6^G}$ defined in Eq. (4.25) can be exactly evaluated with the help of the following results:

$$\int xD_nF\, dx = \int x\frac{1}{x}\frac{d}{dx}(D_{n-1}F)dx = D_{n-1}F + c_1 \quad (n = 1, 2, ..., 5),$$

$$\int x^3 D_2\Gamma\, dx = \int (x\Gamma'' - \Gamma')\, dx = \int \left[(x\Gamma')' - 2\Gamma'\right] dx = x\Gamma' - 2\Gamma + c_2,$$

$$\int x^3 D_3\Gamma\, dx = \int (\Gamma''' - 3\frac{\Gamma''}{x} + 3\frac{\Gamma'}{x^2})\, dx = \Gamma'' - 3\frac{\Gamma'}{x} + c_3,$$

$$\int x^5 D_4\Gamma \, dx = \int [(x\Gamma''')' - 7\Gamma''' + 15(\frac{\Gamma'}{x})'] \, dx = x\Gamma''' - 7\Gamma'' + 15\frac{\Gamma'}{x} + c_4, \tag{4.26}$$

where c_1~c_4 are integration constants, F is a smooth function of x (with $x = |\mathbf{x}| = \sqrt{x_1^2 + x_2^2}$) which can be $\Phi(x)$, $\Lambda(x)$ or $\Gamma(x)$, D_1F~D_5F are differentials defined in Eq. (4.6), and $D_0F \equiv F$.

It then follows from Eqs. (4.10a–f), (4.1a), (4.3a) and (4.22)–(4.26) that the volume averages of the non-zero components of the gradient part of the Eshelby tensor, $\langle \mathbf{S}^{\mathrm{G}} \rangle_{\mathrm{V}}$, are

$$\langle S^G_{\alpha\beta\gamma\theta} \rangle_{\mathrm{V}} = \left[\frac{1-4\nu}{4(1-\nu)} \delta_{\alpha\beta}\delta_{\gamma\theta} + \frac{4\nu-3}{4(1-\nu)} (\delta_{\alpha\gamma}\delta_{\beta\theta} + \delta_{\alpha\theta}\delta_{\beta\gamma}) \right] K_1\left(\frac{a}{L}\right) I_1\left(\frac{a}{L}\right), \tag{4.27a}$$

$$\langle S^G_{3\alpha 3\beta} \rangle_{\mathrm{V}} = -\frac{1}{2} K_1\left(\frac{a}{L}\right) I_1\left(\frac{a}{L}\right) \delta_{\alpha\beta}, \tag{4.27b}$$

$$\langle S^G_{\alpha\beta 33} \rangle_{\mathrm{V}} = -\frac{\nu}{1-\nu} K_1\left(\frac{a}{L}\right) I_1\left(\frac{a}{L}\right) \delta_{\alpha\beta}, \tag{4.27c}$$

where $I_1(\cdot)$ and $K_1(\cdot)$ are modified Bessel functions of the indicated argument a/L. A comparison of the expressions of $\langle \mathbf{S}^{\mathrm{G}} \rangle_{\mathrm{V}}$ in Eqs. (4.27a–c) with those of $\langle \mathrm{S}^{\mathrm{C}} \rangle_{\mathrm{V}} \equiv \mathbf{S}^{\mathrm{C}}$ given in Eqs. (4.15a–c) shows that

$$\langle S^G_{ijkl} \rangle_{\mathrm{V}} = -2K_1\left(\frac{a}{L}\right) I_1\left(\frac{a}{L}\right) S^C_{ijkl}. \tag{4.28}$$

Hence, the volume average of the Eshelby tensor over the cylindrical inclusion of the unit length is obtained from Eqs. (2.44a), (4.15a–c), (4.19) and (4.28) as

$$\langle S_{ijkl} \rangle_{\mathrm{V}} = \left[1 - 2K_1\left(\frac{a}{L}\right) I_1\left(\frac{a}{L}\right) \right] S^C_{ijkl}, \tag{4.29}$$

where S^C_{ijkl} are given in Eq. (4.15a–c). Eq. (4.29) shows that $\langle S_{ijkl} \rangle_{\mathrm{V}}$ depends on a/L. When $L = 0$ (or $a/L \to \infty$), Eq. (4.4) gives $K_1\left(\frac{a}{L}\right) I_1\left(\frac{a}{L}\right) \to 0$, and hence Eq. (4.29) reduces to $\langle S_{ijkl} \rangle_{\mathrm{V}} = S^C_{ijkl}$, as will be further illustrated in the next section. Based on the closed-form expression of the average Eshelby tensor derived in Eq. (4.29), the inhomogeneity problem

involving the cylindrical inclusion of a different material (e.g., Mura, 1987) and the related homogenization of strain gradient composites reinforced by cylindrical fibers can then be analyzed by using Eshelby's equivalent eigenstrain method, as was done by Xun et al. (2004) for micropolar composites.

The volume averages of the components of the fifth-order Eshelby-like tensor **T** inside the cylindrical inclusion of the unit length are, based on Eq. (4.19),

$$\left\langle T_{ijklm} \right\rangle_{\mathrm{V}} = \frac{1}{\pi\, a^2} \int_0^a \int_0^{2\pi} T_{ijklm}\, x\, d\theta\, dx \tag{4.30}$$

where T_{ijklm}, given in Eqs. (4.12) and (4.13a,b), is odd in x_α^0. As a result, the integration of T_{ijklm} with respect to θ on the interval of [0, 2π] vanishes, thereby leading to $\left\langle T_{ijklm} \right\rangle_{\mathrm{V}} = 0$.

Finally, the Eshelby tensor for exterior points $\mathbf{x} \notin \Omega$ (or $x > a$) can be similarly determined as follows. Using Eqs. (4.1b), (4.2b), (4.3b) and (4.6) in Eqs. (4.7)–(4.9a,b) yields the non-vanishing components of $\mathbf{S}^{\mathrm{C}}$ as

$$\begin{aligned} S^C_{\alpha\beta\gamma\theta} = \frac{R^2}{8(1-\nu)x^4}\Big[&(4\nu x^2 - 2x^2 + R^2)\delta_{\alpha\beta}\delta_{\gamma\theta} + (-4\nu x^2 + 2x^2 + R^2)(\delta_{\alpha\gamma}\delta_{\beta\theta} + \delta_{\alpha\theta}\delta_{\beta\gamma}) \\ &- 4(2\nu x^2 - x^2 + R^2)\delta_{\gamma\theta}x^0_\alpha x^0_\beta + 4(x^2 - R^2)\delta_{\alpha\beta}x^0_\gamma x^0_\theta + 4(\nu x^2 - R^2)(\delta_{\alpha\gamma}x^0_\beta x^0_\theta \\ &+ \delta_{\alpha\theta}x^0_\beta x^0_\gamma + \delta_{\beta\gamma}x^0_\alpha x^0_\theta + \delta_{\beta\theta}x^0_\alpha x^0_\gamma) + 8(3R^2 - 2x^2)x^0_\alpha x^0_\beta x^0_\gamma x^0_\theta\Big], \end{aligned} \tag{4.31a}$$

$$S^C_{\alpha 3\beta 3} = \frac{R^2}{4x^2}\left(\delta_{\alpha\beta} - 2x^0_\alpha x^0_\beta\right), \tag{4.31b}$$

$$S^C_{\alpha\beta 33} = \frac{\nu}{2(1-\nu)}\frac{R^2}{x^2}\left(\delta_{\alpha\beta} - 2x^0_\alpha x^0_\beta\right), \tag{4.31c}$$

which are the same as those of the Eshelby tensor outside a cylindrical inclusion based on classical elasticity (Cheng and He, 1997). Clearly, Eqs. (4.31a–c) show that the classical part of the Eshelby tensor, $\mathbf{S}^{\mathrm{C}}$, is not uniform outside the inclusion (with $\mathbf{x} \notin \Omega$ or $x > a$) but changes with x, which is the distance from **x** (the point of interest) to the central line of the cylindrical inclusion. This is different from the case for **x** inside the inclusion (with $\mathbf{x} \in \Omega$

or $x < a$), where $\mathbf{S}^{\mathrm{C}}$ is uniform for all $\mathbf{x} \in \Omega$, as shown in Eqs. (4.15a–c).

Substituting Eqs. (4.1b), (4.2b), (4.3b) and (4.6) into Eqs. (4.10a–f) and (4.11a,b) yields

$$J_1^G = -\frac{aI_1}{(1-\nu)x^3}\left[LxK_0 + (\nu x^2 + 2L^2)K_1\right] + \frac{L^2R^2}{(1-\nu)x^4}, \tag{4.32a}$$

$$J_2^G = \frac{aI_1}{(1-\nu)x^3}\left[-LxK_0 + (-x^2 + \nu x^2 - 2L^2)K_1\right] + \frac{L^2R^2}{(1-\nu)x^4}, \tag{4.32b}$$

$$J_3^G = \frac{aI_1}{(1-\nu)x^3L}\left[x(\nu x^2 + 4L^2)K_0 + L(x^2 + 2\nu x^2 + 8L^2)K_1\right] - \frac{4L^2R^2}{(1-\nu)x^4}, \tag{4.32c}$$

$$J_4^G = \frac{aI_1}{(1-\nu)x^3}\left[4LxK_0 + (x^2 + 8L^2)K_1\right] - \frac{4L^2R^2}{(1-\nu)x^4}, \tag{4.32d}$$

$$J_5^G = \frac{aI_1}{2(1-\nu)x^3L}\left[x(x^2 - \nu x^2 + 8L^2)K_0 + 2L(2x^2 - \nu x^2 + 8L^2)K_1\right] - \frac{4L^2R^2}{(1-\nu)x^4}, \tag{4.32e}$$

$$J_6^G = -\frac{aI_1}{(1-\nu)x^3L}\left[x(x^2 + 24L^2)K_0 + 8L(x^2 + 6L^2)K_1\right] + \frac{24L^2R^2}{(1-\nu)x^4}, \tag{4.32f}$$

and

$$S^G_{3\alpha 3\beta} = \frac{a}{2xL}I_1\left[x^0_\alpha x^0_\beta(xK_0 + 2LK_1) - \delta_{\alpha\beta}LK_1\right], \tag{4.33a}$$

$$S^G_{\alpha\beta 33} = \frac{\nu}{1-\nu}\frac{aI_1}{xL}\left[-\delta_{\alpha\beta}LK_1 + x^0_\alpha x^0_\beta(xK_0 + 2LK_1)\right]. \tag{4.33b}$$

In Eqs. (4.32a–f) and (4.33a,b), $I_1 = I_1(\frac{a}{L})$, $K_0 = K_0(\frac{x}{L})$ and $K_1 = K_1(\frac{x}{L})$ are modified Bessel functions of the indicated arguments, with $x > a$. Using Eqs. (4.32a–f) in Eq. (4.7) will then yield the expression for $S^G_{\alpha\beta\gamma\theta}$, which has 9 independent components. The other 6 non-vanishing components of $\mathbf{S}^{\mathrm{G}}$ in this case are obtained from Eqs. (4.33a,b). It is observed from Eqs. (4.7), (4.4), (4.32a–f) and (4.33a,b) that the components of $\mathbf{S}^{\mathrm{G}}$ in this exterior case (with $\mathbf{x} \notin \Omega$ or $x > a$) will vanish when $L = 0$ (or $x/L \to \infty$, $a/L \to \infty$). By substituting the components of $\mathbf{S}^{\mathrm{G}}$ obtained here and the components of $\mathbf{S}^{\mathrm{C}}$ derived in Eqs. (4.31a–c) into Eq. (2.44a) will finally give the explicit expressions of the Eshelby tensor $\mathbf{S}$ ($= \mathbf{S}^{\mathrm{C}} + \mathbf{S}^{\mathrm{G}}$) for any point $\mathbf{x}$ outside the cylindrical inclusion (i.e., $\mathbf{x} \notin \Omega$ or $x > a$).

4.3. Numerical Results

In this section, some numerical results are presented to quantitatively illustrate how the components of the Eshelby tensor for the cylindrical inclusion vary with position and inclusion size, which has been analytically demonstrated in the preceding section.

From Eqs. (4.16)–(4.18a,b), the non-zero components of the gradient part of the Eshelby tensor, $\mathbf{S}^{\mathrm{G}}$, for any $\mathbf{x}$ inside the cylindrical inclusion (i.e., $\mathbf{x} \in \Omega$ or $x < a$) along the x_1 axis (with $x_2 = 0$, $x = x_1$) can be obtained as

$$S^G_{1111} = \frac{aK_1}{(1-\nu)x^3 L}\left[x(3L^2 + \nu x^2 - x^2)I_0 - L(\nu x^2 + 6L^2)I_1\right], \tag{4.34a}$$

$$S^G_{2222} = \frac{aK_1}{(1-\nu)x^3}\left[(-6L^2 + \nu x^2 - 2x^2)I_1 + 3LxI_0\right], \tag{4.34b}$$

$$S^G_{1122} = \frac{aK_1}{(1-\nu)x^3 L}\left[-x(3L^2 + \nu x^2)I_0 + L(\nu x^2 + 6L^2 + x^2)I_1\right], \tag{4.34c}$$

$$S^G_{2211} = \frac{aK_1}{(1-\nu)x^3}\left[-3LxI_0 + (6L^2 + x^2 - \nu x^2)I_1\right], \tag{4.34d}$$

$$S^G_{1212} = \frac{aK_1}{2(1-\nu)x^3 L}\left[-x(6L^2 + x^2 - \nu x^2)I_0 + 2L(x^2 + 6L^2)I_1\right], \tag{4.34e}$$

$$S^G_{3131} = \frac{a}{2xL}K_1(-xI_0 + LI_1), \quad S^G_{3232} = -\frac{a}{2x}K_1 I_1, \tag{4.34f,g}$$

$$S^G_{1133} = -\frac{\nu}{1-\nu}\frac{aK_1}{xL}(xI_0 - LI_1), \quad S^G_{2233} = -\frac{\nu}{1-\nu}\frac{aK_1 I_1}{x}, \tag{4.34h,i}$$

where $I_0 = I_0(\frac{x}{L})$, $I_1 = I_1(\frac{x}{L})$ and $K_1 = K_1(\frac{a}{L})$ are modified Bessel functions of the indicated arguments. As shown in Eqs. (4.34a–i), in this special case (with $x = x_1$, $x_2 = 0$) there are only 9 non-zero components among the 15 independent non-zero components of $\mathbf{S}^{\mathrm{G}}$.

The distribution of $S_{1111} = S^C_{1111} + S^G_{1111}$ along the x_1 axis (a generic radial direction of the inclusion due to the axial symmetry) for five different values of a is shown in Fig. 4.1, where the values of S^C_{1111} and S^G_{1111} are, respectively, obtained from Eqs. (4.15a) and (4.34a). For illustration purpose, in the numerical analysis leading to the results displayed in Figs.

4.1–4.3, Poisson's ratio v is taken to be 0.3, and the length scale parameter L to be 17.6 μm.

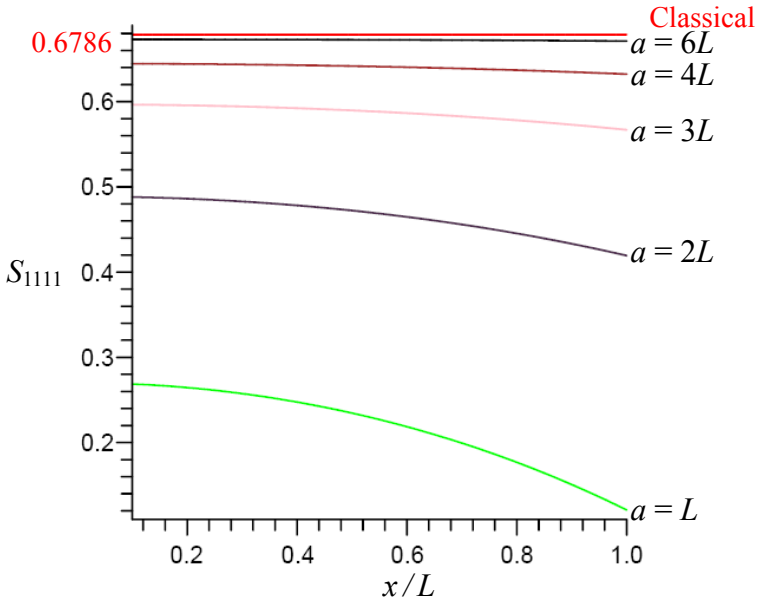

Fig. 4.1. S_{1111} along a radial direction of the cylindrical inclusion.

It is seen from Fig. 4.1 that S_{1111} varies with x (the position) and depends on a and L, unlike its counterpart S^C_{1111} in classical elasticity, which is a constant (i.e., $S^C_{1111} = 0.6786$ from Eq. (4.15a), as shown) independent of x, a and L. When a is small (comparable to the value of L here), S_{1111} is much smaller than S^C_{1111}, which indicates that the magnitude of $S^G_{1111} (= S_{1111} - S^C_{1111})$ is large and the strain gradient effect is significant. As a increases, the value of S_{1111} approaches from below S^C_{1111} (= 0.6786), and the curves of S_{1111} become increasingly flatter. When a is much larger than L (e.g., $a = 6L = 105.6$ μm here), the curves of S_{1111} and S^C_{1111} almost coincide, which means that the magnitude of S^G_{1111} is very small and the strain gradient effect becomes insignificant and can therefore be ignored.

Similar trends are observed from Fig. 4.2, where the values of S_{1212} varying with x and a are displayed and compared to the value of S^C_{1212}, which is a constant (i.e., 0.3214)

independent of both x and a. The values of S_{1212}^{G} (included in $S_{1212} = S_{1212}^{C} + S_{1212}^{G}$) showing in Fig. 4.2 are from Eq. (4.34e), while that of S_{1212}^{C} is determined using Eq. (4.15a).

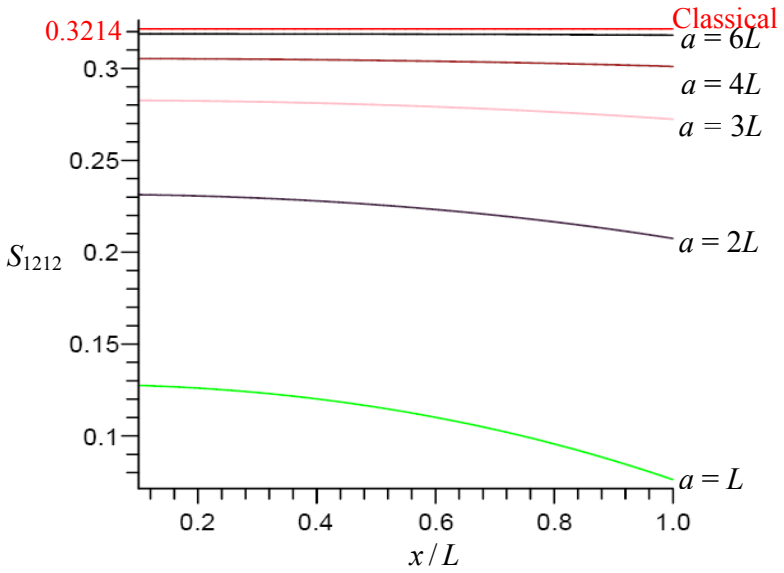

Fig. 4.2. S_{1212} along a radial direction of the cylindrical inclusion.

The variation of the volume averaged component $\langle S_{1111} \rangle_{\mathrm{V}}$ inside the cylindrical inclusion with the inclusion size is plotted in Fig. 4.3, where its counterpart in classical elasticity, $\langle S_{1111}^{C} \rangle_{\mathrm{V}} (= S_{1111}^{C})$, is also displayed for comparison. Note that $\langle S_{1111} \rangle_{\mathrm{V}}$ is obtained from Eq. (4.29), while S_{1111}^{C} (= 0.6786) is from Eq. (4.15a). It is observed from Fig. 4.3 that $\langle S_{1111} \rangle_{\mathrm{V}}$ indeed depends on the inclusion size: the smaller a, the smaller $\langle S_{1111} \rangle_{\mathrm{V}}$. Also, Fig. 4.3 shows that as a increases, $\langle S_{1111} \rangle_{\mathrm{V}}$ approaches S_{1111}^{C} (from below), which is a constant independent of a. Moreover, the difference between $\langle S_{1111} \rangle_{\mathrm{V}}$ and S_{1111}^{C}, which is $\langle S_{1111}^{G} \rangle_{\mathrm{V}} (= \langle S_{1111} \rangle_{\mathrm{V}} - S_{1111}^{C})$, is seen to be significantly large only when the inclusion is small (with $a/L < 20$ or $a < 352$ μm here). The same is true for all of the other non-vanishing

components of $\langle S_{ijkl} \rangle_V$, which is mathematically dictated by Eq. (4.29). These observations indicate that the strain gradient effect is insignificant for large inclusions and may therefore be neglected, which agrees with what is observed above from examining Figs. 4.1 and 4.2.

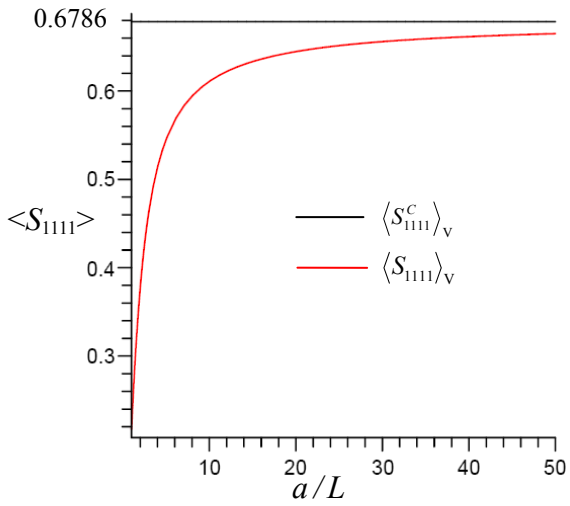

Fig. 4.3. $\langle S_{1111} \rangle_V$ varying with the inclusion radius.

4.4. Summary

The Eshelby tensor for a cylindrical inclusion in the two regions inside and outside the inclusion is obtained in explicit expressions for the first time using the general form of the Eshelby tensor for a plane strain inclusion based on the strain gradient theory. The newly obtained Eshelby tensor has 15 independent non-zero components (as opposed to 36 such components in the case of a 3-D inclusion of arbitrary shape) and consists of a classical part (depending only on Poisson's ratio) and a gradient part (depending on the length scale parameter additionally). The gradient part vanishes when the strain gradient effect is not considered. This non-classical Eshelby tensor contains a material length scale parameter and can explain the size effect at the micron scale, unlike that based on classical elasticity. When the strain gradient effect is suppressed, this Eshelby tensor reduces to that

for a cylindrical inclusion based on classical elasticity.

To further illustrate the newly derived Eshelby tensor, sample numerical results are provided. These results quantitatively show that the new Eshelby tensor depends on both the position and inclusion size and can capture the size effect at the micron scale.

In addition, the volume average of the newly derived position-dependent Eshelby tensor over the cylindrical inclusion of a unit length is obtained in a closed form, which is needed in homogenization analyses of fiber-reinforced composites. The volume averaged components of the Eshelby tensor are found to become smaller as the inclusion radius decreases, but they are observed to approach (from below) the constant values of the corresponding components of the Eshelby tensor based on classical elasticity when the inclusion size becomes sufficiently large.

CHAPTER V

STRAIN GRADIENT SOLUTION FOR ESHELBY'S ELLIPSOIDAL INCLUSION PROBLEM

5.1. Introduction

The simplified strain elasticity theory (SSGET) introduced in Chapter II has been found a success in capturing the size effect exhibited by composite materials filled with inhomogeneities of micron scale, as discussed in the preceding chapters. A spherical inclusion and a cylindrical inclusion problem have been solved in the framework of the SSGET. This chapter aims to solve a more general and complex ellipsoidal inclusion problem based on the SSGET, which are of fundamental interest in a wide range of physical and engineering problems in the micromechanics of heterogeneous solids.

The rest of this chapter is organized as follows. In Section 5.2, analytical expressions of the Eshelby tensor inside and outside an ellipsoidal inclusion are deduced by applying the general form of the Eshelby tensor derived in Chapter II. The volume average of this Eshelby tensor over the ellipsoidal inclusion is analytically evaluated. Numerical results are provided in Section 5.3 to quantitatively illustrate the position dependence and the inclusion size dependence of the newly obtained Eshelby tensor for the ellipsoidal inclusion problem. This chapter concludes with a summary in Section 5.4.

5.2. Ellipsoidal Inclusion

Consider an ellipsoidal inclusion of three semi-axes a_1, a_2 and a_3 and centered at the

origin of the coordinate system (x_1, x_2, x_3) in the physical space, as shown in Fig. 5.1. Then, the region Ω occupied by the inclusion is given by

$$\frac{x_1^2}{a_1^2}+\frac{x_2^2}{a_2^2}+\frac{x_3^2}{a_3^2}\le 1. \tag{5.1}$$

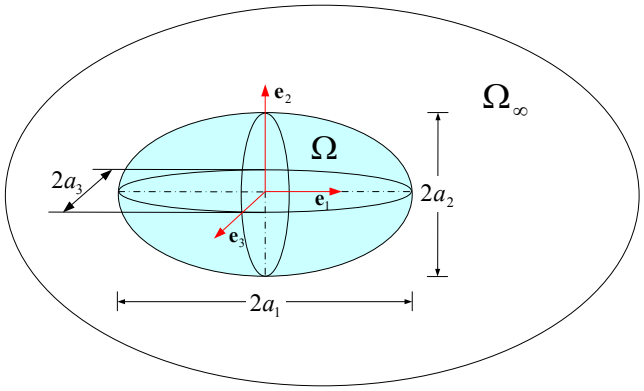

Fig. 5.1. Ellipsoidal inclusion problem.

For this ellipsoidal inclusion, $\Phi(\mathbf{x})$ and $\Lambda(\mathbf{x})$ defined in Eqs. (2.43a,b) can be shown by integration and differentiation to satisfy (Mura, 1982)

$$\Phi_{,ijkl}(\mathbf{x})=\begin{cases} -\left[I_K(0)-a_I^2 I_{IK}(0)\right]\delta_{ij}\delta_{kl}-\left[I_J(0)-a_I^2 I_{IJ}(0)\right](\delta_{ik}\delta_{jl}+\delta_{il}\delta_{jk}), & \mathbf{x}\in\Omega, \\ -\left[I_K(\gamma)-a_I^2 I_{IK}(\gamma)\right]\delta_{ij}\delta_{kl}-\left[I_J(\gamma)-a_I^2 I_{IJ}(\gamma)\right](\delta_{ik}\delta_{jl}+\delta_{il}\delta_{jk}) \\ -\left[I_K(\gamma)-a_I^2 I_{IK}(\gamma)\right]_{,l}\delta_{ij}x_k-\left[I_J(\gamma)-a_I^2 I_{IJ}(\gamma)\right]_{,l}(\delta_{ik}x_j+\delta_{jk}x_i) \\ -\left[I_J(\gamma)-a_I^2 I_{IJ}(\gamma)\right]_{,k}(\delta_{il}x_j+\delta_{jl}x_i)-\left[I_J(\gamma)-a_I^2 I_{IJ}(\gamma)\right]_{,kl}x_i x_j, & \mathbf{x}\notin\Omega; \end{cases} \tag{5.2a,b}$$

$$\Lambda_{,ij}(\mathbf{x})=\begin{cases} -I_I(0)\delta_{ij}, & \mathbf{x}\in\Omega, \\ -I_I(\gamma)\delta_{ij}-I_{I,j}(\gamma)x_i, & \mathbf{x}\notin\Omega, \end{cases} \tag{5.2c,d}$$

where

$$I_I(\gamma)=2\pi a_1 a_2 a_3\int_\gamma^\infty \frac{dt}{(a_I^2+t)\sqrt{(a_1^2+t)(a_2^2+t)(a_3^2+t)}}, \tag{5.3a}$$

$$I_{IJ}(\gamma) = 2\pi a_1 a_2 a_3 \int_\gamma^\infty \frac{dt}{(a_I^2 + t)(a_J^2 + t)\sqrt{(a_1^2 + t)(a_2^2 + t)(a_3^2 + t)}}, \tag{5.3b}$$

which are functions of γ, with $I, J \in \{1, 2, 3\}$. For $\mathbf{x} \in \Omega$ (interior points) $\gamma = 0$, and for $\mathbf{x} \notin \Omega$ (exterior points) γ is the largest positive root of the following equation:

$$\frac{x_1^2}{a_1^2 + \gamma} + \frac{x_2^2}{a_2^2 + \gamma} + \frac{x_3^2}{a_3^2 + \gamma} = 1, \tag{5.4}$$

which shows that γ is a function of **x.** Note that in Eqs. (5.2a–d) and in the sequel each repeated lower-case index implies summation from 1 to 3, while each upper-case index takes the same value as its corresponding lower-case index but implies no summation.

For interior points with $\mathbf{x} \in \Omega$, it follows from Eqs. (2.47a) and (5.2a,c) that the classical part of the Eshelby tensor is

$$\begin{aligned} S_{ijlm}^{C,IN} = \frac{1}{8\pi(1-\nu)} \Big\{ & \Big[2\nu I_I(0) - I_L(0) + a_I^2 I_{IL}(0)\Big]\delta_{ij}\delta_{lm} \\ & + \Big[(1-\nu)I_L(0) + (1-\nu)I_M(0) - I_J(0) + a_I^2 I_{IJ}(0)\Big](\delta_{il}\delta_{jm} + \delta_{im}\delta_{jl}) \Big\}, \end{aligned} \tag{5.5}$$

which is the same as that provided in Li and Wang (2008). It is clear from Eq. (5.5) that the Eshelby tensor $S_{ijlm}^{C,IN}$ is uniform (i.e., independent of position **x)** inside the ellipsoidal inclusion, which is a well-known result (e.g., Markenscoff, 1998) and has recently been elaborated in a broader context by Liu (2008). In fact, it can be shown that the components of $S_{ijlm}^{C,IN}$ given in Eq. (5.5) depend only on the two aspect ratios of the ellipsoidal inclusion, defined by $\alpha_1 = a_1/a_3$ and $\alpha_2 = a_2/a_3$, and Poisson's ratio of the matrix material, ν.

For exterior points with $\mathbf{x} \notin \Omega$, it can be shown that the use of Eqs. (2.47a) and (5.2b,d) yields the classical part of the Eshelby tensor as (Mura, 1982)

$$
\begin{aligned}
S_{ijlm}^{C,EX} &= S_{ijlm}^{C}(\gamma)+\frac{\nu}{4\pi(1-\nu)}I_{I,j}(\gamma)\delta_{lm}x_i+\frac{1}{8\pi}\Big[I_{L,j}(\gamma)\delta_{im}x_l+I_{L,i}(\gamma)\delta_{jm}x_l+I_{M,j}(\gamma)\delta_{il}x_m \\
&\quad +I_{M,i}(\gamma)\delta_{jl}x_m\Big]-\frac{1}{8\pi(1-\nu)}\Big\{\Big[I_L(\gamma)-a_I^2I_{IL}(\gamma)\Big]_m\delta_{ij}x_l+\Big[I_J(\gamma)-a_I^2I_{IJ}(\gamma)\Big]_m(\delta_{il}x_j+\delta_{jl}x_i) \\
&\quad +\Big[I_J(\gamma)-a_I^2I_{IJ}(\gamma)\Big]_l(\delta_{im}x_j+\delta_{jm}x_i)+\Big[I_J(\gamma)-a_I^2I_{IJ}(\gamma)\Big]_{lm}x_ix_j\Big\},
\end{aligned}
\tag{5.6}
$$

where

$$
\begin{aligned}
S_{ijlm}^{C}(\gamma) &= \frac{1}{8\pi(1-\nu)}\Big\{\Big[2\nu I_I(\gamma)-I_L(\gamma)+a_I^2I_{IL}(\gamma)\Big]\delta_{ij}\delta_{lm} \\
&\quad +\Big[(1-\nu)I_L(\gamma)+(1-\nu)I_M(\gamma)-I_J(\gamma)+a_I^2I_{IJ}(\gamma)\Big](\delta_{il}\delta_{jm}+\delta_{im}\delta_{jl})\Big\}.
\end{aligned}
\tag{5.7}
$$

Clearly, Eq. (5.6) involves the first- and second-order derivatives of $I_I(\gamma)$ and $I_{IJ}(\gamma)$ defined in Eqs. (5.3a,b), which are not explicit and will be replaced with more direct expressions. It can be shown from Eqs. (5.3a,b), after some lengthy algebra, that

$$
I_{J,p}(\gamma)=\frac{-4\pi a_1a_2a_3\varpi_J\varpi_Px_p}{\Delta Z},\quad I_{IJ,p}(\gamma)=\frac{-4\pi a_1a_2a_3\varpi_I\varpi_J\varpi_Px_p}{\Delta Z},
\tag{5.8a,b}
$$

$$
x_ix_j\Big[I_J(\gamma)-a_I{}^2I_{IJ}(\gamma)\Big]_{pq}=-\frac{4\pi a_1a_2a_3}{\Delta}\left\{\left[2-2\gamma\left(\varpi_I+\varpi_J+\varpi_P+\varpi_Q\right)-\gamma\vartheta+\frac{4\gamma\eta}{Z}\right]\hat{n}_i\hat{n}_j\hat{n}_p\hat{n}_q+\gamma\varpi_P\delta_{pq}\hat{n}_i\hat{n}_j\right\},
\tag{5.8c}
$$

where

$$
\Delta\equiv\sqrt{(a_1^2+\gamma)(a_2^2+\gamma)(a_3^2+\gamma)},\quad Z\equiv\frac{x_mx_m}{(a_M^2+\gamma)^2},\quad \varpi_I\equiv\frac{1}{a_I^2+\gamma},
\tag{5.9a–c}
$$

$$
\vartheta\equiv\varpi_1+\varpi_2+\varpi_3,\quad \eta\equiv\frac{x_mx_m}{(a_M^2+\gamma)^3},\quad \hat{n}_i\equiv\frac{x_i}{(a_I^2+\gamma)\sqrt{Z}}.
\tag{5.9d–f}
$$

Using Eqs. (5.7) and (5.8a–c) in Eq. (5.6) then gives

$$
\begin{aligned}
S_{ijlm}^{C,EX} &= S_{IL}^{(1)}\delta_{ij}\delta_{lm}+S_{IJ}^{(2)}(\delta_{il}\delta_{jm}+\delta_{im}\delta_{jl})+S_I^{(3)}\varpi_L\varpi_M\delta_{ij}x_lx_m+S_L^{(4)}\varpi_I\varpi_J\delta_{lm}x_ix_j \\
&\quad +S_I^{(5)}(\varpi_J\varpi_M\delta_{il}x_jx_m+\varpi_J\varpi_L\delta_{im}x_jx_l)+S_J^{(6)}(\varpi_I\varpi_M\delta_{jl}x_ix_m+\varpi_I\varpi_L\delta_{jm}x_ix_l) \\
&\quad +S_{IJLM}^{(7)}x_ix_jx_lx_m,
\end{aligned}
\tag{5.10}
$$

where

$$
\begin{aligned}
S_{IL}^{(1)} &= \frac{1}{8\pi(1-\nu)}\left[2\nu I_I(\gamma) - I_L(\gamma) + a_I^2 I_{IL}(\gamma)\right], \\
S_{IJ}^{(2)} &= \frac{1}{8\pi(1-\nu)}\left\{(1-\nu)\left[I_I(\gamma) + I_J(\gamma)\right] - I_J(\gamma) + a_I^2 I_{IJ}(\gamma)\right\}, \\
S_I^{(3)} &= \frac{a_1 a_2 a_3}{\Delta Z}\frac{\gamma}{2(1-\nu)}\varpi_I, \quad S_L^{(4)} = \frac{a_1 a_2 a_3}{\Delta Z}\frac{1}{2(1-\nu)}(\gamma\varpi_L - 2\nu), \\
S_I^{(5)} &= \frac{a_1 a_2 a_3}{\Delta Z}\frac{1}{2(1-\nu)}(\gamma\varpi_I - 1 + \nu), \quad S_J^{(6)} = \frac{a_1 a_2 a_3}{\Delta Z}\frac{1}{2(1-\nu)}(\gamma\varpi_J - 1 + \nu), \\
S_{IJLM}^{(7)} &= \frac{a_1 a_2 a_3}{\Delta Z^2}\frac{1}{2(1-\nu)}\varpi_I\varpi_J\varpi_L\varpi_M\left[2 - 2\gamma\left(\varpi_I + \varpi_J + \varpi_L + \varpi_M\right) - \gamma\vartheta + \frac{4\gamma\eta}{Z}\right].
\end{aligned}
\tag{5.11}
$$

Note that the expression for the classical part of the Eshelby tensor outside the ellipsoidal inclusion (i.e., for exterior points with $\mathbf{x} \notin \Omega$) given in Eqs. (5.10) and (5.11) no longer contains derivatives of $I_I(\lambda)$ and $I_{IJ}(\lambda)$ and is therefore more convenient and more accurate to use (since differentiation tends to introduce more errors in numerical approximations). It can be readily shown that the expression of $S_{ijlm}^{C,EX}$ in Eq. (5.10) is the same as that derived earlier by Ju and Sun (1999) using a different notation. Clearly, it is seen from Eqs. (5.6) and (5.7) that $S_{ijlm}^{C,EX}$, being dependent on the position $\mathbf{x}$, is not uniform outside the ellipsoidal inclusion, although $S_{ijlm}^{C,IN}$ (see Eq. (5.5)) is uniform inside the same inclusion.

The determination of the gradient part of the Eshelby tensor requires the evaluation of the integral defining $\Gamma(\mathbf{x})$ in Eq. (2.43c). For the ellipsoidal inclusion described in Eq. (5.1), a closed-form expression for $\Gamma(\mathbf{x})$ can hardly be derived. However, the following results can be obtained (see Appendix E for derivations):

$$
\Gamma(\mathbf{x}) = 4\pi L^2 - L^2\int_0^{2\pi}\int_0^{\pi}\left(1 + \frac{s}{L}\right)\exp\left(-\frac{s}{L}\right)\exp\left(-\frac{m}{L}\right)\sin\theta\, d\theta\, d\varphi \tag{5.12}
$$

for interior points $\mathbf{x} \in \Omega$, where

$$
s = \left[\left(\frac{\sin\theta\cos\varphi}{a_1}\right)^2 + \left(\frac{\sin\theta\sin\varphi}{a_2}\right)^2 + \left(\frac{\cos\theta}{a_3}\right)^2\right]^{-1/2} = s(\theta,\varphi), \tag{5.13a}
$$

$$m = s|\mathbf{X}|\cos\theta, \quad \mathbf{X} = \frac{x_1}{a_1}\mathbf{e_1} + \frac{x_2}{a_2}\mathbf{e_2} + \frac{x_3}{a_3}\mathbf{e_3}, \tag{5.13b,c}$$

and

$$\Gamma(\mathbf{x}) = -\frac{4L^2}{\pi}\int_0^{2\pi}\left(\int_0^{\alpha} F^{(1)}\sin\theta\, d\theta + \int_{\alpha}^{\pi/2} F^{(2)}\sin\theta\, d\theta\right)d\varphi \tag{5.14}$$

for exterior points $\mathbf{x} \notin \Omega$, where

$$F^{(1)} \equiv \frac{\pi}{2}e^{-\frac{m}{L}}\left[\frac{s}{L}\cosh\left(\frac{s}{L}\right) - \sinh\left(\frac{s}{L}\right)\right], \tag{5.15a}$$

$$F^{(2)} \equiv -\frac{\pi}{2} + \frac{\pi}{2}\left(1 + \frac{s}{L}\right)e^{-\frac{s}{L}}\cosh\left(\frac{m}{L}\right), \tag{5.15b}$$

$$\alpha \equiv \cos^{-1}\frac{1}{|\mathbf{X}|}. \tag{5.15c}$$

Clearly, Eqs. (5.12) and (5.14) show that $\Gamma(\mathbf{x}) = 0$ when $L = 0$ (i.e., when the strain gradient effect is not considered), as expected.

It should be mentioned that for interior points $\mathbf{x} \in \Omega$, evaluating $\Gamma(\mathbf{x})$ defined in Eq. (2.43c) can also be reduced to the evaluation of one line integral on the interval $[0, \infty)$ by using an expression of the Helmholtz potential inside an ellipsoidal region derived in Michelitsch et al. (2003) (see their Eq. (3.18)), as was done in Ma and Hu (2006) for spheroidal inclusion cases with $a_1 = a_2$.

For the special case of a spherical inclusion with $a_1 = a_2 = a_3 = R$, thereby $s = R$ and $m = x\cos\theta$ according to Eqs. (5.13a–c), it can be readily shown by using Eqs. (5.12) and (5.14) respectively that

$$\Gamma(\mathbf{x}) = \begin{cases} 4\pi L^2 - \dfrac{4\pi L^2}{x}(L+R)e^{-\frac{R}{L}}\sinh\left(\dfrac{x}{L}\right), & \mathbf{x} \in \Omega, \\ \dfrac{-4\pi L^3}{x}\left[\sinh\left(\dfrac{R}{L}\right) - \dfrac{R}{L}\cosh\left(\dfrac{R}{L}\right)\right]e^{-\frac{x}{L}}, & \mathbf{x} \notin \Omega, \end{cases} \tag{5.16a,b}$$

which are the same as those obtained in Eqs.(3.1e,f) by direct integration.

For the special case of a cylindrical inclusion with $a_1 = a_2 = a$ and $a_3 \to \infty$, it can be shown, after evaluating the integrals analytically, that Eqs. (5.12) and (5.14) give

$$\Gamma(\mathbf{x}) = \begin{cases} 4\pi L\left[L - aI_0\left(\frac{x}{L}\right)K_1\left(\frac{a}{L}\right)\right], & \mathbf{x} \in \Omega, \\ 4\pi LaI_1\left(\frac{a}{L}\right)K_0\left(\frac{x}{L}\right), & \mathbf{x} \notin \Omega, \end{cases} \tag{5.17a,b}$$

where $I_n(\cdot)$ and $K_n(\cdot)$ (n = 0, 1) are, respectively, the modified Bessel functions of the first and second kinds of the nth order. Eqs. (5.17a,b) are the same as those derived in Eqs. (4.3a,b). In reaching Eqs. (5.17a,b), use has been made of the identities:

$$e^{z\cos\theta} = I_0(z) + 2\sum_{k=1}^{\infty} I_k(z)\cos(k\theta)\,,\ \int_0^{2\pi}\cos[k(\varphi-\varphi_0)]\,d\varphi = 0 \quad (k = 1, 2, ...). \tag{5.17c,d}$$

It can be shown that differentiating Eq. (5.12) or Eq. (5.14) leads to

$$\Gamma_{,i} = \frac{x_i}{Pa_I^2} f(P), \tag{5.18a}$$

where

$$P \equiv |\mathbf{X}| = \left[\left(\frac{x_1}{a_1}\right)^2 + \left(\frac{x_2}{a_2}\right)^2 + \left(\frac{x_3}{a_3}\right)^2\right]^{1/2}, \tag{5.18b}$$

$$f(P) \equiv \int_0^{2\pi}\int_0^{\pi} s(L+s)\exp\left(-\frac{s}{L}\right)\exp\left(-\frac{s}{L}P\cos\theta\right)\cos\theta\sin\theta\,d\theta\,d\varphi \quad \text{for } \mathbf{x} \in \Omega, \tag{5.18c}$$

or

$$f(P) = -\frac{4}{\pi}L^2\int_0^{2\pi}\left(\int_0^{\alpha}\frac{\partial F_1}{\partial P}\sin\theta\,d\theta + \int_{\alpha}^{\pi/2}\frac{\partial F_2}{\partial P}\sin\theta\,d\theta\right)d\varphi \quad \text{for } \mathbf{x} \notin \Omega. \tag{5.18d}$$

Clearly, it is seen from Eqs. (5.18c,d) that $f(P) = 0$ in both the interior and exterior cases when $L = 0$, as expected. Note that in reaching Eq. (5.18a) use has been made of the coordinate transformation:

$$x_i = Pa_I n_i\,, \tag{5.19}$$

which transforms the ellipsoidal region Ω defined in Eq. (5.1) into a unit sphere $|\mathbf{X}| \le 1$

with the unit outward normal **n** on its surface $|\mathbf{X}| = 1$.

It then follows from Eqs. (5.18a,b) and (5.19) that

$$\Gamma_{,ij} = \frac{1}{a_I a_J}\left[P^2 (d_1 f) n_i n_j + \frac{f}{P}\delta_{ij} \right], \tag{5.20a}$$

$$\Gamma_{,ijl} = \frac{1}{a_I a_J a_L}\left[P^3 (d_2 f)\, n_i n_j n_l + P(d_1 f)\left\langle \delta_{ij} n_l \right\rangle_3 \right], \tag{5.20b}$$

$$\Gamma_{,ijlm} = \frac{1}{a_I a_J a_L a_M}\left[P^4 (d_3 f) n_i n_j n_l n_m + P^2 (d_2 f)\left\langle \delta_{ij} n_l n_m \right\rangle_6 + (d_1 f)\left\langle \delta_{ij}\delta_{lm} \right\rangle_3 \right], \tag{5.20c}$$

$$\Gamma_{,ijlmp} = \frac{1}{a_I a_J a_L a_M a_P}\left[P^5 (d_4 f) n_i n_j n_l n_m n_p + P^3 (d_3 f)\left\langle \delta_{ip} n_j n_l n_m \right\rangle_{10} + P(d_2 f)\left\langle \delta_{ij}\delta_{lm} n_p \right\rangle_{15} \right], \tag{5.20d}$$

where

$$\begin{aligned}
&d_1 f \equiv \frac{1}{P}\frac{d}{dP}\left(\frac{f}{P}\right) = \frac{1}{P^3}\left(Pf' - f\right), \quad d_2 f \equiv \frac{1}{P}\frac{d}{dP}(d_1 f) = \frac{1}{P^5}\left(P^2 f'' - 3Pf' + 3f\right), \\
&d_3 f \equiv \frac{1}{P}\frac{d}{dP}(d_2 f) = \frac{1}{P^7}\left(P^3 f''' - 6P^2 f'' + 15Pf' - 15f\right), \\
&d_4 f \equiv \frac{1}{P}\frac{d}{dP}(d_3 f) = \frac{1}{P^9}\left(P^4 f^{(4)} - 10P^3 f''' + 45P^2 f'' - 105Pf' + 105f\right), \\
&\left\langle \delta_{ij} n_l \right\rangle_3 \equiv \delta_{ij} n_l + \delta_{il} n_j + \delta_{jl} n_i, \quad \left\langle \delta_{ij}\delta_{lm} \right\rangle_3 \equiv \delta_{ij}\delta_{lm} + \delta_{il}\delta_{jm} + \delta_{im}\delta_{jl}, \\
&\left\langle \delta_{ij} n_l n_m \right\rangle_6 \equiv \delta_{ij} n_l n_m + \delta_{il} n_j n_m + \delta_{im} n_j n_l + \delta_{jl} n_i n_m + \delta_{jm} n_i n_l + \delta_{lm} n_i n_j, \\
&\left\langle \delta_{ip} n_j n_l n_m \right\rangle_{10} \equiv \delta_{ip} n_j n_l n_m + \delta_{jp} n_i n_l n_m + \delta_{lp} n_i n_j n_m + \delta_{mp} n_i n_j n_l + \delta_{lm} n_i n_j n_p + \delta_{im} n_j n_l n_p \\
&\qquad + \delta_{jm} n_i n_l n_p + \delta_{il} n_j n_m n_p + \delta_{jl} n_i n_m n_p + \delta_{ij} n_l n_m n_p, \\
&\left\langle \delta_{ij}\delta_{lm} n_p \right\rangle_{15} \equiv \delta_{ij}\delta_{lm} n_p + \delta_{il}\delta_{jm} n_p + \delta_{jl}\delta_{im} n_p + \delta_{jp}\delta_{lm} n_i + \delta_{ip}\delta_{lm} n_j + \delta_{im}\delta_{jp} n_l + \delta_{im}\delta_{lp} n_j + \delta_{jm}\delta_{lp} n_i \\
&\qquad + \delta_{ip}\delta_{jm} n_l + \delta_{il}\delta_{mp} n_j + \delta_{il}\delta_{jp} n_m + \delta_{jl}\delta_{mp} n_i + \delta_{ip}\delta_{jl} n_m + \delta_{ij}\delta_{mp} n_l + \delta_{ij}\delta_{lp} n_m,
\end{aligned} \tag{5.21}$$

with $n_i = x_i/(Pa_\mathrm{I})$ according to Eq. (5.19).

Note that Eqs. (5.20a–d) hold for both the interior and exterior cases, with f defined in Eq. (5.18c) and Eq. (5.18d), respectively. In Eq. (5.21), f', f'', f''' and $f^{(4)}$ denote, respectively, the first-, second-, third- and fourth-order derivatives of f with respect to P. For the interior case with $\mathbf{x} \in \Omega$, f', f'', f''' and $f^{(4)}$ can be obtained from Eq. (5.18c) by direct differentiation. For the exterior case with $\mathbf{x} \notin \Omega$, the use of Eq. (5.18d) leads to

$$
\begin{aligned}
f' &= -\frac{4}{\pi}L^2\left[\int_0^{2\pi}\left(\int_0^{\alpha}\frac{\partial^2 F^{(1)}}{\partial P^2}\sin\theta\, d\theta + \int_{\alpha}^{\pi/2}\frac{\partial^2 F^{(2)}}{\partial P^2}\sin\theta\, d\theta\right)d\varphi\right],\\
f'' &= -\frac{4}{\pi}L^2\left[\int_0^{2\pi}\left(\int_0^{\alpha}\frac{\partial^3 F^{(1)}}{\partial P^3}\sin\theta\, d\theta + \int_{\alpha}^{\pi/2}\frac{\partial^3 F^{(2)}}{\partial P^3}\sin\theta\, d\theta\right)d\varphi\right],\\
f''' &= -\frac{4}{\pi}L^2\left[\int_0^{2\pi}\left(\int_0^{\alpha}\frac{\partial^4 F^{(1)}}{\partial P^4}\sin\theta\, d\theta + \int_{\alpha}^{\pi/2}\frac{\partial^4 F^{(2)}}{\partial P^4}\sin\theta\, d\theta\right)d\varphi\right],\\
f^{(4)} &= -\frac{4}{\pi}L^2\left[\int_0^{2\pi}\left(\int_0^{\alpha}\frac{\partial^5 F^{(1)}}{\partial P^5}\sin\theta\, d\theta + \int_{\alpha}^{\pi/2}\frac{\partial^5 F^{(2)}}{\partial P^5}\sin\theta\, d\theta\right)d\varphi\right],
\end{aligned}
\tag{5.22}
$$

where $F^{(1)}$ and $F^{(2)}$ are defined in Eqs. (5.15a,b). In reaching Eq. (5.22) use has also been made of the result $[F^{(1)}-F^{(2)}]\big|_{\theta=\alpha}=0$, which enables the terms involving $\partial\alpha/\partial P$ to vanish.

Using Eqs. (5.20a,c) in Eq. (2.47b) then yields the gradient part of the Eshelby tensor as

$$
\begin{aligned}
S^G_{ijlm} = \frac{1}{8\pi(1-\nu)}\Bigg\{\Bigg[&\frac{2\nu}{a_I a_J}\left[P^2(d_1 f)n_i n_j + \frac{f}{P}\delta_{ij}\right]\delta_{lm} + (1-\nu)P^2(d_1 f)\left(\frac{\delta_{il}n_j n_m}{a_J a_M} + \frac{\delta_{jl}n_i n_m}{a_I a_M}\right.\\
&\left. + \frac{\delta_{im}n_j n_l}{a_J a_L} + \frac{\delta_{jm}n_i n_l}{a_I a_L}\right) + (1-\nu)\frac{f}{P}\left(\frac{\delta_{il}\delta_{jm}}{a_I a_L} + \frac{\delta_{il}\delta_{jm}}{a_J a_M} + \frac{\delta_{im}\delta_{jl}}{a_I a_M} + \frac{\delta_{im}\delta_{jl}}{a_J a_L}\right)\\
&- \frac{2L^2}{a_I a_J a_L a_M}\left[P^4(d_3 f)n_i n_j n_l n_m + P^2(d_2 f)\langle\delta_{ij}n_l n_m\rangle_6 + (d_1 f)\langle\delta_{ij}\delta_{lm}\rangle_3\right] + 2L^2\Lambda_{,ijlm}\Bigg\},
\end{aligned}
\tag{5.23}
$$

where $n_i = x_i/(Pa_1)$ from Eq (5.19), and P is defined in Eq. (5.18b).

Equation (5.23) applies to both the interior and exterior cases, but the expressions for $f(P)$ and $\Lambda_{,ijlm}$ are different in each case. For the interior case with $\mathbf{x}\in\Omega$, $f(P)$ is given in Eq. (5.18c) and $\Lambda_{,ijlm}=0$ (see Eq. (5.2c)), while for the exterior case with $\mathbf{x}\notin\Omega$, $f(P)$ is provided in Eq. (5.18d) and $\Lambda_{,ijlm}$ is obtained from Eq. (5.2d), after some lengthy algebra, as

$$
\begin{aligned}
\Lambda_{,ijlm} = 4\pi a_1 a_2 a_3\Bigg[&\frac{1}{\Delta Z}(\delta_{ij}\delta_{lm}\varpi_I\varpi_L + \delta_{il}\delta_{jm}\varpi_I\varpi_J + \delta_{im}\delta_{jl}\varpi_I\varpi_J) + 4x_i x_j x_l x_m N_{IJLM}\\
&+ 2(\delta_{ij}x_l x_m M_{ILM} + \delta_{il}x_j x_m M_{IJM} + \delta_{im}x_j x_l M_{IJL} + \delta_{jl}x_i x_m M_{IJM}\\
&+ \delta_{jm}x_i x_l M_{IJL} + \delta_{lm}x_i x_j M_{IJL})\Bigg],
\end{aligned}
\tag{5.24}
$$

where

$$M_{ILM} \equiv \varpi_I \varpi_L \varpi_M \frac{1}{\Delta Z^2}\left[-(\varpi_I+\varpi_L+\varpi_M)-\frac{1}{2}\vartheta+\frac{2\eta}{Z}\right], \tag{5.25a}$$

$$\begin{aligned} N_{IJLM} \equiv \varpi_I \varpi_J \varpi_L \varpi_M \frac{1}{\Delta Z^3}\Big[&(\varpi_I^2+\varpi_J^2+\varpi_L^2+\varpi_M^2)+(\varpi_I+\varpi_J+\varpi_L+\varpi_M)^2 \\ &+(\vartheta-\frac{6\eta}{Z})(\varpi_I+\varpi_J+\varpi_L+\varpi_M)+\frac{1}{4}\vartheta^2+\frac{1}{2}\varsigma-\frac{3(\eta\vartheta+2\beta)}{Z}+\frac{12\eta^2}{Z^2}\Big], \end{aligned} \tag{5.25b}$$

$$\varsigma \equiv \varpi_1{}^2+\varpi_2{}^2+\varpi_3{}^2, \quad \beta \equiv \varpi_1^4 x_1^2+\varpi_2^4 x_2^2+\varpi_3^4 x_3^2. \tag{5.25c,d}$$

From Eqs. (5.23)–(5.25a–d) it is seen that the gradient part of the Eshelby tensor, S^G_{ijlm}, is position-dependent inside and outside the ellipsoidal inclusion, since f, P, n_i, and $\Lambda_{,ijlm}$ (for the exterior case) involved in S^G_{ijlm} are all functions of **x**. This differs from the classical part, $S^{C,IN}_{ijlm}$, which is uniform inside the same inclusion.

Next, substituting Eqs. (5.20b,d) into Eq. (2.48) gives the fifth-order Eshelby-like tensor as

$$\begin{aligned} T_{ijlmp} = &\frac{L^2}{8\pi(1-\nu)}\frac{1}{a_I a_J a_L a_M a_P}\Big\{-2\nu\delta_{lm}a_L a_M\left[P^3(d_2 f)n_i n_j n_p+P(d_1 f)\left\langle\delta_{ip}n_j\right\rangle_3\right] \\ &-(1-\nu)P^3(d_2 f)(n_i n_m n_p\delta_{jl}a_J a_L+n_j n_m n_p\delta_{il}a_I a_L+n_i n_l n_p\delta_{jm}a_J a_M+n_j n_l n_p\delta_{im}a_I a_M) \\ &-(1-\nu)P(d_1 f)(\left\langle\delta_{ip}n_m\right\rangle_3\delta_{jl}a_J a_L+\left\langle\delta_{jm}n_p\right\rangle_3\delta_{il}a_I a_L+\left\langle\delta_{il}n_p\right\rangle_3\delta_{jm}a_J a_M+\left\langle\delta_{jl}n_p\right\rangle_3\delta_{im}a_I a_M) \\ &+2L^2\left[P^5(d_4 f)n_i n_j n_l n_m n_p+P^3(d_3 f)\left\langle\delta_{ip}n_j n_l n_m\right\rangle_{10}+P(d_2 f)\left\langle\delta_{ij}\delta_{lm}n_p\right\rangle_{15}\right]\Big\} \\ &+\frac{L^2}{8\pi(1-\nu)}\left[2\nu\Lambda_{,ijp}\delta_{lm}+(1-\nu)(\Lambda_{,imp}\delta_{jl}+\Lambda_{,jmp}\delta_{il}+\Lambda_{,ilp}\delta_{jm}+\Lambda_{,jlp}\delta_{im})-(2L^2\Lambda+\Phi)_{,ijlmp}\right], \end{aligned} \tag{5.26}$$

where $n_i = x_i/(Pa_1)$ from Eq (5.19), P is defined in Eq. (5.18b), and $\Lambda_{,ijp}$, $\Lambda_{,ijlmp}$, $\Phi_{,ijlmp}$ can be obtained from Eqs. (5.2a–d). Clearly, $T_{ijlmp} = 0$ whenever $L = 0$. That is, this fifth-order Eshelby-like tensor vanishes both inside and outside the ellipsoidal inclusion when the strain gradient effect is not considered.

Equation (5.26) is valid for both the interior and exterior cases, but the expressions

for $f(P)$, Λ and Φ are different in each case. For the interior case with $\mathbf{x} \in \Omega$, $f(P)$ is given in Eq. (5.18c) and the derivatives of Φ and Λ involved are obtained from Eqs. (5.2a,c) as

$$\Phi_{,ijlmp} = 0,\ \Lambda_{,ijp} = \Lambda_{,imp} = \Lambda_{,jmp} = \Lambda_{,ilp} = \Lambda_{,jlp} = 0,\ \ \Lambda_{,ijlmp} = 0. \tag{5.27}$$

For the exterior case with $\mathbf{x} \notin \Omega$, $f(P)$ is provided in Eq. (5.18d) and the derivatives of Φ and Λ are determined from Eqs. (5.2b,d), after some tedious derivations, as

$$\begin{aligned}
\frac{\Phi_{,ijlmp}}{4\pi a_1 a_2 a_3} = {} & \frac{\gamma\varpi_I}{\Delta Z}[\varpi_L\varpi_P\delta_{ij}\delta_{lm}x_p + \varpi_J\varpi_P(\delta_{il}\delta_{jm} + \delta_{im}\delta_{jl})x_p + \varpi_L\varpi_M\delta_{ij}\delta_{lp}x_m \\
& + \varpi_J\varpi_M(\delta_{il}\delta_{jp} + \delta_{ip}\delta_{jl})x_m + \varpi_J\varpi_L(\delta_{im}\delta_{jp} + \delta_{ip}\delta_{jm})x_l] \\
& + \delta_{ij}x_l\left[\frac{2a_I^2\varpi_I^2\varpi_L\varpi_M\varpi_P}{\Delta Z^2}x_m x_p + \gamma\varpi_I(\delta_{mp}\frac{\varpi_L\varpi_M}{\Delta Z} + 2x_m x_p M_{LMP})\right] \\
& + (\delta_{il}x_j + \delta_{jl}x_i)\left[\frac{2a_I^2\varpi_I^2\varpi_J\varpi_M\varpi_P}{\Delta Z^2}x_m x_p + \gamma\varpi_I(\delta_{mp}\frac{\varpi_J\varpi_M}{\Delta Z} + 2x_m x_p M_{JMP})\right] \\
& + (\delta_{im}x_j + \delta_{jm}x_i)\left[\frac{2a_I^2\varpi_I^2\varpi_J\varpi_L\varpi_P}{\Delta Z^2}x_l x_p + \gamma\varpi_I(\delta_{lp}\frac{\varpi_J\varpi_L}{\Delta Z} + 2x_l x_p M_{JLP})\right] \\
& + (\delta_{ip}x_j + \delta_{jp}x_i)\left[\frac{2a_I^2\varpi_I^2\varpi_J\varpi_L\varpi_M}{\Delta Z^2}x_l x_m + \gamma\varpi_I(\delta_{lm}\frac{\varpi_J\varpi_L}{\Delta Z} + 2x_l x_m M_{JLM})\right] \\
& + x_i x_j\left\{2a_I^2\left[\delta_{mp} - \frac{2\varpi_P}{Z}x_m x_p\left(2\varpi_I + \varpi_M + \varpi_P - \frac{2\eta}{Z}\right)\right]\frac{\varpi_I^2\varpi_J\varpi_L\varpi_M}{\Delta Z^2}x_l\right. \\
& + \frac{2a_I^2\varpi_I^2}{Z}\left[x_m\varpi_M(\delta_{lp}\frac{\varpi_J\varpi_L}{\Delta Z} + 2x_l x_p M_{JLP}) + x_p\varpi_P(\delta_{lm}\frac{\varpi_J\varpi_L}{\Delta Z} + 2x_l x_m M_{JLM})\right] \\
& \left. + 2\gamma\varpi_I\left(\delta_{mp}x_l M_{JLM} + \delta_{lp}x_m M_{JLM} + \delta_{lm}x_p M_{JLP} + 2x_l x_m x_p N_{JLMP}\right)\right\},
\end{aligned} \tag{5.28a}$$

$$\begin{aligned}
\Lambda_{,ijp} = {} & \frac{4\pi a_1 a_2 a_3}{\Delta Z}\left(\varpi_I\varpi_P\delta_{ij}x_p + \varpi_I\varpi_J\delta_{ip}x_j + \varpi_I\varpi_J\delta_{jp}x_i\right) \\
& + \frac{8\pi a_1 a_2 a_3}{\Delta Z^2}\varpi_I\varpi_J\varpi_P x_i x_j x_p\left[-\left(\varpi_I + \varpi_J + \varpi_P\right) - \frac{1}{2}\vartheta + \frac{2\eta}{Z}\right],
\end{aligned} \tag{5.28b}$$

$$\frac{\Lambda_{,ijlmp}}{4\pi a_1 a_2 a_3} = 2x_p(\delta_{ij}\delta_{lm}M_{ILP} + \delta_{il}\delta_{jm}M_{IJP} + \delta_{im}\delta_{jl}M_{IJP}) + 2x_i(\delta_{jm}\delta_{lp}M_{IJL} + \delta_{jp}\delta_{lm}M_{IJL} + \delta_{jl}\delta_{mp}M_{IJM}) + 2x_j(\delta_{il}\delta_{mp}M_{IJM} + \delta_{im}\delta_{lp}M_{IJL} + \delta_{ip}\delta_{lm}M_{IJL}) + 2x_m(\delta_{il}\delta_{jp}M_{IJM} + \delta_{jl}\delta_{ip}M_{IJM} + 2\delta_{ij}\delta_{lp}M_{ILM}) + 2x_l(\delta_{ip}\delta_{jm}M_{IJL} + \delta_{ij}\delta_{mp}M_{ILM} + \delta_{im}\delta_{jp}M_{IJL}) + 4\left(\delta_{ip}x_j x_l x_m + \delta_{jp}x_i x_l x_m + \delta_{lp}x_i x_j x_m + \delta_{mp}x_i x_j x_l\right)N_{IJLM} + 4(\delta_{ij}x_l x_m x_p N_{ILMP} + \delta_{il}x_j x_m x_p N_{IJMP} + \delta_{im}x_j x_l x_p N_{IJLP} + \delta_{jl}x_i x_m x_p N_{IJMP} + \delta_{jm}x_i x_l x_p N_{IJLP} + \delta_{lm}x_i x_j x_p N_{IJLP}) + 8x_i x_j x_l x_m x_p H_{IJLMP}, \tag{5.28c}$$

where

$$H_{IJLMP} \equiv -\frac{\varpi_I\varpi_J\varpi_L\varpi_M\varpi_P}{\Delta Z^4}\Bigg\{2(\varpi_I+\varpi_J+\varpi_L+\varpi_M+\varpi_P)^3 + (\frac{3}{2}\vartheta - \frac{24\eta}{Z})(\varpi_I+\varpi_J+\varpi_L+\varpi_M+\varpi_P)^2 - \left[\frac{60\eta^2}{Z^2} - \frac{12}{Z}(\eta\vartheta+2\beta) + \frac{3}{4}\vartheta^2 + \frac{3}{2}\varsigma\right](\varpi_I+\varpi_J+\varpi_L+\varpi_M+\varpi_P) + 6(\varpi_I^3+\varpi_J^3+\varpi_L^3+\varpi_M^3+\varpi_P^3) + (\frac{3}{2}\vartheta - \frac{12\eta}{Z})(\varpi_I^2+\varpi_J^2+\varpi_L^2+\varpi_M^2+\varpi_P^2) - \frac{120\eta^3}{Z^3} + \frac{30}{Z^2}\left(\eta^2\vartheta + 4\eta\beta\right) + \frac{1}{Z}\left[-3\eta\vartheta^2 - 12\beta\vartheta - 6\eta\varsigma - 24\left(x_1^2\varpi_1^5 + x_2^2\varpi_2^5 + x_3^2\varpi_3^5\right)\right] + \frac{3}{4}\vartheta\varsigma + \frac{1}{8}\vartheta^3 + \left(\varpi_1^3+\varpi_2^3+\varpi_3^3\right) - 6\left(\varpi_I\varpi_L\varpi_M + \varpi_J\varpi_L\varpi_M + \varpi_I\varpi_J\varpi_L + \varpi_I\varpi_J\varpi_M + \varpi_I\varpi_J\varpi_P + \varpi_J\varpi_L\varpi_P + \varpi_I\varpi_L\varpi_P + \varpi_I\varpi_M\varpi_P + \varpi_J\varpi_M\varpi_P + \varpi_L\varpi_M\varpi_P\right)\Bigg\}, \tag{5.28d}$$

and M_{IJK} and N_{IJKL} are given in Eqs. (5.25a,b).

Considering that S^G_{ijlm} is position-dependent inside the ellipsoidal inclusion, its volume average over the ellipsoidal region occupied by the inclusion is examined next. This averaged Eshelby tensor is needed for predicting the effective elastic properties of a heterogeneous composite containing ellipsoidal inhomogeneities.

The volume average of a sufficiently smooth function $F(\mathbf{x})$ over the ellipsoidal inclusion occupying region Ω is defined by, with the help of the coordinate transformation defined in Eq. (5.19),

$$\left\langle F(\mathbf{x})\right\rangle_{\mathrm{V}} = \frac{1}{\mathrm{Vol}(\Omega)}\iiint_{\Omega} F(\mathbf{x})dV = \frac{3}{4\pi}\int_0^1\int_0^{2\pi}\int_0^{\pi} F(\mathbf{x})P^2\sin\theta\, d\theta\, d\varphi\, dP, \tag{5.29}$$

where $dV = a_1 a_2 a_3 P^2 \sin\theta \, dP \, d\theta \, d\varphi$, with $P = |\mathbf{X}|$ (see Eq. (5.18b)). It then follows from Eqs. (2.47b), (5.2c) and (5.29) that

$$\left\langle S^G_{ijlm} \right\rangle_{\mathrm{V}} = \frac{1}{8\pi(1-\nu)} \Big[2\nu \left\langle \Gamma_{,ij} \right\rangle_{\mathrm{V}} \delta_{lm} + (1-\nu) \Big(\left\langle \Gamma_{,jm} \right\rangle_{\mathrm{V}} \delta_{il} + \left\langle \Gamma_{,im} \right\rangle_{\mathrm{V}} \delta_{jl} + \left\langle \Gamma_{,jl} \right\rangle_{\mathrm{V}} \delta_{im} + \left\langle \Gamma_{,il} \right\rangle_{\mathrm{V}} \delta_{jm} \Big) - 2L^2 \left\langle \Gamma_{,ijlm} \right\rangle_{\mathrm{V}} \Big], \tag{5.30}$$

where

$$\left\langle \Gamma_{,ij} \right\rangle_{\mathrm{V}} = \left(f\big|_{P=1} \right) \frac{\delta_{ij}}{a_I a_J}, \quad \left\langle \Gamma_{,ijlm} \right\rangle_{\mathrm{V}} = \frac{1}{5} \Big[(f'' + 2f' - 2f)\big|_{P=1} + (2f)\big|_{P=0} \Big] \frac{\left\langle \delta_{im} \delta_{jl} \right\rangle_3}{a_I a_J a_L a_M}, \tag{5.31a,b}$$

with f defined in Eq. (5.18c). Note that in reaching Eqs. (5.31a,b) use has been made of the integral identities given in Eq. (3.13). Using Eqs. (5.31a,b) in Eq. (5.30) finally gives

$$\begin{aligned} \left\langle S^G_{ijlm} \right\rangle_{\mathrm{V}} = \frac{1}{8\pi(1-\nu)} \Bigg\{ & 2\nu \left(f\big|_{P=1} \right) \frac{\delta_{ij}\delta_{lm}}{a_I a_J} + (1-\nu) \left(f\big|_{P=1} \right) \Bigg[\left(\frac{1}{a_I a_L} + \frac{1}{a_J a_M} \right) \delta_{il}\delta_{jm} \\ & + \left(\frac{1}{a_I a_M} + \frac{1}{a_J a_L} \right) \delta_{im}\delta_{jl} \Bigg] - \frac{2L^2}{5} \Big[(f'' + 2f' - 2f)\big|_{P=1} + (2f)\big|_{P=0} \Big] \frac{\left\langle \delta_{il}\delta_{jm} \right\rangle_3}{a_I a_J a_L a_M} \Bigg\} \end{aligned} \tag{5.32}$$

as the average of the gradient part of the Eshelby tensor over the ellipsoidal inclusion Ω. It can be readily shown that for the spherical inclusion case with $a_1 = a_2 = a_3 = R$, Eq. (5.32) recovers the closed-form expression of $\left\langle S^G_{ijlm} \right\rangle_{\mathrm{V}}$ derived in Eq. (3.18).

Since $S^{C,IN}_{ijlm}$ is uniform inside the inclusion, the use of Eqs. (5.5) and (5.29) gives $\left\langle S^{C,IN}_{ijlm} \right\rangle_{\mathrm{V}} = S^{C,IN}_{ijlm}$. It then follows from Eqs. (2.44a), (5.5) and (5.32) that

$$\begin{aligned} \left\langle S_{ijlm} \right\rangle_{\mathrm{V}} = \frac{1}{8\pi(1-\nu)} \Bigg\{ & \left[2\nu I_I(0) - I_L(0) + a_I^2 I_{IL}(0) + \frac{2\nu \left(f\big|_{P=1} \right)}{a_I a_J} \right] \delta_{ij}\delta_{lm} \\ & + \Big[(1-\nu) I_L(0) + (1-\nu) I_M(0) - I_J(0) + a_I^2 I_{IJ}(0) \Big] \left(\delta_{il}\delta_{jm} + \delta_{im}\delta_{jl} \right) \\ & + (1-\nu) \left(f\big|_{P=1} \right) \Bigg[\left(\frac{1}{a_I a_L} + \frac{1}{a_J a_M} \right) \delta_{il}\delta_{jm} + \left(\frac{1}{a_I a_M} + \frac{1}{a_J a_L} \right) \delta_{im}\delta_{jl} \Bigg] \\ & - \frac{2L^2}{5} \Big[(f'' + 2f' - 2f)\big|_{P=1} + (2f)\big|_{P=0} \Big] \frac{\left\langle \delta_{il}\delta_{jm} \right\rangle_3}{a_I a_J a_L a_M} \Bigg\} \end{aligned} \tag{5.33}$$

as the volume average of the Eshelby tensor inside the ellipsoidal inclusion based on the SSGET. In Eq. (5.33), $I_I(0)$ and $I_{LJ}(0)$ are constants obtainable from Eqs. (5.3a,b), and $f = f(P)$ is defined in Eq. (5.18c). Clearly, when $L = 0$, Eq. (5.33) reduces to $\left\langle S_{ijlm}^{C,IN} \right\rangle_{\mathrm{V}} = S_{ijlm}^{C,IN}$ given in Eq. (5.5), since $f(P) \equiv 0$ for any value of P (> 0) when $L = 0$ (see Eq. (5.18c)).

The volume average of T_{ijlmp} for $\mathbf{x}$ locating inside the ellipsoidal inclusion (i.e., $\mathbf{x} \in \Omega$) can be readily shown to vanish, i.e.,

$$\left\langle T_{ijlmp}(\mathbf{x}) \right\rangle_{\mathrm{V}} = \frac{1}{\mathrm{Vol}(\Omega)} \iiint_{\Omega} T_{ijlmp}(\mathbf{x}) dV = \frac{3}{4\pi} \int_0^1 \int_0^{2\pi} \int_0^{\pi} T_{ijlmp} P^2 \sin\theta d\theta d\phi dP \equiv 0. \quad (5.34)$$

This is based on the fact that $T_{ijlmp}(\mathbf{x})$ involved in Eq. (5.34), which is to be substituted from Eqs. (5.26) and (5.27), contains the components of the unit normal vector $\mathbf{n} = n_i \mathbf{e}_i = (\sin\theta\cos\phi)\mathbf{e}_1 + (\sin\theta\sin\phi)\mathbf{e}_2 + (\cos\theta)\mathbf{e}_3$ on the unit sphere surface $|\mathbf{X}| = 1$ through n_i, $n_i n_j n_l$ and $n_i n_j n_l n_m n_p$, which satisfy the following integral identities:

$$\int_0^{2\pi} \int_0^{\pi} n_i \sin\theta d\theta d\phi = 0, \quad \int_0^{2\pi} \int_0^{\pi} n_i n_j n_l \sin\theta d\theta d\phi = 0, \quad \int_0^{2\pi} \int_0^{\pi} n_i n_j n_l n_m n_p \sin\theta d\theta d\phi = 0. \quad (5.35)$$

It then follows from Eqs. (2.40), (5.29) and (5.34) that

$$\left\langle \varepsilon_{ij} \right\rangle_{\mathrm{V}} = \left\langle S_{ijlm} \right\rangle_{\mathrm{V}} \varepsilon_{lm}^{*}, \quad (5.36)$$

where $\left\langle S_{ijlm} \right\rangle_{\mathrm{V}}$ is given in Eq. (5.33). Equation (5.36) shows that the average disturbed strain is only related to the eigenstrain $\boldsymbol{\varepsilon}^*$ even in the presence of the eigenstrain gradient $\boldsymbol{\kappa}^*$.

5.3. Numerical Results

To quantitatively illustrate how the newly derived Eshelby tensor changes with the position and inclusion size, some numerical results are presented in this section.

Figure 5.2 shows the distribution of $S_{3333} = S_{3333}^{C} + S_{3333}^{G}$ along the x_3 axis (with $x_1 =$

$0 = x_2$) for four different values of a_3, where the values of S^C_{3333} and S^G_{3333} are, respectively, obtained from Eqs. (5.5) and (5.23), with $f(P)$ given in Eq. (5.18c) and $\Lambda_{,ijlm} = 0$ from Eq. (5.2c). For comparison, the value of the counterpart component of the classical Eshelby tensor, which is the same as S^C_{3333}, is also displayed in Fig. 5.2, where $\alpha_1 = a_1/a_3$ and $\alpha_2 = a_2/a_3$ are the two aspect ratios of the ellipsoidal inclusion.

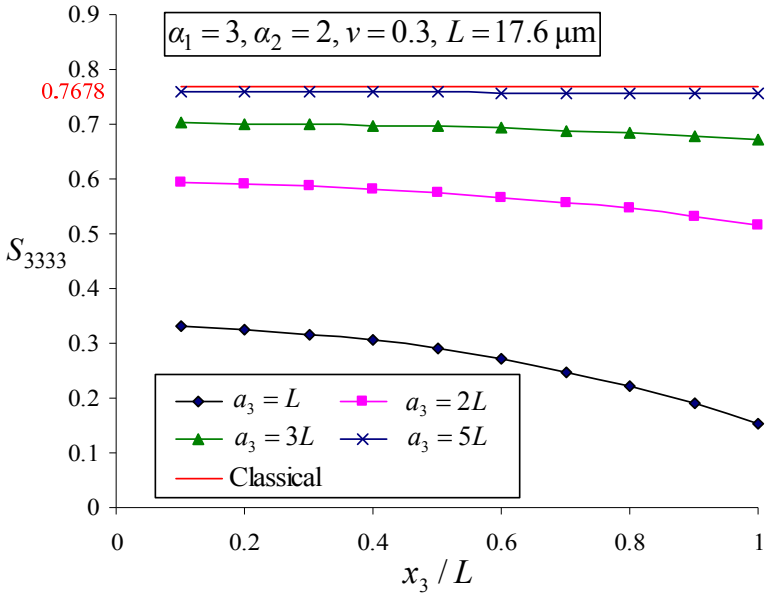

Fig. 5.2. S_{3333} along the x_3 axis of the ellipsoidal inclusion.

From Fig. 5.2 it is observed that S_{3333} varies with the position (with $x_1 = x_2 = 0$, $x = x_3$) and depends on the inclusion size (a_3), unlike its classical part S^C_{3333} which, for the specified values of the aspect ratios α_1 and α_2, is a constant independent of both x_3 and a_3 (i.e., $S^C_{3333} = 0.7678$ from Eq. (5.5), as shown). When a_3 is small (with $a_3 = L = 17.6$ μm here), S_{3333} is much smaller than S^C_{3333}, which indicates that the magnitude of $S^G_{3333} (= S_{3333} - S^C_{3333})$ is very large and the strain gradient effect is significant. However,

when a_3 is much greater than L (e.g., $R = 5L = 88.0$ μm shown here), S_{3333} is seen to be quite uniform and its value approaches S^C_{3333} from below, meaning that the magnitude of S^G_{3333} is very small. This indicates that for large inclusions the strain gradient effect is insignificant and may be neglected. Similar trends have been observed for other components of S_{ijlm} $(= S^C_{ijlm} + S^G_{ijlm})$.

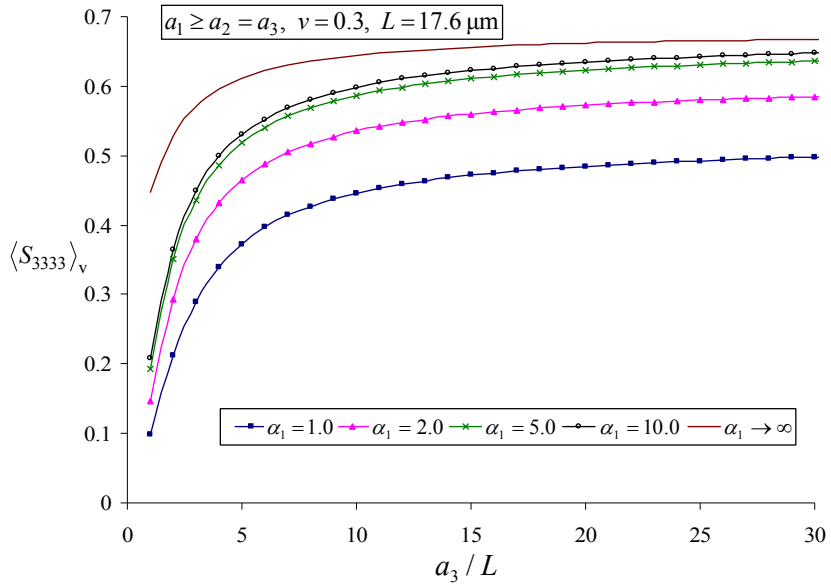

Fig. 5.3. $\langle S_{3333} \rangle_V$ changing with the inclusion size for different aspect ratio values.

The variation of the component of the averaged Eshelby tensor inside the ellipsoidal inclusion, $\langle S_{3333} \rangle_V$, with the inclusion size a_3 is shown in Figs. 5.3 and 5.4. In Fig. 5.3, the spherical inclusion and the cylindrical inclusion cases are included as two limiting cases of the ellipsoidal inclusion problem solution with $\alpha_1 = 1$ and with $\alpha_1 \to \infty$, respectively. Note that $\langle S_{3333} \rangle_V$ is obtained from Eq. (5.33) for all cases displayed in Figs. 5.3 and 5.4.

For the spherical inclusion (with $\alpha_1 = 1 = \alpha_2$) and cylindrical inclusion (with $\alpha_1 \to$

∞ and $\alpha_2 = 1$) cases, the numerical results of $\langle S_{3333} \rangle_V$ obtained using Eq. (5.33) and shown in Fig. 5.3 are almost identical to those determined using the closed-form formulas derived in Eqs. (3.18) and (4.29). Moreover, it is clearly seen from Fig. 5.3 that the spherical inclusion case having $\alpha_1 = 1 = \alpha_2$ provides a lower bound, while the cylindrical inclusion case having $\alpha_1 \to \infty$ and $\alpha_2 = 1$ furnishes an upper bound for the ellipsoidal (spheroidal) inclusion cases with $1 < \alpha_1 < \infty$ (and $\alpha_2 = 1$), as expected. These facts verify and support the current analysis of the ellipsoidal inclusion problem.

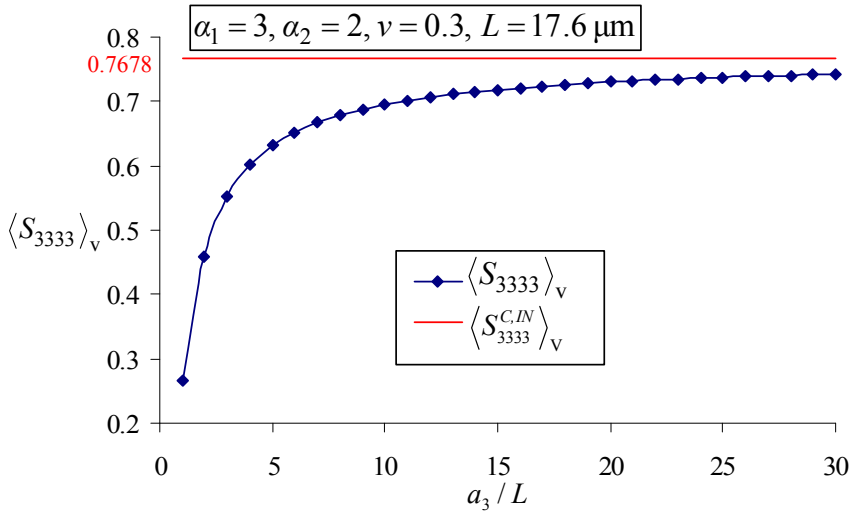

Fig. 5.4. Comparison of $\langle S_{3333} \rangle_V$ and $\langle S_{3333}^{C,IN} \rangle_V$.

It is observed from Fig. 5.3 that $\langle S_{3333} \rangle_V$ is indeed varying with the inclusion size for all five cases considered: the smaller a_3, the smaller $\langle S_{3333} \rangle_V$. This size effect is seen to be significant when the inclusion is small (with $a_3/L < 10$ or $a_3 < 176$ μm here). However, as the inclusion size increases, $\langle S_{3333} \rangle_V$ in each case approaches from below the corresponding value of $\langle S_{3333}^{C,IN} \rangle_V$ ($= S_{3333}^{C,IN}$) based on classical elasticity, which, for given

values of the aspect ratios, is a constant independent of a_3, as discussed in Section 5.2. This comparison is further illustrated in Fig. 5.4, where it is shown that the classical Eshelby tensor component, as a constant (i.e., $\left\langle S_{3333}^{C,IN} \right\rangle_{\mathrm{V}} = 0.7678$ from Eq. (5.5) for $\alpha_1 = 3$ and $\alpha_2 = 2$), cannot explain the inclusion size effect.

5.4. Summary

The Eshelby problem of an ellipsoidal inclusion (with three distinct semi-axes) in an infinite homogeneous isotropic elastic material is analytically solved by using a simplified strain gradient elasticity theory (SSGET) that involves one material length scale parameter. Analytical expressions for the Eshelby tensor are derived for both the interior and exterior cases in terms of two line integrals with an unbounded upper limit and two surface integrals over a unit sphere.

The newly obtained fourth-order Eshelby tensor for each case consists of two parts: a classical part depending only on Poisson's ratio, and a gradient part depending on the length scale parameter additionally. As a result, the new Eshelby tensor based on the SSGET can capture the inclusion size effect, unlike its classical counterpart. The fourth-order Eshelby tensor is accompanied by a fifth-order Eshelby-like tensor that links the eigenstrain gradient to the disturbed strain and contains only a gradient part. In the absence of the microstructure-dependent strain gradient effect, both the gradient part of the Eshelby tensor and the Eshelby-like tensor vanish, and the non-classical Eshelby tensor is reduced to that based on classical elasticity. Moreover, the Eshelby tensors for the spherical and cylindrical inclusion problems based on the SSGET are included in the current Eshelby tensor as two limiting cases.

In addition, the newly obtained Eshelby tensor inside or outside the ellipsoidal inclusion depends on the position, differing from the classical Eshelby tensor that is uniform inside the inclusion. This necessitates the determination of the volume average of the new Eshelby tensor over the ellipsoidal inclusion needed in homogenization analyses, which is done analytically in this study.

To further illustrate the newly derived non-classical Eshelby tensor, sample numerical results are provided. These results reveal that the non-classical Eshelby tensor varies with both the position and the inclusion size, thereby capturing the size effect at the micron scale, unlike the classical Eshelby tensor. The components of the averaged Eshelby tensor are found to decrease as the inclusion size decreases, and these components are observed to approach (from below) the values of the corresponding components of the Eshelby tensor based on classical elasticity when the inclusion size is large enough.

CHAPTER VI

SOLUTION OF AN ESHELBY-TYPE INCLUSION PROBLEM WITH A BOUNDED DOMAIN AND THE ESHELBY TENSOR FOR A SPHERICAL INCLUSION IN A FINITE SPHERICAL MATRIX

6.1. Introduction

In the last four chapters, the Eshelby tensor for an inclusion embedded in an infinite homogeneous isotropic elastic body is obtained using the simplified strain gradient elastic theory (SSGET). This non-classical Eshelby tensor contains a material length scale parameter and, therefore, is capable of explaining the microstructure-dependent size effect in the composites at the micro- or nano- scale. However, both the classical Eshelby tensor and the newly derived non-classical Eshelby tensor are for an inclusion embedded in an *infinite* elastic matrix. This implies that the disturbed displacement due to the inclusion makes no influence on the displacement at the boundary of the elastic body, and vice versa. Consequently, these Eshelby tensors and the subsequent homogenization methods cannot account for the boundary effect of a finite body. Hence, there has been a need to obtain the Eshelby tensor for an inclusion in a *finite* matrix subject to traction, displacement or mixed boundary conditions.

A few analytical studies have been performed using *classical elasticity* to solve the problem of an inclusion in a *finite* homogeneous isotropic elastic body. Kinoshita and Mura

(1984) provided the first theoretical study of the finite-domain inclusion problem based on classical elasticity. They proved the existence and uniqueness of the Neumann tensor for a bounded homogeneous elastic body, which reduces to the Green's function (also a second-order tensor) when the body is unbounded. The use of this Neumann tensor would then lead to solutions of finite-domain eigenstrain problems. However, the determination of the Neumann tensor for a bounded elastic body is rather challenging, and only the Neumann tensor for a half space was given in Kinoshita and Mura (1984). By using a displacement method in classical elasticity and solving the boundary-value problems directly, Luo and Weng (1987) determined the elastic field in a spherically concentric three-phase solid consisting of an inclusion, an interphase layer, and an infinite matrix. The presence of the finite interphase layer between the inclusion and matrix enabled a modification of the Mori-Tanaka method, but no explicit expression of Eshelby tensor for the modified problem was provided there. More recently, Eshelby tensor for a spherical inclusion in a finite spherical elastic matrix was analytically obtained in Li et al. (2007) by using Somigliana's identity and Green's function for an infinite three-dimensional (3-D) elastic body in classical elasticity. In contrast, no analytical solution has been provided for the finite-domain inclusion problem using any higher-order elasticity theory. This motivated the current study.

In the present chapter, a solution for the Eshelby inclusion problem of a finite homogeneous isotropic elastic body containing an inclusion prescribed with a uniform eigenstrain and a uniform eigenstrain gradient is first derived in a general form. It makes use of an extended Betti's reciprocal theorem and an extended Somigliana's identity based on a simplified strain gradient elasticity theory elaborated in Gao and Park (2007), which involves only one material length scale parameter and has been successfully employed to obtain analytical solutions of several problems (e.g., Gao and Ma, 2009; Gao et al., 2009;

Ma and Gao, 2009). The problem of a spherical inclusion embedded concentrically in a finite spherical elastic body is then analytically solved by applying the general solution, with the Eshelby tensor and its volume average derived in closed forms.

The rest of this chapter is organized as follows. In Section 6.2, an extended Betti's reciprocal theorem is first proposed and proved. It is then followed by the derivation of a general solution for the finite-domain Eshelby inclusion problem based on this reciprocal theorem and an extended Somigliana's identity that arises subsequently. The finite-domain spherical inclusion problem is solved in Section 6.3 by using the general formulas derived in Section 6.2, which leads to closed-form expressions of the Eshelby tensor and its volume average. In Section 6.4, sample numerical results are presented to quantitatively show how the components of the Eshelby tensor obtained in Section 6.3 vary with the position, inclusion size, matrix size, and inclusion volume fraction, where the size and boundary effects are observed and discussed. The chapter concludes with a summary in Section 6.5.

6.2. Strain Gradient Solution of Eshelby's Inclusion Problem in a Finite Domain

6.2.1. Extended Betti's reciprocal theorem

For an elastic body satisfying the SSGET reviewed in Section 2.1, Betti's first reciprocal theorem in classical elasticity (e.g., Sadd, 2009) can be extended to

$$\int_{\Omega}\left[\tau_{ij}^{(I)}\varepsilon_{ij}^{(II)}+\mu_{ijk}^{(I)}\kappa_{ijk}^{(II)}\right]dV=\int_{\Omega}\left[\tau_{ij}^{(II)}\varepsilon_{ij}^{(I)}+\mu_{ijk}^{(II)}\kappa_{ijk}^{(I)}\right]dV\,, \tag{6.1}$$

where the superscripts "(*I*)" and "(*II*)" represent two loading sets, and Ω is the region occupied by the elastic body.

To prove this extended Betti's reciprocal theorem based on the SSGET, it is noted that the second term in the strain energy density function on each side of Eq. (6.1), which is

absent in classical elasticity, is required in the SSGET (see Eq. (2.4)). Also,

$$\begin{aligned}\tau_{ij}^{(I)}\varepsilon_{ij}^{(II)} &= C_{ijkl}\varepsilon_{kl}^{(I)}\varepsilon_{ij}^{(II)} = C_{klij}\varepsilon_{ij}^{(II)}\varepsilon_{kl}^{(I)} = \tau_{kl}^{(II)}\varepsilon_{kl}^{(I)},\\ \mu_{ijk}^{(I)}\kappa_{ijk}^{(II)} &= L^2 C_{ijmn}\kappa_{mnk}^{(I)}\kappa_{ijk}^{(II)} = L^2 C_{mnij}\kappa_{ijk}^{(II)}\kappa_{mnk}^{(I)} = \mu_{mnk}^{(II)}\kappa_{mnk}^{(I)},\end{aligned} \tag{6.2}$$

where use has been made of Eqs. (2.5a,b) and the major symmetry of the stiffness tensor (i.e., $C_{ijkl} = C_{klij}$). Substituting Eq. (6.2) into the left hand side of Eq. (6.1) will immediately give the right hand side of Eq. (6.1), thereby proving Eq. (6.1).

Physically, the extended Betti's theorem expressed in Eq. (6.1) states that the strain energy in the elastic body induced by the loading set (*I*) through the displacement field caused by the loading set (*II*) is equal to that induced by the loading set (*II*) through the displacement field caused by loading set (*I*).

Using Eqs. (2.5a–d) and (2.7) gives, with the help of the divergence theorem,

$$\int_\Omega \left[\tau_{ij}^{(I)}\varepsilon_{ij}^{(II)} + \mu_{ijk}^{(I)}\kappa_{ijk}^{(II)}\right]dV = -\int_\Omega \sigma_{ij,j}^{(I)}u_i^{(II)}dV + \int_{\partial\Omega}\left[t_i^{(I)}u_i^{(II)} + q_i^{(I)}u_{i,l}^{(II)}n_l\right]dA \tag{6.3}$$

for any region Ω bounded by a smooth surface $\partial\Omega$ (without any edge), where $\mathbf{n} = n_i\mathbf{e}_i$ is the outward unit normal vector on $\partial\Omega$, and t_i and q_i are, respectively, the Cauchy traction and double stress traction defined by (Gao and Park, 2007),

$$t_i = \sigma_{ij}n_j - (\mu_{ijk}n_k)_{,j} + (\mu_{ijk}n_k n_l)_{,l}n_j, \quad q_i = \mu_{ijk}n_j n_k. \tag{6.4a,b}$$

With the help of Eq. (6.3), Eq. (6.1) can be rewritten as

$$-\int_\Omega \sigma_{ij,j}^{(I)}u_i^{(II)}dV + \int_{\partial\Omega}\left[t_i^{(I)}u_i^{(II)} + q_i^{(I)}u_{i,l}^{(II)}n_l\right]dA = -\int_\Omega \sigma_{ij,j}^{(II)}u_i^{(I)}dV + \int_{\partial\Omega}\left[t_i^{(II)}u_i^{(I)} + q_i^{(II)}u_{i,l}^{(I)}n_l\right]dA. \tag{6.5}$$

Eq. (6.5), as the extended Betti's second reciprocal theorem based on the SSGET, will be directly used to derive the solution of the finite-domain inclusion problem next.

6.2.2. Extended Somigliana's identity and solution of Eshelby's inclusion problem in a finite domain

Consider an inclusion Ω_I of arbitrary shape embedded in a finite homogeneous isotropic elastic body Ω of arbitrary shape, as shown in Fig.6.1(a). A uniform eigenstrain $\boldsymbol{\varepsilon}^*$ and a uniform eigenstrain gradient $\boldsymbol{\kappa}^*$ are independently prescribed inside the inclusion, as discussed in Section 2.4. Besides $\boldsymbol{\varepsilon}^*$ and $\boldsymbol{\kappa}^*$, there is no body force or surface force acting in the elastic body containing the inclusion. Hence, the displacement, strain and stress fields induced by the presence of $\boldsymbol{\varepsilon}^*$ and $\boldsymbol{\kappa}^*$ here are disturbed fields, which may be superposed to those caused by applied body and/or surface forces.

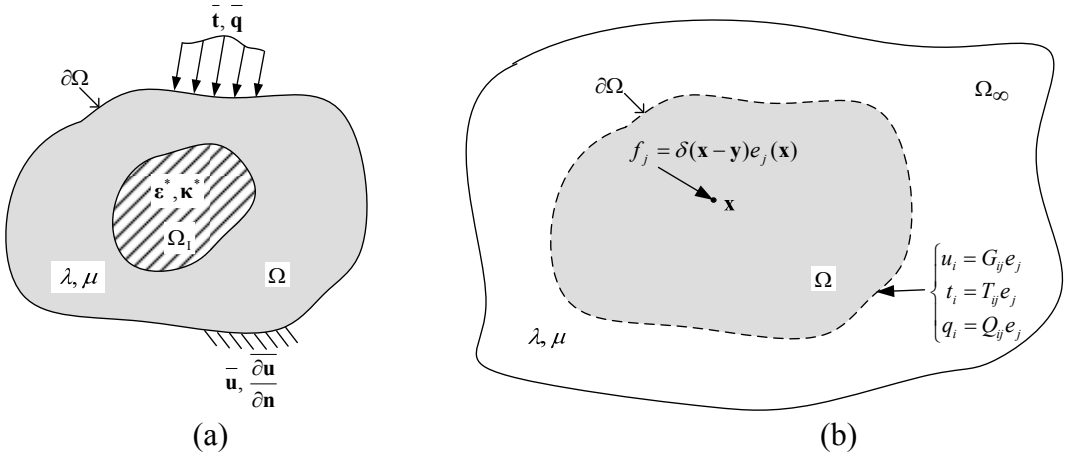

Fig. 6.1. Inclusion in a finite elastic body.

According to the derivation in Section 2.4, in the absence of body forces, the equations of equilibrium for this inclusion problem can be written as (See Eq. (2.32))

$$C_{ijkl}\,(\varepsilon_{kl} - L^2\kappa_{klp,p})_{,j} - C_{ijkl}\,(\varepsilon^*_{kl,j} - L^2\kappa^*_{klp,pj}) = 0\,. \tag{6.6}$$

It can be seen from comparing Eqs. (2.7) and (6.6) that Eq. (2.7) will be the same as Eq. (6.6) if the total stress σ_{ij} and the body force f_j in Eq. (2.7) are, respectively, replaced by

$$\sigma_{ij} = C_{ijkl}(\varepsilon_{kl} - L^2 \kappa_{klp,p}), \tag{6.7}$$

$$f_i = -C_{ijkl}(\varepsilon^*_{kl,j} - L^2 \kappa^*_{klp,pj}). \tag{6.8}$$

The total stress expression listed in Eq. (6.7) is exactly what is given by Eqs. (2.5a,b) and (2.7). Hence, Eqs. (2.7), (6.7) and (6.8) can be used as an alternative to the equilibrium equations provided in Eq. (6.6).

On the other hand, consider an infinite homogeneous isotropic elastic body Ω_∞ subject to a unit concentrated body force applied at point **x**, as shown in Fig.6.1(b). Substituting the special body force $f_i(\mathbf{y}) = \delta(\mathbf{x} - \mathbf{y})e_i(\mathbf{x})$ into Eq. (2.7), leads to the equilibrium equations for this point-force problem as

$$\sigma_{ij,j}(\mathbf{y}) + \delta(\mathbf{x}-\mathbf{y})\, e_i(\mathbf{x}) = 0, \tag{6.9}$$

where $\delta(\mathbf{x}-\mathbf{y})$ is the 3-D Dirac delta function, and $e_i(\mathbf{x})$ is the ith component of the unit force. Note that the Green's function $\mathbf{G}(\mathbf{x}-\mathbf{y})$ in the SSGET, given in Eq. (2.28) and (2.29) is a second-order tensor whose component $G_{ij}(\mathbf{x}-\mathbf{y})$ represents the displacement component u_i at point **y** in a 3-D infinite elastic body due to a unit concentrated body force applied at point **x** in the body in the jth direction. That is, $G_{ij}(\mathbf{x}-\mathbf{y})$ (= $G_{ji}(\mathbf{x}-\mathbf{y})$) satisfies the equilibrium equations in Eq. (6.9). Actually, the use of this Green's function will give the solution of the this concentrated-force problem based on the SSGET for the displacement, stress, traction and double stress traction at point **y** in the 3-D infinite elastic body due to the unit concentrated body force applied at point **x** (see Eqs. (6.11a–c)).

The complete boundary conditions in the SSGET have been derived in Gao and Park (2007) using a variational formulation. Two typical kinds of such boundary conditions are the Dirichlet-like boundary conditions:

$$u_i = \overline{u_i}, \quad u_{i,l} n_l = \overline{\frac{\partial u_i}{\partial n}} \quad \text{on} \quad \partial\Omega, \tag{6.10a}$$

i.e., the displacement and displacement gradient are specified on the smooth boundary $\partial\Omega$, and the Neumann-like boundary conditions:

$$t_i = \overline{t_i}, \quad q_i = \overline{q_i} \quad \text{on} \quad \partial\Omega, \tag{6.10b}$$

i.e., the Cauchy traction and double stress traction are specified on $\partial\Omega$. For the inclusion problem under consideration, the disturbed displacement, strain and stress fields due to $\boldsymbol{\varepsilon}^*$ and $\boldsymbol{\kappa}^*$ can be obtained by setting the prescribed field quantities on $\partial\Omega$ to zero (i.e., using homogeneous boundary conditions), as was done in Li et al. (2007) in the context of classical elasticity.

To solve the finite-domain inclusion problem satisfying Eqs. (6.6) and (6.10a) or Eqs. (6.6) and (6.10b), the extended Betti's theorem expressed in Eq. (6.5) can be used. The loading by $\boldsymbol{\varepsilon}^*$ and $\boldsymbol{\kappa}^*$ in the current inclusion problem shown Fig. 6.1(a) is taken to be the loading set (*II*), while that by a unit concentrated body force applied at a point inside a finite elastic body identical to that of Ω (see Fig. 6.1(b)) as the loading set (*I*). For the latter, the finite elastic body is cut out of an infinite body Ω_∞ having the same elastic properties (λ and μ), and the displacement, Cauchy traction and double stress traction at any point $\mathbf{y}$ on the boundary (cutting surface) $\partial\Omega$ are respectively given by

$$u_i(\mathbf{y}) = G_{ij}(\mathbf{x}-\mathbf{y}) e_j(\mathbf{x}), \tag{6.11a}$$

$$t_i(\mathbf{y}) = T_{ij}(\mathbf{x}-\mathbf{y}) e_j(\mathbf{x}), \tag{6.11b}$$

$$q_i(\mathbf{y}) = Q_{ij}(\mathbf{x}-\mathbf{y}) e_j(\mathbf{x}), \tag{6.11c}$$

where $G_{ij}(\mathbf{x} - \mathbf{y})$ is the 3-D Green's function based on the SSGET listed in Eq. (2.28), and $T_{ij}(\mathbf{x} - \mathbf{y})$ and $Q_{ij}(\mathbf{x} - \mathbf{y})$ are, respectively, the second-order Cauchy traction and double stress traction transformation tensors related to the Green's function $G_{ij}(\mathbf{x} - \mathbf{y})$, which lead

to, respectively, the traction and double stress traction in the *i*th direction at point **y** due to the unit concentrated body force applied in the *j*th direction at point **x**. The expressions of $T_{ij}(\mathbf{x}-\mathbf{y})$ and $Q_{ij}(\mathbf{x}-\mathbf{y})$ based on the SSGET can be obtained from Eqs. (6.11a), (2.5a–d) (2.7) and (6.4a,b) as (see Appendix F)

$$\begin{aligned}
T_{ik} &= \frac{1}{32\pi\mu(1-\nu)}\left[\lambda(A-B_{,mm})_{,k}n_i+\mu(A_{,i}n_k+A_{,j}\delta_{ik}n_j-2B_{,ijk}n_j)\right]\\
&+\frac{L^2}{32\pi\mu(1-\nu)}\Big\{-\lambda[\nabla^2(A-B_{,mm})_{,k}n_i+(A-B_{,mm})_{,ikp}n_p-(A-B_{,mm})_{,kpl}n_in_pn_l]\\
&-\mu[\nabla^2(A_{,i}n_k)+\nabla^2(A_{,j}\delta_{ik}-2B_{,ijk})n_j+(A_{,ipk}+\nabla^2A_{,p}\delta_{ik}-2\nabla^2B_{,ikp})n_p\\
&-A_{,ipl}n_kn_pn_l-(A\delta_{ik}-2B_{,ik})_{,jpl}n_jn_pn_l]\Big\}+\frac{L^2}{32\pi\mu(1-\nu)}[\lambda(A-B_{,mm})_{,kp}\delta_{ij}\\
&+\mu(A_{,ip}\delta_{jk}+A_{,jp}\delta_{ik}-2B_{,ijkp})](-n_{p,j}+n_{p,l}n_ln_j+n_pn_{l,l}n_j),
\end{aligned} \tag{6.12a}$$

$$Q_{ik}=\frac{L^2}{32\pi\mu(1-\nu)}\left[\lambda(A-B_{,mm})_{,kp}\delta_{ij}+\mu(A_{,ip}\delta_{jk}+A_{,jp}\delta_{ik}-2B_{,ijkp})\right]n_jn_p, \tag{6.12b}$$

where $A = A(r)$ and $B = B(r)$ are defined in Eqs. (2.29). When $L = 0$, T_{ik} and Q_{ik} in Eqs. (6.12a,b) reduce to

$$T_{ik}^C=\frac{1}{8\pi(1-\nu)r^3}\left\{(1-2\nu)(r_kn_i-r_in_k)+r_jn_j\left[(2\nu-1)\delta_{ik}-\frac{3r_ir_k}{r^2}\right]\right\},\quad Q_{ik}^C=0, \tag{6.12c,d}$$

which are the traction transformation tensors based on classical elasticity. It can be readily shown that Eq. (6.12c) is the same as that provided in Paris and Canas (1997) (see Eq. (5.4.20) there).

Using Eqs. (2.7), (6.7–6.9) and (6.11a–c) in Eq. (6.5) yields, with the help of the divergence theorem, the disturbed displacement field at any point $\mathbf{x} \in \Omega$ for the finite domain inclusion problem as

$$\begin{aligned}
u_m^{(II)}(\mathbf{x}) &= \int_\Omega C_{ijkl}\left[G_{im,j}(\mathbf{x}-\mathbf{y})\varepsilon_{kl}^*(\mathbf{y})+L^2G_{im,jp}(\mathbf{x}-\mathbf{y})\kappa_{klp}^*(\mathbf{y})\right]dV_y\\
&-\int_{\partial\Omega}\left[T_{im}(\mathbf{x}-\mathbf{y})u_i^{(II)}(\mathbf{y})+Q_{im}(\mathbf{x}-\mathbf{y})u_{i,l}^{(II)}(\mathbf{y})n_l(\mathbf{y})\right]dA_y\\
&+\int_{\partial\Omega}\left[G_{im}(\mathbf{x}-\mathbf{y})t_i^{(II)}+G_{im,l}(\mathbf{x}-\mathbf{y})q_i^{(II)}n_l(\mathbf{y})\right]dA_y,
\end{aligned} \tag{6.13}$$

where the derivatives are with respective to **y** (the integration variable), and use has been made of the fact that the eigenstrain and eigenstrain gradient vanish on the boundary of the finite body $\partial\Omega$, which is outside the inclusion. It is seen from Eq. (6.13) that the displacement contains contributions from field quantities distributed both in the volume Ω and on its surface $\partial\Omega$. If the two surface integrals in Eq. (6.13) are suppressed, the disturbed displacement field given in Eq. (6.13) reduces to that for the problem of an inclusion in an infinite elastic body based on the SSGET (see Eq. (2.34)). This means that the two surface integrals in Eq. (6.13) represent the boundary effect due to the finite size of the elastic body and/or the constraints existing on the finite boundary. Eq. (6.13) can be viewed as an extended Somigliana's identity based on the SSGET, which plays a role similar to that of the Somigliana's identity in classical elasticity (e.g., Paris and Canas, 1997; Sadd, 2009).

Furthermore, if the microstructure-dependent strain gradient effect is neglected by setting $L = 0$, the higher-order terms involved in Eq. (6.13) vanish (with $\mu_{ijk} = 0$, $q_i = 0$ and $Q_{ij} = 0$ from Eqs. (2.5b), (6.4b) and (6.12b), respectively), and Eq. (6.13) reduces to

$$u_m^{(II)}(\mathbf{x}) = \int_\Omega C_{ijkl}\left[G^C_{im,j}(\mathbf{x}-\mathbf{y})\varepsilon^*_{kl}(\mathbf{y})\right]dV_y - \int_{\partial\Omega}\left[T^C_{im}(\mathbf{x}-\mathbf{y})u_i^{(II)}(\mathbf{y}) - G^C_{im}(\mathbf{x}-\mathbf{y})t_i^{(II)}\right]dA_y, \quad (6.14)$$

where G^C_{ij} is the Green's function for a 3-D infinite elastic body in classical elasticity listed in Eq. (2.23), $G^C_{im,j} \equiv \partial G^C_{im}(\mathbf{x}-\mathbf{y})/\partial y_j$, T^C_{im} is the classical Cauchy traction transformation tenor given in Eq. (6.12c), and $t_i^{(II)}$ is the traction related to the Cauchy stress $\tau_{ij}^{(II)}$ by $t_i^{(II)} = \tau_{ij}^{(II)} n_j$. It can be readily verified that Eq. (6.14) is the same as the Somigliana's identity in classical elasticity used by Li et.al. (2007).

Now, with $\overline{u_i} = 0$, $\overline{\dfrac{\partial u_i}{\partial n}} = 0$ on $\partial\Omega$ for the loading set (*II*), it follows from Eqs. (6.10a)

and (6.13) that

$$u_m^{(II)}(\mathbf{x}) = \int_\Omega C_{ijkl}\left[G_{im,j}(\mathbf{x}-\mathbf{y})\varepsilon_{kl}^*(\mathbf{y}) + L^2 G_{im,jp}(\mathbf{x}-\mathbf{y})\kappa_{klp}^*(\mathbf{y})\right]dV_y + \int_{\partial\Omega}\left[G_{im}(\mathbf{x}-\mathbf{y})t_i^{(II)} + G_{im,l}(\mathbf{x}-\mathbf{y})q_i^{(II)}n_l(\mathbf{y})\right]dA_y, \tag{6.15}$$

which is the disturbed displacement field in the finite elastic body subject to the homogeneous Dirichlet-like boundary conditions. Similarly, using Eq. (6.10b) in Eq. (6.13) gives, with $\overline{t_i} = 0, \overline{q_i} = 0$ on $\partial\Omega$ for the loading set (*II*),

$$u_m^{(II)}(\mathbf{x}) = \int_\Omega C_{ijkl}\left[G_{im,j}(\mathbf{x}-\mathbf{y})\varepsilon_{kl}^*(\mathbf{y}) + L^2 G_{im,jp}(\mathbf{x}-\mathbf{y})\kappa_{klp}^*(\mathbf{y})\right]dV_y - \int_{\partial\Omega}\left[T_{im}(\mathbf{x}-\mathbf{y})u_i^{(II)}(\mathbf{y}) + Q_{im}(\mathbf{x}-\mathbf{y})u_{i,l}^{(II)}(\mathbf{y})n_l(\mathbf{y})\right]dA_y, \tag{6.16}$$

which is the disturbed displacement field in the finite elastic body subject to the homogeneous Neumann-like boundary conditions.

Clearly, Eqs. (6.15) and (6.16) are integral equations that involve the unknown displacement components in the integrands of the surface integrals. It is very challenging to obtain analytical solutions of such integral equations even for inclusion problems involving simple-shape elastic bodies and inclusions. Hence, only the inclusion problems defined in Eq. (6.15), which are associated with the simpler Dirichlet-like boundary conditions, will continue to be formulated in the rest of this section.

As stated earlier, the derivatives involved in the integrals in Eqs. (6.13)–(6.16) are with respect to **y**, which is the integration variable. Note that

$$\frac{\partial G_{ij}(\mathbf{x}-\mathbf{y})}{\partial y_k} = -\frac{\partial G_{ij}(\mathbf{x}-\mathbf{y})}{\partial x_k}. \tag{6.17}$$

Using Eq. (6.17) in Eq. (6.15) then gives

$$u_m^{(II)}(\mathbf{x}) = \int_\Omega C_{ijkl}\left[-G_{im,j}(\mathbf{x}-\mathbf{y})\varepsilon_{kl}^*(\mathbf{y}) + L^2 G_{im,jp}(\mathbf{x}-\mathbf{y})\kappa_{klp}^*(\mathbf{y})\right]dV_y + \int_{\partial\Omega}\left[G_{im}(\mathbf{x}-\mathbf{y})t_i^{(II)} - G_{im,l}(\mathbf{x}-\mathbf{y})q_i^{(II)}n_l(\mathbf{y})\right]dA_y. \tag{6.18}$$

In Eq. (6.18) and all of the ensuing equations, the derivatives are taken with respect to **x** unless otherwise stated.

Substituting Eq. (6.18) into Eq. (2.5c) yields the disturbed strain as

$$\begin{aligned}\varepsilon_{mn}(\mathbf{x}) = \frac{1}{2}\int_{\Omega} C_{ijkl}\Big[-(G_{im,jn}+G_{in,jm})\varepsilon^{*}_{kl} + L^{2}(G_{im,jpn}+G_{in,jpm})\kappa^{*}_{klp}\Big]dV_{y} \\ + \frac{1}{2}\int_{\partial\Omega}\Big[(G_{im,n}+G_{in,m})t_{i} - (G_{im,ln}+G_{in,lm})q_{i}n_{l}\Big]dA_{y},\end{aligned} \tag{6.19}$$

where the surface integral term represents the boundary effect on the disturbed strain field for the finite-domain inclusion problem. Note that in Eq. (6.19) and other subsequent equations, the superscript "(*II*)" is dropped for convenience, since the strain, traction and double stress traction involved in Eq. (6.19) and ensuing equations are all for the inclusion problem under the loading set (*II*) shown in Fig. 6.1(a).

For uniform $\boldsymbol{\varepsilon}^{*}$ and $\boldsymbol{\kappa}^{*}$, the volume integral term in Eq. (6.19) represents the disturbed strain field in an infinite (unbounded) elastic body containing the inclusion (see Eq. (2.34)), which can be written as

$$\varepsilon^{\infty}_{mn}(\mathbf{x}) = S^{\bullet,\infty}_{mnkl}\varepsilon^{*}_{kl} + T^{\bullet,\infty}_{mnklp}\kappa^{*}_{klp}\ , \tag{6.20a}$$

$$S^{\bullet,\infty}_{mnkl} = -\frac{1}{2}\int_{\Omega} C_{ijkl}(G_{im,jn}+G_{in,jm})dV_{y}, \tag{6.20b}$$

$$T^{\bullet,\infty}_{mnklp} = \frac{L^{2}}{2}\int_{\Omega} C_{ijkl}(G_{im,jpn}+G_{in,jpm})dV_{y}, \tag{6.20c}$$

where $S^{\bullet,\infty}_{mnkl}$ and $T^{\bullet,\infty}_{mnklp}$, as defined, are, respectively, the fourth-order Eshelby tensor and the fifth-order Eshelby-like (gradient) tenor for the unbounded-domain inclusion problem, and the superscript "$\bullet$" can be either "*I*", representing the *interior* case with **x** located inside the inclusion, or "*E*", representing the *exterior* case with **x** located outside the inclusion.

Based on Eqs. (6.20a–c) and the similarity between the unbounded and bounded cases, it is postulated that for the present bounded-domain inclusion problem the disturbed

strain field has the following form:

$$\varepsilon_{mn}(\mathbf{x}) = S^{\bullet,F}_{mnkl}(\mathbf{x})\varepsilon^*_{kl} + T^{\bullet,F}_{mnklp}(\mathbf{x})\kappa^*_{klp}, \tag{6.21}$$

which is similar to the one given in Eqs. (6.20a–c) for the unbounded-domain inclusion problem. In Eq. (6.21), $S^{\bullet,F}_{mnkl}$, and $T^{\bullet,F}_{mnklp}$ denote, respectively, the Eshelby tensor and the Eshelby-like tensor for the current finite-domain inclusion problem.

Using Eqs. (2.5a,b), (2.7) and (6.21) in Eqs. (6.4a,b) gives

$$t_i = g_{imn}\varepsilon^*_{mn} + f_{imnr}\kappa^*_{mnr}, \quad q_i = h_{imn}\varepsilon^*_{mn} + t_{imnr}\kappa^*_{mnr}, \tag{6.22a,b}$$

where

$$g_{imn} \equiv C_{ijkl}[(1-L^2\nabla^2)S^{\bullet,F}_{klmn}n_j - (L^2 S^{\bullet,F}_{klmn,p}n_p)_{,j} + (L^2 S^{\bullet,F}_{klmn,p}n_p n_q)_{,q}n_j], \tag{6.23a}$$

$$f_{imnr} \equiv C_{ijkl}[(1-L^2\nabla^2)T^{\bullet,F}_{klmnr}n_j - (L^2 T^{\bullet,F}_{klmnr,p}n_p)_{,j} + (L^2 T^{\bullet,F}_{klmnr,p}n_p n_q)_{,q}n_j], \tag{6.23b}$$

$$h_{imn} \equiv L^2 C_{ijkl} S^{\bullet,F}_{klmn,p}n_j n_p, \tag{6.23c}$$

$$t_{imnr} \equiv L^2 C_{ijkl} T^{\bullet,F}_{klmnr,p}n_j n_p. \tag{6.23d}$$

Substituting Eqs. (6.20a–c), (6.21) and (6.22a,b) into Eq. (6.19) then yields

$$\begin{aligned} S^{\bullet,F}_{mnkl}\varepsilon^*_{kl} + T^{\bullet,F}_{mnklp}\kappa^*_{klp} &= S^{\bullet,\infty}_{mnkl}\varepsilon^*_{kl} + T^{\bullet,\infty}_{mnklp}\kappa^*_{klp} \\ &+ \frac{1}{2}\int_{\partial\Omega}\Big[\big(g_{ikl}\varepsilon^*_{kl} + f_{iklp}\kappa^*_{klp}\big)(G_{im,n} + G_{in,m}) - \big(h_{ikl}\varepsilon^*_{kl} + t_{iklp}\kappa^*_{klp}\big)(G_{im,qn} + G_{in,qm})n_q\Big]dA_y. \end{aligned} \tag{6.24}$$

From Eq. (6.24) it follows that

$$S^{\bullet,F}_{mnkl} = S^{\bullet,\infty}_{mnkl} + S^{B,F}_{mnkl}, \qquad T^{\bullet,F}_{mnklp} = T^{\bullet,\infty}_{mnklp} + T^{B,F}_{mnklp}, \tag{6.25a,b}$$

where

$$S^{B,F}_{mnkl} \equiv \frac{1}{2}\int_{\partial\Omega}\Big[g_{ikl}(G_{im,n} + G_{in,m}) - h_{ikl}(G_{im,qn} + G_{in,qm})n_q\Big]dA_y, \tag{6.26a}$$

$$T^{B,F}_{mnklp} \equiv \frac{1}{2}\int_{\partial\Omega}\Big[f_{iklp}(G_{im,n} + G_{in,m}) - t_{iklp}(G_{im,qn} + G_{in,qm})n_q\Big]dA_y. \tag{6.26b}$$

Here $S^{B,F}_{mnkl}$ and $T^{B,F}_{mnklp}$ can be regarded, respectively, as the boundary parts of the finite-domain Eshelby tensor and Eshelby-like tensor. In the absence of the boundary effect, $S^{B,F}_{mnkl} = 0$, $T^{B,F}_{mnklp} = 0$, and $S^{\bullet,F}_{mnkl}$ and $T^{\bullet,F}_{mnklp}$ reduce, respectively, to their counterparts $S^{\bullet,\infty}_{mnkl}$ and $T^{\bullet,\infty}_{mnklp}$ for the unbounded-domain inclusion problem, as shown in Eqs. (6.25a,b).

Clearly, Eqs. (6.25a,b), (6.26a,b) and (6.23a-d) define the integral equations to solve for $S^{\bullet,F}_{mnkl}$ and $T^{\bullet,F}_{mnklp}$, which depend on the shape and size of both the elastic body (through the surface integrals listed in Eqs. (6.26a,b)) and the inclusion (via $S^{\bullet,\infty}_{mnkl}$ and $T^{\bullet,\infty}_{mnklp}$). Hence, closed-form solutions may be derived only for problems involving simple-shape finite elastic bodies and inclusions. The spherical inclusion problem to be discussed next is one of such problems that have been solved analytically.

6.3. Eshelby Tensor for a Finite-Domain Spherical Inclusion Problem

6.3.1. Position-dependent Eshelby tensor

Consider a finite spherical elastic body Ω of radius H containing a concentric spherical inclusion Ω_I of radius R, as illustrated in Fig. 6.2.

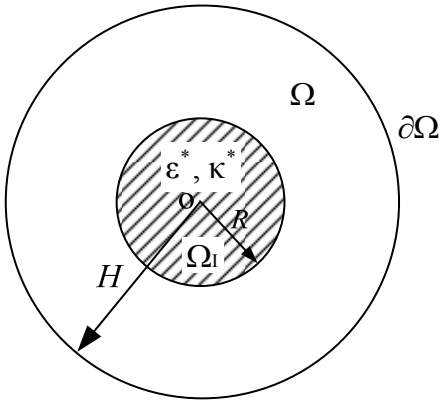

Fig. 6.2. Spherical Inclusion in a finite spherical elastic body.

For the unbounded spherical inclusion problem, the Eshelby tensor *inside* the inclusion based on the SSGET, which is derived in obtained in Section 3.2, can be written as

$$S^{I,\infty}_{mnkl}(\mathbf{x}) = S^{I,C}_{mnkl} + S^{I,G}_{mnkl}(\mathbf{x}), \tag{6.27}$$

where $\mathbf{x}$ is a point located inside the inclusion (i.e., $\mathbf{x} \in \Omega_I$ or $0 < |\mathbf{x}| < R$), $S^{I,C}_{mnkl}$ is the classical part that is uniform for all $\mathbf{x} \in \Omega_I$, and $S^{I,G}_{mnkl}(\mathbf{x})$ is the gradient part that varies with the position of point $\mathbf{x}$. It can be readily shown that $S^{I,\infty}_{mnkl}$ obtained in Eqs. (3.4) – (3.7a–f) and involved in Eq. (6.27) can be written in a matrix form as

$$S^{I,\infty}_{mnkl}(\mathbf{x}) = [\Theta_{mnkl}(\mathbf{x}^0)]^T\,[S^{I,\infty}(x)], \tag{6.28}$$

where

$$\begin{aligned}[\Theta_{mnkl}(\mathbf{x}^0)]^{\mathrm{T}} = [&\delta_{mn}\delta_{kl}, \delta_{mk}\delta_{nl} + \delta_{ml}\delta_{nk}, \delta_{mn}x^0_k x^0_l, \delta_{kl}x^0_m x^0_n,\\ &\delta_{mk}x^0_n x^0_l + \delta_{ml}x^0_n x^0_k + \delta_{nk}x^0_m x^0_l + \delta_{nl}x^0_m x^0_k, x^0_m x^0_n x^0_k x^0_l],\end{aligned} \tag{6.29a}$$

$$[S^{I,\infty}(x)] = [S^{I,C}] + [S^{I,G}(x)], \tag{6.29b}$$

$$[S^{I,C}] = \left[\frac{5\nu-1}{15(1-\nu)}, \frac{4-5\nu}{15(1-\nu)}, 0, 0, 0, 0\right]^T, \tag{6.29c}$$

$$[S^{I,G}(x)] = \left[S^{I,G}_1, S^{I,G}_2, S^{I,G}_3, S^{I,G}_4, S^{I,G}_5, S^{I,G}_6\right]^T, \tag{6.29d}$$

with

$$S^{I,G}_1 = \frac{1}{4\pi(1-\nu)}\left[\frac{2\nu(1-\nu)}{1-2\nu}D_1\Gamma - \frac{\nu}{1-2\nu}L^2x^2D_3(\Gamma-\Lambda) - \frac{1+3\nu}{1-2\nu}L^2D_2(\Gamma-\Lambda)\right], \tag{6.30a}$$

$$S^{I,G}_2 = \frac{1}{4\pi(1-\nu)}\left[(1-\nu)\,D_1\Gamma - L^2D_2(\Gamma-\Lambda)\right], \tag{6.30b}$$

$$S^{I,G}_3 = \frac{x^2}{4\pi(1-\nu)}\left[\frac{2\nu(1-\nu)}{1-2\nu}D_2\Gamma - \frac{\nu}{1-2\nu}L^2x^2D_4(\Gamma-\Lambda) - \frac{1+5\nu}{1-2\nu}L^2D_3(\Gamma-\Lambda)\right], \tag{6.30c}$$

$$S^{I,G}_4 = -\frac{L^2x^2}{4\pi(1-\nu)}D_3(\Gamma-\Lambda), \tag{6.31d}$$

$$S_5^{I,G} = \frac{x^2}{8\pi(1-\nu)}\left[(1-\nu)D_2\Gamma - 2L^2 D_3(\Gamma-\Lambda)\right], \tag{6.30e}$$

$$S_6^{I,G} = -\frac{L^2 x^4}{4\pi(1-\nu)} D_4(\Gamma-\Lambda). \tag{6.30f}$$

The differentials $D_1\Lambda$, $D_2\Lambda$, $D_3\Lambda$, $D_4\Lambda$ and $D_1\Gamma$, $D_2\Gamma$, $D_3\Gamma$, $D_4\Gamma$ involved in Eqs. (6.30a–f) are given by Eq. (3.10). In Eq. (6.29a) and throughout this dissertation, $x_i^0 = x_i / x$ is the *i*th component of the unit vector $\mathbf{x}^0 = \mathbf{x}/x$, and $x = |\mathbf{x}| = \sqrt{x_m x_m}$ is the distance from point **x** to the center of the spherical body that serves as the origin of the coordinate system.

For the unbounded spherical inclusion problem, the Eshelby tensor *outside* the inclusion based on the SSGET has been obtained in Section 3.2 and is summarized here,

$$S_{mnkl}^{E,\infty}(\mathbf{x}) = S_{mnkl}^{E,C}(\mathbf{x}) + S_{mnkl}^{E,G}(\mathbf{x}), \tag{6.31}$$

where **x** is a point located outside the inclusion (i.e., $\mathbf{x} \notin \Omega_I$ or $R < |\mathbf{x}| < H$), $S_{mnkl}^{E,C}(\mathbf{x})$ is the classical part, and $S_{mnkl}^{E,G}(\mathbf{x})$ is the gradient part. Both $S_{mnkl}^{E,C}$ and $S_{mnkl}^{E,G}$ vary with the position of **x** in this exterior case, unlike in the interior case. In a matrix form, Eq. (6.31) can be written as

$$[S_{mnkl}^{E,\infty}(\mathbf{x})] = [\Theta_{mnkl}(\mathbf{x}^0)]^T [S^{E,\infty}(x)], \tag{6.32}$$

where $[\Theta_{mnkl}(\mathbf{x}^0)]^T$ is the same as that defined in Eq. (6.29a), and

$$[S^{E,\infty}(x)] = [S^{E,C}(x)] + [S^{E,G}(x)], \tag{6.33}$$

in which

$$[S^{E,C}(x)] = \frac{1}{30(1-\nu)}\left(\frac{R}{x}\right)^3\left[3\left(\frac{R}{x}\right)^2 - 5(1-2\nu),\ 3\left(\frac{R}{x}\right)^2 + 5(1-2\nu),\ 15-15\left(\frac{R}{x}\right)^2,\right.$$
$$\left. 15(1-2\nu) - 15\left(\frac{R}{x}\right)^2,\ 15\nu - 15\left(\frac{R}{x}\right)^2,\ 105\left(\frac{R}{x}\right)^2 - 75\right]^T, \tag{6.34a}$$

$$S^{E,G}(x) = \left[S_1^{E,G}, S_2^{E,G}, S_3^{E,G}, S_4^{E,G}, S_5^{E,G}, S_6^{E,G}\right]^T, \tag{6.34b}$$

with $S_1^{E,G} - S_6^{E,G}$ obtainable from using Eq. (3.20) in their interior counterparts $S_1^{I,G} - S_6^{I,G}$ given in Eqs. (6.30a–f).

Based on the similarity between the unbounded- and bounded-domain inclusion problems and the forms of the Eshelby tensor for the unbounded-domain problem given in Eqs. (6.28) and (6.32), it is postulated that the Eshelby tensor for the current bounded-domain spherical inclusion problem can be expressed in a similar form as

$$S^{\bullet,F}_{mnkl}(\mathbf{x}) = [\Theta_{mnkl}(\mathbf{x}^0)]^T\ [S^{\bullet,F}(x)], \tag{6.35}$$

where $[\Theta_{mnkl}(\mathbf{x}^0)]^T$ is the same as that defined in Eq. (6.29a), and

$$[S^{\bullet,F}(x)] = \left[S_1^{\bullet,F}(x), S_2^{\bullet,F}(x), S_3^{\bullet,F}(x), S_4^{\bullet,F}(x), S_5^{\bullet,F}(x), S_6^{\bullet,F}(x)\right]^T \tag{6.36}$$

is an array of six components yet to be determined.

Using Eq. (6.35) in Eqs. (6.23a,b) yields, after carrying out the algebra,

$$g_{ikl} = \left[\Xi_{ikl}\right]\left[S^{E,F}(H)\right], \quad h_{ikl} = 0, \tag{6.37a,b}$$

on $\partial\Omega$, where

$$\left[\Xi_{ikl}\right] \equiv \left[\delta_{kl}n_i,\ \delta_{ik}n_l + \delta_{il}n_k,\ n_i n_k n_l\right]\left[M\right]^T, \tag{6.38}$$

$$[M]^T \equiv \begin{bmatrix} 3\lambda+2\mu & 0 & 0 \\ 2\lambda & 2\mu & 0 \\ -2\alpha(3\lambda+2\mu) & 0 & (3\lambda+2\mu)(1+6\alpha) \\ \lambda+2\mu+8\mu\alpha & 0 & 0 \\ -8\lambda\alpha & 2\mu(1+2\alpha) & 4(\lambda+\mu)(1+6\alpha) \\ -2(\lambda+2\mu)\alpha & -4\mu\alpha & \lambda+2\mu+2(3\lambda+14\mu)\alpha \end{bmatrix}^T, \tag{6.39}$$

with $\alpha \equiv L^2/H^2$, λ and μ being the Lamé constants, $n_i = y_i / y$ being the *i*th component of the unit vector **n** representing the direction of **y**, and $y = |\mathbf{y}| = \sqrt{y_m y_m}$.

Using Eqs. (6.37a,b)–(6.39) in Eq. (6.26a) gives the boundary part of the finite-domain Eshelby tensor, in a matrix form, as

$$S^{B,F}_{mnkl} = \frac{1}{2}[Q_1, Q_2, Q_3][M]^T\left[S^{E,F}(H)\right], \tag{6.40}$$

where

$$\begin{aligned} Q_1 &= \int_{\partial\Omega} \delta_{kl} n_i (G_{im,n} + G_{in,m}) dA_y, \qquad Q_2 = \int_{\partial\Omega} (\delta_{ik} n_l + \delta_{il} n_k)(G_{im,n} + G_{in,m}) dA_y, \\ Q_3 &= \int_{\partial\Omega} n_i n_k n_l (G_{im,n} + G_{in,m}) dA_y, \end{aligned} \tag{6.41}$$

with G_{ij}, given in Eqs. (2.28) and (2.29), being the 3-D Green's function for an infinite elastic body based on the SSGET. The use of Eqs. (2.28) and (2.29) in Eq. (6.41) results in

$$Q_1 = \delta_{kl}\left(\left\langle n_n \overline{A}\right\rangle_{,m} + \left\langle n_m \overline{A}\right\rangle_{,n} - 2\left\langle n_i \overline{B}\right\rangle_{,imn}\right), \tag{6.42a}$$

$$Q_2 = \delta_{km}\left\langle n_l \overline{A}\right\rangle_{,n} + \delta_{kn}\left\langle n_l \overline{A}\right\rangle_{,m} + \delta_{lm}\left\langle n_k \overline{A}\right\rangle_{,n} + \delta_{ln}\left\langle n_k \overline{A}\right\rangle_{,m} - 2\left\langle n_l \overline{B}\right\rangle_{,kmn} - 2\left\langle n_k \overline{B}\right\rangle_{,lmn} \tag{6.42b}$$

$$Q_3 = \left\langle \overline{A} n_m n_k n_l \right\rangle_{,n} + \left\langle \overline{A} n_n n_k n_l \right\rangle_{,m} - 2\left\langle \overline{B} n_i n_k n_l \right\rangle_{,imn}, \tag{6.42c}$$

where

$$\overline{A}(r) \equiv \frac{1}{4\pi\mu}\frac{1}{r}\left(1 - e^{-\frac{r}{L}}\right), \quad \overline{B}(r) \equiv \frac{1}{16\pi\mu(1-\nu)}\left(r + \frac{2L^2}{r} - \frac{2L^2}{r}e^{-\frac{r}{L}}\right), \tag{6.43a,b}$$

with $r = |\mathbf{x} - \mathbf{y}|$. In Eqs. (6.42a–c) and in the sequel, $\langle f \rangle$ denotes the surface integral of function *f* over ∂Ω (i.e., the surface of the spherical elastic body of radius *H*) defined by

$$\langle f \rangle = \int_{\partial\Omega} f \, dA_y \, . \tag{6.44}$$

The integrals in Eqs. (6.42a–c) can be analytically evaluated with the help of the following relations (see Appendices G and H):

$$\langle f(r) n_i \rangle = f_0(x) x_i \, , \tag{6.45}$$

$$\langle f(r) n_i n_j n_k \rangle = f_1(x) \left(x_i \, \delta_{jk} + x_j \delta_{ik} + x_k \delta_{ij} \right) + f_2(x) x_i \, x_j \, x_k \, , \tag{6.46}$$

where

$$f_0(x) = \frac{2\pi H^2}{x} \int_{-1}^{1} f(r) t \, dt \, , \tag{6.47a}$$

$$f_1(x) = \frac{\pi H^2}{x} \int_{-1}^{1} f(r) t (1 - t^2) \, dt \, , \tag{6.47b}$$

$$f_2(x) = \frac{\pi H^2}{x^3} \int_{-1}^{1} f(r) t (5t^2 - 3) \, dt \, , \tag{6.47c}$$

with

$$r = |\mathbf{x} - \mathbf{y}| = \sqrt{x^2 + H^2 - 2xHt} \, , \; t \equiv \cos\theta \, , \tag{6.48a,b}$$

in which θ is the angle between $\mathbf{x}$ ($\in \Omega$) and $\mathbf{y}$ ($\in \partial\Omega$), as shown in Fig. 6.3. Clearly, Eq. (6.48a) follows directly from the cosine law.

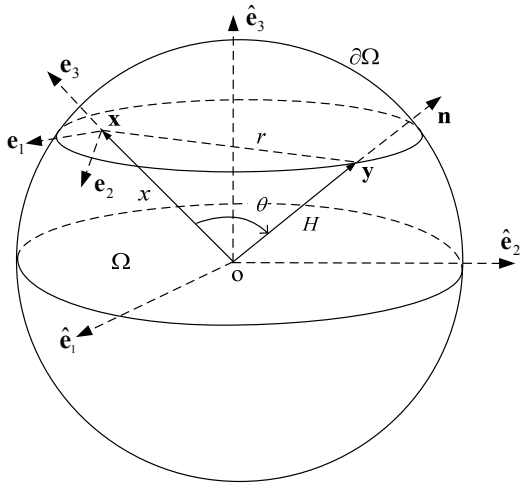

Fig. 6.3. Locations of $\mathbf{x}$ ($\in \Omega$) and $\mathbf{y}$ ($\in \partial\Omega$).

Applying Eqs. (6.45) and (6.47a) to $\overline{A}(r)$ and $\overline{B}(r)$ defined in Eqs. (6.43a,b), respectively, yields, together with Eq. (6.44),

$$\left\langle \overline{A}(r)n_i \right\rangle = A_0(x)x_i\,, \quad \left\langle \overline{B}(r)n_i \right\rangle = B_0(x)x_i\,, \tag{6.49a,b}$$

where

$$A_0(x) = \frac{1}{3\mu} + \frac{\Psi_1(x)}{\mu x^3}\,, \quad B_0(x) = \frac{x^2 - 5H^2 + 10L^2}{60\mu(1-\nu)} + \frac{L^2\Psi_1(x)}{2\mu(1-\nu)x^3}\,, \tag{6.50a,b}$$

with

$$\Psi_1(x) \equiv e^{-H/L}L(H+L)[L\sinh(x/L) - x\cosh(x/L)]\,. \tag{6.51}$$

Similarly, the application of Eqs. (6.46) and (6.47b,c) to $\overline{A}(r)$ and $\overline{B}(r)$ respectively results in

$$\begin{aligned} \left\langle \overline{A}(r)n_i n_j n_k \right\rangle &= A_1(x)\left(x_i\,\delta_{jk} + x_j\delta_{ik} + x_k\delta_{ij}\right) + A_2(x)x_i\,x_j x_k\,, \\ \left\langle \overline{B}(r)n_i n_j n_k \right\rangle &= B_1(x)\left(x_i\,\delta_{jk} + x_j\delta_{ik} + x_k\delta_{ij}\right) + B_2(x)x_i\,x_j x_k\,, \end{aligned} \tag{6.52a,b}$$

where

$$A_1(x) = \frac{-3x^2 + 7H^2}{105\mu H^2} - \frac{1}{\mu H^2 x^5}\Psi_2(x),$$

$$B_1(x) = \frac{1}{1260\mu(\nu-1)H^2}[21H^2(H^2 - 2L^2) + 6x^2(3L^2 - H^2) + x^4] + \frac{L^2}{2\mu(\nu-1)H^2x^5}\Psi_2(x)\,,$$

$$A_2(x) = \frac{1}{7\mu H^2} + \frac{1}{\mu H^2 x^7}\Psi_3(x)\,,$$

$$B_2(x) = \frac{90L^2 + 5x^2 - 9H^2}{1260\mu(1-\nu)H^2} + \frac{L^2}{2\mu(1-\nu)H^2x^7}\Psi_3(x)\,,$$

$$\begin{aligned} \Psi_2(x) \equiv e^{-H/L}\{&18L^4[(LH^2 + Lx^2 + Hx^2)\sinh(x/L) - H^2x\cosh(x/L)] \\ &+ 3L^3[LH^3\sinh(x/L) - x(H^3 + Lx^2 + Hx^2)\cosh(x/L)] + 7L^3H^2x^2\sinh(x/L) + \\ &+ 45L^5(L+H)[L\sinh(x/L) - x\cosh(x/L)] + L^2H^2x^2[H\sinh(x/L) - x\cosh(x/L)]\}, \end{aligned}$$

$$\begin{aligned} \Psi_3(x) \equiv e^{-H/L}\{&90L^4[(LH^2 + Lx^2 + Hx^2)\sinh(x/L) - H^2x\cosh(x/L)] - H^3Lx^3\cosh(x/L) \\ &+ 15L^3[LH^3\sinh(x/L) - x(H^3 + Lx^2 + Hx^2)\cosh(x/L)] + 36L^3H^2x^2\sinh(x/L) + \\ &+ 225L^5(L+H)[L\sinh(x/L) - x\cosh(x/L)] + 6L^2H^2x^2[H\sinh(x/L) - x\cosh(x/L)]\}. \end{aligned}$$

(6.53a–f)

Using Eqs. (6.49a,b)–(6.53a–f) in Eqs. (5.42a–c) then leads to, in a matrix form,

$$[Q_1, Q_2, Q_3] = \left[\Theta_{mnkl}(\mathbf{x}^0)\right]^T [Q(x)]^T, \tag{6.54}$$

where $\left[\Theta_{mnkl}(\mathbf{x}^0)\right]^T$ is the same as that given in Eq. (6.29a), and $[Q(x)]$ is a 3 by 6 matrix whose components are given by

$$\begin{aligned}
&Q_{11} = 2(A_0 - D_1\mathrm{N}), \quad Q_{14} = 2x^2(D_1A_0 - D_2\mathrm{N}), \quad Q_{12} = Q_{13} = Q_{15} = Q_{16} = 0,\\
&Q_{21} = -4D_1B_0, \quad Q_{22} = 2A_0 - 4D_1B_0, \quad Q_{23} = -4x^2D_2B_0, \quad Q_{24} = Q_{23},\\
&Q_{25} = x^2(D_1A_0 - 4D_2B_0), \quad Q_{26} = -4x^4D_3B_0,\\
&Q_{31} = 2(A_1 - D_1\mathrm{Z} - 2D_1B_1), \quad Q_{32} = 2(A_1 - \mathrm{X} - 2D_1B_1), \quad Q_{33} = 2x^2(A_2 - 2D_2B_1 - D_1\mathrm{X}),\\
&Q_{34} = 2x^2(D_1A_1 - D_2\mathrm{Z} - 2D_2B_1), \quad Q_{35} = x^2(A_2 + D_1A_1 - 2D_1\mathrm{X} - 4D_2B_1),\\
&Q_{36} = 2x^4(D_1A_2 - D_2\mathrm{X} - 2D_3B_1),
\end{aligned} \tag{6.55}$$

with

$$\mathrm{N}(x) \equiv xB_0' + 3B_0, \quad \mathrm{Z}(x) \equiv xB_1' + 3B_1, \quad \mathrm{X}(x) \equiv xB_2' + 5B_2. \tag{6.56}$$

The differential operators $D_1(\cdot)$, $D_2(\cdot)$ and $D_3(\cdot)$ involved in Eq. (6.55) are defined in Eq. (3.3).

Substituting Eq. (6.54) into Eq. (6.40) then yields the boundary part of the finite-domain Eshelby tensor as

$$S_{mnkl}^{B,F}(\mathbf{x}) = \frac{1}{2}\left[\Theta_{mnkl}(\mathbf{x}^0)\right]^T [Q(x)]^T [M]^T \left[S^{E,F}(H)\right], \tag{6.57}$$

where $[Q(x)]$ is the 3 by 6 matrix whose components are listed in Eq. (6.55), $[M]$ is given in Eq. (6.39), and $[S^{E,F}(H)]$ can be determined as follows.

Note that Eq. (6.57) can be rewritten as

$$S_{mnkl}^{B,F}(\mathbf{x}) = \left[\Theta_{mnkl}(\mathbf{x}^0)\right]^T [K(x)] \left[S^{E,F}(H)\right], \tag{6.58}$$

where

$$[K(x)] \equiv \frac{1}{2}[Q(x)]^T [M]^T \tag{6.59}$$

is a six by six matrix. Using Eqs. (6.28), (6.32), (6.35) and (6.58) in Eq. (6.25a) gives,

noting that the six components of $\left[\Theta_{mnkl}(\mathbf{x}^0)\right]$ are linearly independent,

$$[S^{I,F}(x)] = [S^{I,\infty}(x)] + [K(x)][S^{E,F}(H)] \tag{6.60}$$

for the interior case with $0 < x < R$, and

$$[S^{E,F}(x)] = [S^{E,\infty}(x)] + [K(x)][S^{E,F}(H)] \tag{6.61}$$

for the exterior case with $R < x < H$. By setting $x \to H$, Eq. (6.61) gives

$$[S^{E,F}(H)] = [\mathrm{I} - K(H)]^{-1}[S^{E,\infty}(H)] \ , \tag{6.62}$$

where [I] is the six by six identity matrix, $[K(H)]$ is obtainable from Eq. (6.59) with $x = H$, and $[S^{E,\infty}(H)]$ can be determined from Eq. (6.33) with $x = H$.

Finally, it follows from Eqs. (6.62), (6.60), (6.29b) and (6.35) that the Eshelby tensor inside the spherical inclusion for the finite-domain inclusion problem can be expressed as

$$S^{I,F}_{mnkl}(\mathbf{x}) = [\Theta_{mnkl}(\mathbf{x}^0)]^T \left\{[S^{I,C}] + [S^{I,G}(x)] + [S^{B,F}(x)]\right\}, \tag{6.63}$$

$$[S^{B,F}(x)] \equiv [K(x)][\mathrm{I} - K(H)]^{-1}[S^{E,\infty}(H)], \tag{6.64}$$

where $\mathbf{x} \in \Omega_\mathrm{I}$, $0 < x < R$, and $[S^{I,C}]$, $[S^{I,G}]$ and $[S^{B,F}]$ are, respectively, the classical, gradient and boundary parts of the interior Eshelby tensor based on the SSGET. Note that $[S^{I,C}]$, as given in Eq. (6.29c), is uniform inside the inclusion, while $[S^{I,G}]$, as listed in Eqs. (6.29d) and (6.30a–f), depends on L, R and x in a complicated manner. In addition, $[S^{B,F}]$ given in Eq. (6.64) varies with L, R, H and x. That is, $[S^{B,F}]$ is non-uniform inside the inclusion and is different for the elastic body with different body and/or inclusion sizes (i.e., with varying H and/or R) and different materials (with changing L).

6.3.2. Volume averaged Eshelby tensor

Considering that the finite-domain Eshelby tensor $\mathbf{S}^{I,F}$ is position-dependent inside the inclusion, the volume average of $\mathbf{S}^{I,F}$ over the spherical inclusion will be needed in predicting effective properties of a heterogeneous particle-reinforced composite. Hence, the volume average of $\mathbf{S}^{I,F}$ is evaluated here.

The volume average of a sufficiently smooth function $F(\mathbf{x})$ over the spherical inclusion occupying the region Ω_I is defined in Eq. (3.11). Replacing $F(\mathbf{x})$ in Eq. (3.11) with $S^{I,F}_{mnkl}(\mathbf{x})$ given in Eq. (6.63) then leads to, with the help of Eqs. (3.11) and (6.29a),

$$\left\langle S^{I,F}_{mnkl} \right\rangle_{\mathrm{V}} = \left\langle S^{I,\infty}_{mnkl} \right\rangle_{\mathrm{V}} + \left\langle S^{B,F}_{mnkl} \right\rangle_{\mathrm{V}}, \tag{6.65}$$

where the volume averaged Eshelby tensor for the unbounded spherical inclusion problem has been obtained in a closed-form in Eq. (3.16). And the volume averaged boundary part of the Eshelby tensor for the bounded spherical inclusion problem is given by

$$\left\langle S^{B,F}_{mnkl} \right\rangle_{\mathrm{V}} = S_1(R, L, H)\, \delta_{mn}\delta_{kl} + S_2(R, L, H)\, (\delta_{mk}\delta_{nl} + \delta_{ml}\delta_{nk}), \tag{6.66}$$

with

$$S_1(R, L, H) \equiv \frac{1}{R^3}\left(3\overline{S^{B,F}_1} + \overline{S^{B,F}_3} + \overline{S^{B,F}_4} + \frac{1}{5}\overline{S^{B,F}_6} \right), \tag{6.67a}$$

$$S_2(R, L, H) \equiv \frac{1}{R^3}\left[\left(3\overline{S^{B,F}_2} + 2\overline{S^{B,F}_5} + \frac{1}{5}\overline{S^{B,F}_6} \right) \right], \tag{6.67b}$$

$$\overline{S^{B,F}_n} \equiv \int_0^R x^2 S^{B,F}_n(x)\, dx\,. \tag{6.67c}$$

Note that $S^{B,F}_n(x)$ (n = 1, 2, …, 6) in Eq. (6.67c) is the nth component of the array $[S^{B,F}(x)]$ given in Eq. (6.64).

By following a similar procedure, the volume average of the fifth-order Eshelby-like tensor $T^{I,F}_{mnklp}$ over the spherical inclusion can also be evaluated, which gives

$\left\langle T^{I,F}_{mnklp} \right\rangle_{\mathrm{V}} = 0$. It then follows from Eqs. (5.21) and (3.11) that

$$\left\langle \varepsilon_{mn} \right\rangle_{\mathrm{V}} = \left\langle S^{I,F}_{mnkl} \right\rangle_{\mathrm{V}} \varepsilon^{*}_{kl}, \tag{6.68}$$

where $\left\langle S^{I,F}_{mnkl} \right\rangle_{\mathrm{V}}$ is given in Eq. (6.65) along with Eqs. (6.67a–c). Equation (6.68) shows that the average disturbed strain is only related to the eigenstrain $\boldsymbol{\varepsilon}^*$ even in the presence of the eigenstrain gradient $\boldsymbol{\kappa}^*$. This result will have important applications in homogenization analyses.

6.4. Numerical Results

To demonstrate how the components of the Eshelby tensor for the finite-domain spherical inclusion problem derived in Section 6.3 quantitatively change with the position $\mathbf{x}$, inclusion size R and matrix size H, some numerical results are provided in this section. In the numerical analysis presented here, the Poisson's ratio v is taken to be 0.3, and the material length scale parameter L to be 17.6 μm.

Figure 6.4 shows the distribution of $S^{I,F}_{1111} (= S^{I,C}_{1111} + S^{I,G}_{1111} + S^{B,F}_{1111})$ along the x_1 axis (or any radial direction due to the spherical symmetry) of a spherical inclusion concentrically embedded in a finite spherical elastic matrix. The values of $S^{I,F}_{1111}$ displayed in Fig. 6.4 are obtained from Eqs. (6.63), (6.64), (6.29a,c,d) and (6.30a–f) while those of $S^{I,\infty}_{1111}$ are determined from Eqs. (6.28) and (6.29a–j). The inclusion has a fixed size of $R = L$, while the matrix domain has three different sizes: $H = 2R$, $H = 3R$, and $H = 5R$, as indicated in Fig. 6.4, where the distribution of $S^{I,\infty}_{1111} (= S^{I,C}_{1111} + S^{I,G}_{1111})$ for the unbounded spherical inclusion problem along the same direction is also plotted for comparison. Note that $S^{I,C}_{1111}$ is a constant (i.e., $S^{I,C}_{1111} = 0.5238$ from Eqs. (6.28) and (6.29a–c)).

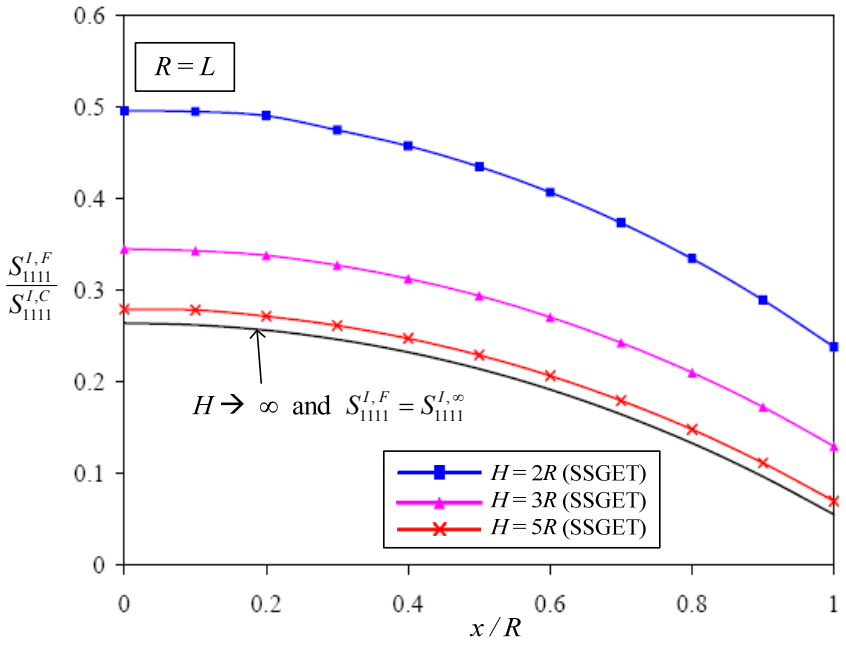

Fig. 6.4. $S_{1111}^{I,F}$ along a radical direction of the inclusion for the matrix with different sizes.

When H=5R, the inclusion volume fraction, defined by $\phi = (R/H)^3$, is very small (with ϕ = 0.8%), and $S_{1111}^{I,F}$ is quite close to $S_{1111}^{I,\infty}$, indicating that the contribution of the boundary part $S_{1111}^{B,F}$ $(=S_{1111}^{I,F}-S_{1111}^{I,\infty})$ is insignificant and may therefore be ignored. However, the contribution of the boundary part $S_{1111}^{B,F}$ to the total value of $S_{1111}^{I,F}$ increases with increasing ϕ. When ϕ increases from 0.8% to 12.5% (i.e., H decreases from 5R to 2R), $S_{1111}^{I,F}$ becomes much larger than $S_{1111}^{I,\infty}$, revealing that the boundary effect is significant and can no longer be neglected. Clearly, these observations based on Fig. 6.4 indicate that the value of $S_{1111}^{I,\infty}$ (a component of the Eshelby tensor for the infinite-domain spherical inclusion problem) provides a lower bound of the values of $S_{1111}^{I,F}$ (the counterpart component of the Eshelby tensor for the finite-domain spherical inclusion problem).

The variation of the component of the averaged Eshelby tensor inside the spherical inclusion, $\left\langle S_{1111}^{I,F}\right\rangle_{\mathrm{V}}$ $(=\left\langle S_{1111}^{I,\infty}\right\rangle_{\mathrm{V}}+\left\langle S_{111}^{B,F}\right\rangle_{\mathrm{V}})$, with the inclusion volume fraction ϕ is illustrated

in Fig. 6.5. The values of $\left\langle S_{1111}^{I,\infty}\right\rangle_{\mathrm{V}}$ based on the SSGET for the unbounded spherical inclusion problem and those of $\left\langle S_{1111}^{I,F}\right\rangle_{\mathrm{V}}$ based on classical elasticity for the finite-domain spherical inclusion problem are also displayed in Fig. 6.5 for comparison. Note that the values of $\left\langle S_{1111}^{I,F}\right\rangle_{\mathrm{V}}$ shown in Fig. 6.5 are obtained from Eqs. (6.65), (3.16), (6.66) and (6.67a–c), with those for the classical elasticity-based cases determined by setting $L \to 0$. From Eq. (3.16) it is seen that $\left\langle S_{1111}^{I,\infty}\right\rangle_{\mathrm{V}}$ based on the SSGET is independent of H and is therefore the same for all of the SSGET-based $\left\langle S_{1111}^{I,F}\right\rangle_{\mathrm{V}}$ curves with different values of ϕ shown in Fig. 6.5 (including the curve with $\phi \to 0$ or $H \to \infty$). Therefore, the distance between a line for $\left\langle S_{1111}^{I,F}\right\rangle_{\mathrm{V}}$ with a specified ϕ ($\neq 0$) and the line for $\left\langle S_{1111}^{I,\infty}\right\rangle_{\mathrm{V}}$ with $\phi \to 0$, based on either the SSGET or classical elasticity, are actually the boundary part $\left\langle S_{111}^{B,F}\right\rangle_{\mathrm{V}}$ (= $\left\langle S_{1111}^{I,F}\right\rangle_{\mathrm{V}} - \left\langle S_{1111}^{I,\infty}\right\rangle_{\mathrm{V}}$) (see Eq. (6.65)).

Figure 6.5 shows that the inclusion size effect is predicted by the current finite-domain inclusion problem solution based on the SSGET – unbounded (with $\phi \to 0$) and bounded (with different values of $\phi \neq 0$). That is, in each case with a fixed inclusion volume fraction ϕ, the smaller the inclusion radius R is, the smaller the value of $\left\langle S_{1111}^{I,F}\right\rangle_{\mathrm{V}}$ is. This size effect is seen to be more significant for the cases with small inclusion volume fractions, where the boundary effect is small, as will be discussed below. However, as the inclusion size becomes large (with $R > 264$ μm or $R/L > 15$ for $\phi = 12.5\%$ here), the size effect is seen to be diminishing. In contrast, the solution based on classical elasticity gives a constant value of $\left\langle S_{1111}^{I,F}\right\rangle_{\mathrm{V}}$ for each value of ϕ, which provides an upper bound of the values

of $\left\langle S_{1111}^{I,F} \right\rangle_{\mathrm{V}}$ based on the SSGET for the same value of ϕ, as shown in Fig. 6.5. However, each of these constant values is independent of the inclusion radius R, indicating that the classical elasticity-based solution for the finite-domain inclusion problem does not have the capability to predict the inclusion size effect.

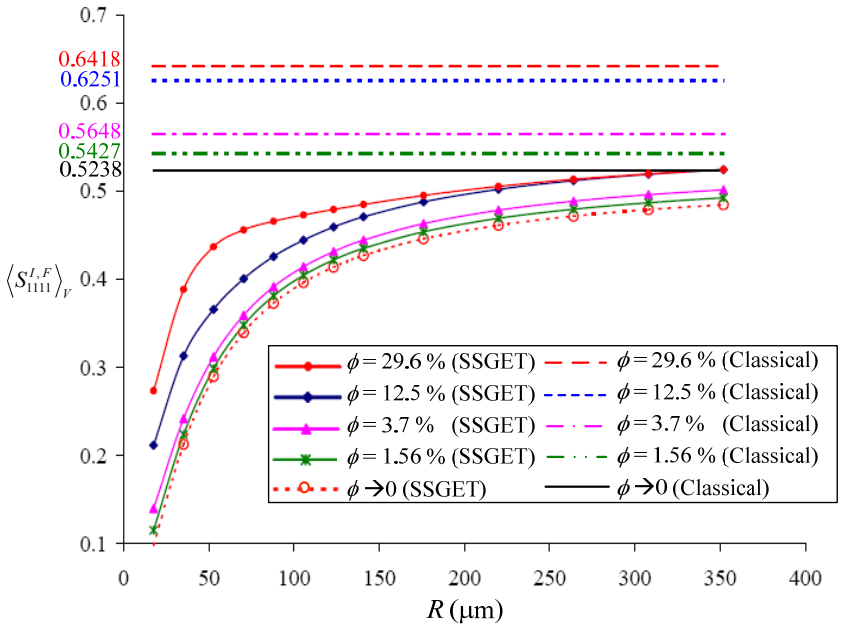

Fig. 6.5. $\left\langle S_{1111}^{I,F} \right\rangle_{\mathrm{V}}$ varying with the inclusion size at different inclusion volume fractions.

From Fig. 6.5 it is also observed that $\left\langle S_{1111}^{I,F} \right\rangle_{\mathrm{V}}$ changes with the inclusion volume fraction ϕ: the smaller ϕ is, the smaller $\left\langle S_{1111}^{I,F} \right\rangle_{\mathrm{V}}$ is, and the closer the curve of $\left\langle S_{1111}^{I,F} \right\rangle_{\mathrm{V}}$ is to that of $\left\langle S_{1111}^{I,\infty} \right\rangle_{\mathrm{V}}$. This indicates that the boundary effect, as measured by $\left\langle S_{111}^{B,F} \right\rangle_{\mathrm{V}}$ (= $\left\langle S_{1111}^{I,F} \right\rangle_{\mathrm{V}} - \left\langle S_{1111}^{I,\infty} \right\rangle_{\mathrm{V}}$), becomes smaller as ϕ gets smaller. However, when ϕ is big enough (with ϕ = 12.5% and above here), $\left\langle S_{111}^{B,F} \right\rangle_{\mathrm{V}}$ and therefore the boundary effect become significantly large. The same is true for all of the other non-vanishing components

of $\left\langle S^{I,F}_{mnkl} \right\rangle_{\mathrm{V}}$, which is dictated by Eqs. (6.66) and (6.67a–c). These observations indicate that the boundary effect is insignificant and may be neglected only when inclusion volume fraction is sufficiently low. In addition, the numerical results reveal that the average Eshelby tensor for the finite-domain spherical inclusion problem is bounded from below by the average Eshelby tensor based on the SSGET for the infinite-domain spherical inclusion problem and is bounded from above by the average Eshelby tensor based on classical elasticity for the same inclusion problem.

6.5. Summary

An Eshelby-type inclusion problem of a finite elastic body of arbitrary shape containing an arbitrarily-shaped inclusion prescribed with a uniform eigenstrain and a uniform eigenstrain gradient is solved using an extended Betti's reciprocal theorem and an extended Somigliana's identity based on a simplified strain gradient elasticity theory (SSGET), which are proposed and proved in this chapter. The solution for the displacement field in the bounded elastic body induced by the eigenstrain and eigenstrain gradient is obtained in a general form in terms of the Green's function for the unbounded 3-D elastic medium based on the SSGET. This solution recovers that for the unbounded-domain inclusion problem if the boundary effect is suppressed.

The solution for the finite-domain spherical inclusion problem is derived by using the general solution, which leads to closed-form expressions of the Eshelby tensor and its volume average. Being dependent on the position, inclusion size, matrix size, and material length scale parameter, this Eshelby tensor can capture the inclusion size and boundary effects, unlike existing Eshelby tensors for bounded or unbounded inclusion problems. In the absence of both the strain gradient and boundary effects, this Eshelby tensor recovers

that for the spherical inclusion in an infinite elastic body based on classical elasticity.

To quantitatively illustrate the Eshelby tensor for the finite-domain spherical inclusion problem, sample numerical results are presented, which show that the inclusion size effect can be significant if the inclusion is small and that the boundary effect can be dominant if the inclusion volume fraction is large. But the inclusion size effect becomes insignificant for a large inclusion, and the boundary effect tends to be vanishingly small at a sufficiently low inclusion volume fraction. In addition, it is found that the components of both the Eshelby tensor and its volume average for the finite-domain spherical inclusion problem are bounded from below by those of the Eshelby tensor and its volume average for the infinite-domain spherical inclusion problem based on the SSGET. Furthermore, the averaged Eshelby tensor for the finite-domain spherical inclusion problem based on the SSGET is bounded from above by its counterpart based on classical elasticity.

CHAPTER VII

A HOMOGENIZATION METHOD BASED ON THE ESHELBY TENSOR

7.1. Introduction

With the solution for an Eshelby-type inclusion problem obtained, the corresponding inhomogeneity problem, where a homogeneous matrix contains a different material (inhomogeneity) subject to uniform boundary conditions, can be solved by using the equivalence between the inclusion and the inhomogeneity problems. Hence, the local elastic fields in the inhomogeneity and in the matrix are obtainable. However, in many engineering applications, the overall or effective properties of a heterogeneous material are more desirable than the local behavior in each constituent, considering that a structure component may contain numerous constituents. This has motivated the development of homogenization methods, which have been recognized as a great success in predicting the effective properties of a composite material based on the geometrical and mechanical characteristics of all constituents and their distributions in the composite (Hashin, 1983; Nemat-Nasser and Hori, 1999).

This chapter aims to develop a homogenization method for predicting the effective elastic properties of a heterogeneous material using the SSGET elaborated in Section 2.2. To this end, an energetically equivalent homogeneous medium, whose elastic behavior is described by the SSGET, is constructed. The effective elastic properties of the heterogeneous material are found to depend not only on the volume fractions, shapes and distributions of the inhomogeneities but also on the inhomogeneity sizes, unlike what is

predicted by the classical elasticity-based homogenization methods. Note that the materials considered in this chapter are primarily heterogeneous materials with non-periodic microstructures. Hence, the term 'heterogeneous material' refers to a heterogeneous material with non-periodic microstructures, unless indicated otherwise.

The chapter is organized as follows. In Section 7.2, a homogenization scheme based on the strain energy equivalence and the SSGET is proposed. A non-classical boundary condition is applied, which gives a uniform strain gradient on the boundary. An effective elastic stiffness tensor and an effective material length scale parameter for a heterogeneous material are obtained in terms of the volume fractions and elastic fields in each constituent. In Section 7.3, an analytical solution for the effective elastic stiffness tensor is derived by using the Mori-Tanaka method and Eshelby's equivalent inclusion method. Numerical examples for a two-phase composite are presented in Section 7.4. This chapter concludes with a summary in Section 7.5.

7.2. Homogenization Scheme Based on the Strain Energy Equivalence

Consider a representative volume element (RVE) of a composite material, as schematically shown in Fig.7.1, where ellipsoidal inhomogeneities, with dimensions being much smaller than the size of the RVE, are aligned along the x_3-axis and are uniformly dispersed in the homogeneous matrix. The matrix and the inhomogeneities are taken to be perfectly bounded. This model composite is heterogeneous (but not necessarily isotropic), while each inhomogeneity and the matrix are assumed to be homogeneous. For convenience, no body force is considered in the remaining part of this chapter unless indicated otherwise.

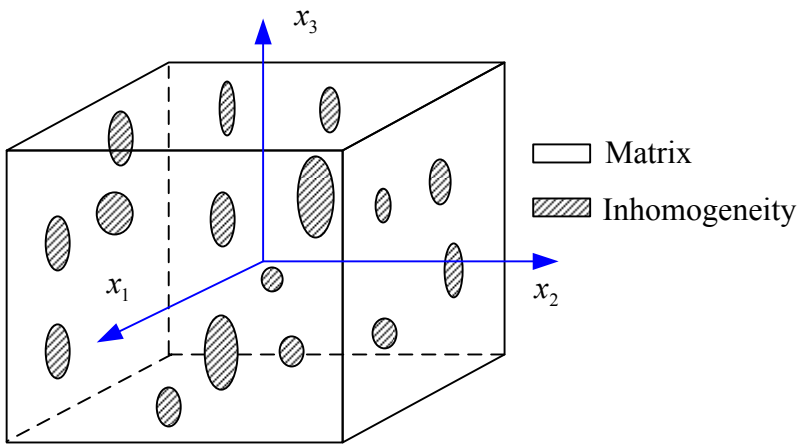

Fig. 7.1. Heterogeneous RVE.

In order the find the effective elastic properties of this heterogeneous composite material using the SSGET, a homogeneous comparison solid element of identical shape and size is introduced. This homogeneous material element is regarded as a strain-gradient elastic medium, whose elastic behavior can be described using the constitutive relations in Eqs. (2.5a,b). The elastic properties of this comparison solid can always be accommodated such that the two volume elements restore the same strain energy under identical boundary conditions. The homogenization method in this chapter aims to find the elastic properties of this homogeneous solid that is energetically equivalent to the heterogeneous material. This strain energy-based homogenization method was first proposed by Hill (1963) using classical elasticity, and is now widely used in predicting effective elastic properties of heterogeneous materials.

In the classical elasticity-based homogenization method, surface displacements that produce a uniform strain in the homogeneous Cauchy elastic medium are prescribed on the boundary (Hill, 1963). By applying such displacement boundary conditions, the strain energy of a Cauchy elastic material, homogeneous or heterogeneous, can be calculated

from the averaged stress and averaged strain. This uniform-strain boundary condition is based on the assumption that the fluctuation wavelength of the applied strain is much larger than the size of the RVE. That is, the applied strain to the RVE is macroscopically uniform. However, when a material experiences a larger deformation gradient such that the mean fields vary with the position of the RVE in the material, non-uniform strain boundary conditions have to be applied to account for the strain gradient. One of such boundary conditions is that the displacement on the boundary is approximated by the following quadratic expression (e.g., Forest, 1998; Bigoni and Drugan, 2007):

$$\hat{u}_i(\mathbf{x}) = \varepsilon^0_{ij} x_j + \beta^0_{ijk} x_j x_k \qquad (\mathbf{x} \in \partial\Omega), \tag{7.1}$$

where ε^0_{ij} and β^0_{ijk} are, respectively, the components of a second-order tensor and a third-order tensor, x_i is the ith component of the position vector $\mathbf{x}$, and $\partial\Omega$ is the boundary of the domain Ω occupied by the RVE. Clearly, Eq. (7.1) shows that $\beta^0_{ijk} = \beta^0_{ikj}$. If $\beta^0_{ijk} = 0$, Eq. (7.1) recoveres the uniform-strain boundary condition used in Hill's homogenization method (Hill, 1963). The displacement in Eq. (7.1) must satisfy the Navier-like displacement equilibrium equations give in Eq. (2.9) without body forces. Using Eq. (7.1) in Eq. (2.9) together with $f_j = 0$, results in

$$\beta^0_{iik} = (2\nu - 1)\beta^0_{kii}, \tag{7.2}$$

which gives three constraints on specifying β^0_{ijk}.

Substituting Eq. (7.1) into Eqs. (2.5c,d) yields the strain and strain gradient on the boundary as

$$\hat{\varepsilon}_{ij}(\mathbf{x}) = \varepsilon^0_{ij} + (\beta^0_{ijp} + \beta^0_{jip}) x_p, \qquad \hat{\kappa}_{ijk}(\mathbf{x}) = \beta^0_{ijk} + \beta^0_{jik} \tag{7.3a,b}$$

for any $\mathbf{x} \in \Omega$. From Eqs. (7.3a,b), it is seen that the strain $\hat{\varepsilon}_{ij}$ is linearly dependent on the position x, while the strain gradient $\hat{\kappa}_{ijk}$ is uniform on the boundary of the RVE. For a homogeneous material subject to the boundary condition in Eqs. (7.3a,b), it is conceivable that the strain gradient will be uniform throughout the material. This indicates that the displacement throughout the material takes the same form as that given in Eq. (7.1), subject to the constraints listed in Eq. (7.2). In other words, for a homogeneous material Eqs. (7.1) and (7.3a,b) also hold for the interior points (i.e., $\mathbf{x} \in \Omega$).

However, if a heterogeneous material model is subject to the boundary condition given in Eq. (7.1), the strain gradient in the interior will not be uniform as shown in Eq. (7.3b) due to the disturbance of existing inhomogeneities. In general, for a heterogeneous material, the strain and stress fields depend on the morphology and properties of the constituents and their distributions in the material.

The volume-averaged strain energy, *U*, stored in a material based on the SSGET can be expressed in terms of quantities on the boundary as (see Appendix I)

$$U = \frac{1}{2\mathrm{Vol}(\Omega)} \int_{\Omega} (\varepsilon_{ij}\tau_{ij} + \kappa_{ijk}\mu_{ijk})\, dV = \frac{1}{2\mathrm{Vol}(\Omega)} \int_{\partial\Omega} (\sigma_{ij}u_i n_j + \mu_{ijk}\varepsilon_{ij}n_k)\, dA, \qquad (7.4)$$

where $\mathbf{n} = n_i\mathbf{e}_i$ is the outward unit normal vector on $\partial\Omega$, κ_{ijk} is the component of the strain gradient tensor defined in Eq. (2.5d), and μ_{ijk} is the component of the double stress tensor defined in Eq. (2.5b). Using Eqs. (7.1) and (7.3a) in Eq. (7.4) gives

$$U = \frac{1}{2\mathrm{Vol}(\Omega)} \int_{\partial\Omega} \left[\sigma_{ij}\ \varepsilon^0_{im} x_m n_j + \mu_{ijk}\ \varepsilon^0_{ij} n_k + \sigma_{ij}\ \beta^0_{imn} x_m x_n n_j + \mu_{ijk}\ (\beta^0_{ijp} + \beta^0_{jip}) x_p n_k \right] dA. \qquad (7.5)$$

Applying the divergence theorem and the equilibrium equations $\sigma_{ij,j} = 0$ in Eq. (7.5) yields

$$U = \frac{1}{2\mathrm{Vol}(\Omega)} \varepsilon^0_{ij} \int_{\Omega} \tau_{ij}\ dV + \frac{1}{\mathrm{Vol}(\Omega)} \beta^0_{ijp} \int_{\Omega} (\tau_{ij} x_p + \mu_{ijp})\, dV. \qquad (7.6)$$

Eq. (7.6) gives the strain energy in an equilibrated material subject to the uniform strain gradient boundary condition listed in Eq. (7.1). Note that Eq. (7.4)–(7.6) are valid for both homogeneous and heterogeneous materials, for no assumption is made on material properties in reaching Eq. (7.4).

For a homogeneous material, using the constitutive equations in Eqs. (2.5a,b) and Eqs. (7.3a,b), which are valid for $\mathbf{x} \in \Omega$, into Eq. (7.6) leads to

$$U_H = \frac{1}{2} C^H_{ijlm} \varepsilon^0_{ij} \varepsilon^0_{lm} + C^H_{ijlm} \varepsilon^0_{ij} \beta^0_{lmk} \langle x_k \rangle_\Omega + C^H_{ijlm} \beta^0_{ijp} \varepsilon^0_{lm} \langle x_p \rangle_\Omega + 2 C^H_{ijlm} \beta^0_{ijp} \beta^0_{lmk} \left(\langle x_k x_p \rangle_\Omega + \overline{L}^2 \delta_{pk} \right), \quad (7.7)$$

where U_H is the volume-averaged strain energy in the homogenous material, C^H_{ijlm} and $\overline{L}$ are, respectively, the stiffness tensor and the material length scale parameter of the homogeneous material, and $\langle\ \rangle_\Omega$ denotes the volume average over the domain Ω.

On the other hand, for a heterogeneous material with (N+1) phases (with each phase defined as a collection of inhomogeneities whose shape, size and elastic properties are identical), the volume-averaged strain energy obtained in Eq. (7.6) can be further expressed as

$$U_C = \frac{1}{2} \varepsilon^0_{ij} \sum_{n=0}^{N} \left[\phi^{(n)} \langle \tau_{ij} \rangle_{\Omega_n} \right] + \beta^0_{ijp} \sum_{n=0}^{N} \left[\phi^{(n)} (\langle \tau_{ij} x_p \rangle_{\Omega_n} + \langle \mu_{ijp} \rangle_{\Omega_n}) \right], \quad (7.8)$$

where use has been made of

$$\langle f \rangle_\Omega = \sum_{n=0}^{N} \phi^{(n)} \langle f \rangle_{\Omega_n}\ , \quad (7.9)$$

in which f is a continuous quantity in the domain Ω, Ω_n is a subdomain of Ω occupied by the nth phase, Ω is the union of Ω_n with n ranging from 0 to N. In Eqs. (7.8) and (7.9) and throughout this chapter, the matrix is designated as the phase with n = 0, $\langle\ \rangle_{\Omega_n}$ represents the volume-averaged value over Ω_n, and $\phi^{(n)}$ is the volume fraction of the nth phase.

Note that in reaching Eq. (7.8), it has been assumed that each constituent of the heterogeneous material is a homogeneous strain-gradient medium whose constitutive behavior can be described by Eqs. (2.5a,b). Using Eqs. (2.5a,b) in Eq. (7.8) yields

$$U_C = \frac{1}{2}\varepsilon_{ij}^0 \sum_{n=0}^{N}\left[\phi^{(n)} C_{ijkl}^{(n)} \left\langle \varepsilon_{kl} \right\rangle_{\Omega_n}\right] + \beta_{ijp}^0 \sum_{n=0}^{N}\left\{\phi^{(n)} C_{ijkl}^{(n)}\left[\left\langle \varepsilon_{kl} x_p \right\rangle_{\Omega_n} + \left(L^{(n)}\right)^2 \left\langle \kappa_{klp} \right\rangle_{\Omega_n}\right]\right\}, \tag{7.10}$$

where $C_{ijkl}^{(n)}$ and $L^{(n)}$ are, respectively, the stiffness tensor and the material length scale parameter for the *n*th phase.

To get the effective elastic property of the heterogeneous material, the volume-averaged strain energy in the homogeneous comparison solid element given in Eq. (7.7) and that in the heterogeneous material element given in Eq. (7.10) should be identical, which requires

$$\begin{aligned} &\frac{1}{2}C_{ijlm}^H \varepsilon_{ij}^0 \varepsilon_{lm}^0 + C_{ijlm}^H \varepsilon_{ij}^0 \beta_{lmk}^0 \left\langle x_k \right\rangle_\Omega + C_{ijlm}^H \beta_{ijp}^0 \varepsilon_{lm}^0 \left\langle x_p \right\rangle_\Omega + 2C_{ijlm}^H \beta_{ijp}^0 \beta_{lmk}^0 \left(\left\langle x_k x_p \right\rangle_\Omega + \overline{L}^2 \delta_{pk}\right) \\ &= \frac{1}{2}\varepsilon_{ij}^0 \sum_{n=1}^{N}\left[\phi^{(n)} C_{ijkl}^{(n)} \left\langle \varepsilon_{kl} \right\rangle_{\Omega_n}\right] + \beta_{ijp}^0 \sum_{n=1}^{N}\left\{\phi^{(n)} C_{ijkl}^{(n)}\left[\left\langle \varepsilon_{kl} x_p \right\rangle_{\Omega_n} + \left(L^{(n)}\right)^2 \left\langle \kappa_{klp} \right\rangle_{\Omega_n}\right]\right\}. \end{aligned} \tag{7.11}$$

From Eq. (7.11) C_{ijlm}^H and $\overline{L}$, which are, respectively, the effective stiffness tensor and the effective material length scale parameter of the heterogeneous material can be determined. Note that C_{ijlm}^H and $\overline{L}$ should be independent of the location of the RVE. Therefore, the origin of the coordinate system can be placed at the centroid of the RVE for convenience. This gives $\left\langle x_p \right\rangle_\Omega = 0$. Then, Eq. (7.11) becomes

$$\begin{aligned} &\frac{1}{2}C_{ijlm}^H \varepsilon_{ij}^0 \varepsilon_{lm}^0 + 2C_{ijlm}^H \beta_{ijp}^0 \beta_{lmk}^0 \left(\left\langle x_k x_p \right\rangle_\Omega + \overline{L}^2 \delta_{pk}\right) \\ &= \frac{1}{2}\varepsilon_{ij}^0 \sum_{n=1}^{N}\left[\phi^{(n)} C_{ijkl}^{(n)} \left\langle \varepsilon_{kl} \right\rangle_{\Omega_n}\right] + \beta_{ijp}^0 \sum_{n=1}^{N}\left\{\phi^{(n)} C_{ijkl}^{(n)}\left[\left\langle \varepsilon_{kl} x_p \right\rangle_{\Omega_n} + \left(L^{(n)}\right)^2 \left\langle \kappa_{klp} \right\rangle_{\Omega_n}\right]\right\}. \end{aligned} \tag{7.12}$$

Considering that ε_{ij}^0 and β_{ijp}^0 can be chosen independently, Eq. (7.12) gives two sets

of equations

$$C_{ijlm}^{H}\varepsilon_{lm}^{0}=\sum_{n=0}^{N}\left[\phi^{(n)}C_{ijkl}^{(n)}\left\langle\varepsilon_{kl}\right\rangle_{\Omega_n}\right] \tag{7.13}$$

$$2C_{ijlm}^{H}\beta_{lmk}^{0}\left(\left\langle x_k x_p\right\rangle_{\Omega}+\bar{L}^{2}\delta_{pk}\right)=\sum_{n=0}^{N}\left\{\phi^{(n)}C_{ijkl}^{(n)}\left[\left\langle\varepsilon_{kl}x_p\right\rangle_{\Omega_n}+\left(L^{(n)}\right)^{2}\left\langle\kappa_{klp}\right\rangle_{\Omega_n}\right]\right\}. \tag{7.14}$$

From Eqs. (7.13) and (7.14), it is seen that once the relation between $\langle\boldsymbol{\varepsilon}\rangle_{\Omega_n}$ and $\boldsymbol{\varepsilon}^0$, and the relation between $\langle\boldsymbol{\varepsilon}\otimes\mathbf{x}\rangle_{\Omega_n}$, $\langle\boldsymbol{\kappa}\rangle_{\Omega_n}$ and $\boldsymbol{\beta}^0$ are known, the effective stiffness tensor C_{ijlm}^{H} and the effective material length scale parameter $\bar{L}$ can be determined for given volume fraction, stiffness tensor and material length scale parameter of each constituent of the composite. Eq. (7.13) is the same as what is obtained from the classical homogenization method (e.g., Weng, 1984; Li and Wang, 2008), where only a uniform strain $\boldsymbol{\varepsilon}^0$ is applied on the boundary and both the constituents of the heterogeneous material and its homogeneous equivalent are treated as Cauchy media.

It is clear from Eq. (7.12) that if only the uniform-strain boundary condition is prescribed, i.e., $\beta_{ijk}^{0}=0$ in Eqs. (7.1) and (7.12), the terms involving β_{ijp}^{0} on the both sides of Eq. (7.12) will vanish. As a result, Eq. (7.12) will be reduced to Eq. (7.13). In this case, the effective material length scale parameter $\bar{L}$ will not be involved. This implies that if the overall behavior of the heterogeneous material is expected to be characterized by the constitutive relations in the SSGET, the uniform strain gradient boundary condition in Eq. (7.1) (at least) has to be applied. This will lead to the determination of the effective material length scale parameter $\bar{L}$ from Eq. (7.14).

C_{ijlm}^{H} and $\bar{L}$ can be readily obtained from Eqs. (7.13) and (7.14) if the exact elastic strain and strain gradient fields in each phase are known. The exact solution for the elastic fields in a heterogeneous RVE subject to the boundary condition in Eq. (7.1) may only be

derived using the SSGET for inhomogeneities of simple shapes such as spherical and cylindrical ones. For inhomogeneities of complex shapes, numerical/approximate solutions will have to be sought and implemented to computationally complete the homogenization analysis.

In the next section, an analytical method is utilized to solve C_{ijlm}^{H} from Eq. (7.13). The volume-averaged strain in each phase will be determined analytically using the Eshelby tensors obtained in Chapters III–V.

7.3. New Homogenization Method Based on the SSGET

To solve Eq. (7.13) subject to the boundary condition in Eq. (7.1), the concept of averaged strain, which was first proposed by Mori and Tanaka (1973), is used. It can be imagined that the volume-averaged strain over the matrix, $\langle \boldsymbol{\varepsilon} \rangle_{\Omega_0}$, is different from that over the whole heterogeneous material due to the presence of inhomogeneities. For simplicity, one inhomogeneity will be considered here. The volume-averaged strain over this inhomogeneity further differs from that over the matrix by a perturbed value $\langle \boldsymbol{\varepsilon}^{d} \rangle_{\Omega_n}$. That is,

$$\langle \boldsymbol{\varepsilon} \rangle_{\Omega_n} = \langle \boldsymbol{\varepsilon} \rangle_{\Omega_0} + \langle \boldsymbol{\varepsilon}^{d} \rangle_{\Omega_n} . \tag{7.15}$$

To determine the volume-averaged strain $\langle \boldsymbol{\varepsilon} \rangle_{\Omega_n}$ in Eq. (7.15), an inclusion problem will be introduced, where a homogeneous body, Ω, made of the same material as that of the matrix, contains an inclusion which is of identical shape and size with those of the inhomogeneity. The inclusion is prescribed with a uniform stress-free eigenstrain $\boldsymbol{\varepsilon}^{*}$ and subject to the same averaged strain as in Eq. (7.15). The volume-averaged stresses over the inclusion and over the inhomogeneity can be made equivalent by suitably adjusting $\boldsymbol{\varepsilon}^{*}$. In

other words, the inclusion and the inhomogeneity problems are equivalent in the sense that their averaged strain and stress fields are identical. This equivalence states (Eshelby, 1957)

$$\mathbf{C}^{(0)} : (\langle \boldsymbol{\varepsilon} \rangle_{\Omega_0} + \langle \boldsymbol{\varepsilon}^d \rangle_{\Omega_n} - \boldsymbol{\varepsilon}^*) = \mathbf{C}^{(n)} : (\langle \boldsymbol{\varepsilon} \rangle_{\Omega_0} + \langle \boldsymbol{\varepsilon}^d \rangle_{\Omega_n}), \tag{7.16}$$

where $\mathbf{C}^{(0)}$ and $\mathbf{C}^{(n)}$ are, respectively, the fourth-order stiffness tensors of the matrix and the inhomogeneity.

From the derivations in Chapter II (see Eq. (2.40)) and considering that the size of the RVE is much larger than that of the inclusion, the volume-averaged disturbed strain due to the uniform eigenstrain $\boldsymbol{\varepsilon}^*$ over the domain occupied by an arbitrarily shaped 3-D inclusion is

$$\langle \boldsymbol{\varepsilon}^d \rangle_{\Omega_n} = \langle \mathbf{S} \rangle_{\Omega_n} : \boldsymbol{\varepsilon}^*, \tag{7.17}$$

where $\langle \mathbf{S} \rangle_{\Omega_n}$ is the volume-averaged Eshelby tensor based on the SSGET over the inclusion domain and has been obtain for spherical, cylindrical and elliptical inclusions in Chapters III–V (see Eqs. (3.18), (4.29) and (5.33)).

Using Eq. (7.17) in Eq. (7.16), the eigenstrain can be obained as

$$\boldsymbol{\varepsilon}^* = \mathbf{Q} : \langle \boldsymbol{\varepsilon} \rangle_{\Omega_0}, \tag{7.18}$$

with

$$\mathbf{Q} \equiv [(\mathbf{C}^{(0)} - \mathbf{C}^{(n)}) : \langle \mathbf{S} \rangle_{\Omega_n} - \mathbf{C}^{(0)}]^{-1} : (\mathbf{C}^{(n)} - \mathbf{C}^{(0)}). \tag{7.19}$$

Then from Eqs. (7.17)–(7.19) and (7.15), the volume-averaged strain over the inclusion domain is related to that over the matrix through

$$\langle \boldsymbol{\varepsilon} \rangle_{\Omega_n} = (\mathbf{I} + \langle \mathbf{S} \rangle_{\Omega_n} : \mathbf{Q}) : \langle \boldsymbol{\varepsilon} \rangle_{\Omega_0}, \tag{7.20}$$

where $\mathbf{I}$ is the fourth-order identity tensor. Using the following identity (Li and Wang,

2008):

$$\mathbf{I}+\langle\mathbf{S}\rangle_{\Omega_n}:\mathbf{Q}=\{\mathbf{I}+\langle\mathbf{S}\rangle_{\Omega_n}:[\mathbf{C}^{(0)}]^{-1}:(\mathbf{C}^{(n)}-\mathbf{C}^{(0)})\}^{-1}, \tag{7.21}$$

Eq. (7.20) is found to be identical to what is obtained using the classical Mori-Tanaka homogenization method based on classical elasticity (see Eqs. (7.16) and (7.17) in Qu and Cherkaoui, 2006) except for the expression of $\langle\mathbf{S}\rangle_{\Omega_n}$. $\langle\mathbf{S}\rangle_{\Omega_n}$ in Eq. (7.20) based on the SSGET contains a material length scale parameter and hence can capture the inclusion size effect, unlike its counterpart based on classical elasticity.

The above analysis involving a single inhomogeneity phase, which is a collection of inhomogeneities with identical size, shape and elastic properties and hence having the same $\langle\mathbf{S}\rangle_{\Omega_n}$ and $\mathbf{Q}$, remains valid for other phases. Therefore, from Eq. (7.20), it follows

$$\langle\boldsymbol{\varepsilon}\rangle_{\Omega}=\sum_{n=0}^{N}\phi^{(n)}\langle\boldsymbol{\varepsilon}\rangle_{\Omega_n}=\left\{\phi^{(0)}\mathbf{I}+\sum_{n=1}^{N}\phi^{(n)}(\mathbf{I}+\langle\mathbf{S}\rangle_{\Omega_n}:\mathbf{Q})\right\}:\langle\boldsymbol{\varepsilon}\rangle_{\Omega_0}, \tag{7.22}$$

where the volume-averaged strain over the matrix domain is related to that over the whole RVE.

Using Eqs. (2.5c) and (7.1) and $\langle\mathbf{x}\rangle_{\Omega}=0$ gives

$$\langle\boldsymbol{\varepsilon}\rangle_{\Omega}=\boldsymbol{\varepsilon}^{0}. \tag{7.23}$$

Through Eqs. (7.20), (7.22) and (7.23) the relation between the applied strain, $\boldsymbol{\varepsilon}^{0}$, on the boundary of the RVE and the volume-averaged strain over the domain of each phase is determined. Then, substituting Eqs. (7.23), (7.22) and (7.20) into (7.13) and letting the coefficients of $\langle\boldsymbol{\varepsilon}\rangle_{\Omega_0}$ on both sides of the equation be equal will result in

$$\mathbf{C}^{H}=\left[\phi^{(0)}\mathbf{C}^{(0)}+\sum_{n=1}^{N}\phi^{(n)}\mathbf{C}^{(n)}:(\mathbf{I}+\langle\mathbf{S}\rangle_{\Omega_n}:\mathbf{Q})\right]:\left[\phi^{(0)}\mathbf{I}+\sum_{n=1}^{N}\phi^{(n)}(\mathbf{I}+\langle\mathbf{S}\rangle_{\Omega_n}:\mathbf{Q})\right]^{-1} \tag{7.24}$$

as the effective stiffness tensor of the heterogeneous material. Note that the inhomogeneities are assumed to be unidirectional. Therefore, the influence of the inhomogeneity orientation distribution is not incorporated in Eq. (7.24).

From Eq. (7.24) it is seen that the effective stiffness tensor $\mathbf{C}^H$ depends not only on the shapes but also on the sizes of the inhomogeneities through the volume-averaged Eshelby tensor, $\langle \mathbf{S} \rangle_{\Omega_n}$, which involves the material length scale parameter of the matrix. Therefore, this effective stiffness tensor based on the SSGET is expected to be able to capture the experimentally observed particle size effect in composites (e.g., Kouzeli and Mortensen, 2002; Vollenberg, and Heikens, 1989; Vollenberg, et al., 1989).

7.4. Numerical Results

Several examples are provided here to quantitatively illustrate the dependence of the effective elastic properties of a heterogeneous material on inhomogeneity sizes, as analytically demonstrated in the preceding section. For simplicity, a composite material with two isotropic phases is chosen for analysis. For such a material, the total phase number $N = 2$, and Eq. (7.24) becomes

$$\mathbf{C}^H = [(1-\varphi)\mathbf{C}^{(0)} + \varphi\, \mathbf{C}^{(1)} : (\mathbf{I} + \langle \mathbf{S} \rangle_{\Omega_1} : \mathbf{Q})] : [(1-\varphi)\mathbf{I} + \varphi(\mathbf{I} + \langle \mathbf{S} \rangle_{\Omega_1} : \mathbf{Q})]^{-1}, \tag{7.25}$$

where $\mathbf{C}^{(0)}$ and $\mathbf{C}^{(1)}$ are, respectively, the fourth-order isotropic stiffness tensors of the matrix and the inhomogeneity phase, ϕ is the volume fraction of the inhomogeneity phase, and $\mathbf{Q}$ can be obtained from Eq. (7.19) with $n = 1$.

For a spherical inclusion with radius R, the volume-averaged Eshelby tensor $\langle \mathbf{S} \rangle_{\Omega_1}$ based on the SSGET given in Eq. (3.18) can be rewritten as

$$\left\langle \mathbf{S} \right\rangle_{\Omega_1} = S_P \mathbf{I}^P + S_S \mathbf{I}^S, \tag{7.26}$$

where

$$\begin{aligned} S_P &= \frac{\nu+1}{3(1-\nu)}\left\{1+\frac{3}{2}\left(\frac{L^{(0)}}{R}\right)^3\left[1-\left(\frac{R}{L^{(0)}}\right)^2-\left(1+\frac{R}{L^{(0)}}\right)^2 e^{-\frac{2R}{L^{(0)}}}\right]\right\}, \\ S_S &= \frac{8-10\nu}{15(1-\nu)}\left\{1+\frac{3}{2}\left(\frac{L^{(0)}}{R}\right)^3\left[1-\left(\frac{R}{L^{(0)}}\right)^2-\left(1+\frac{R}{L^{(0)}}\right)^2 e^{-\frac{2R}{L^{(0)}}}\right]\right\}, \end{aligned} \tag{7.27}$$

and $\mathbf{I}^P$ and $\mathbf{I}^S$ are two fourth-order tensors whose components are, respectively, given by

$$I^P_{ijkl} = \frac{1}{2}\left(\delta_{ik}\delta_{jl}+\delta_{il}\delta_{jk}\right)-\frac{1}{3}\delta_{ij}\delta_{kl}, \qquad I^S_{ijkl} = \frac{1}{3}\delta_{ij}\delta_{kl}. \tag{7.28}$$

When the gradient effect is not considered (i.e., when $L = 0$), Eqs. (7.26) and (7.27) can be reduced to the Eshelby tensor for a spherical inclusion based on classical elasticity:

$$\left\langle \mathbf{S}^{\mathrm{C}} \right\rangle_{\Omega_1} = S^C_P \mathbf{I}^P + S^C_S \mathbf{I}^S, \tag{7.29a}$$

where

$$S^C_P = \frac{\nu+1}{3(1-\nu)}, \qquad S^C_S = \frac{8-10\nu}{15(1-\nu)}. \tag{7.29b}$$

Using $\mathbf{I}^{\mathrm{P}}$ and $\mathbf{I}^S$ given in Eq. (7.28), the stiffness tensors $\mathbf{C}^{(0)}$ and $\mathbf{C}^{(1)}$ can also be decomposed as

$$\mathbf{C}^{(0)} = 3K^{(0)}\mathbf{I}^P + 2G^{(0)}\mathbf{I}^S \ , \quad \mathbf{C}^{(1)} = 3K^{(1)}\mathbf{I}^P + 2G^{(1)}\mathbf{I}^S, \tag{7.30}$$

where $K^{(0)}$ and $K^{(1)}$ are, respectively, the bulk moduli of the matrix and the inhomogeneity, and $G^{(0)}$ and $G^{(1)}$ are, respectively, the shear moduli of the matrix and the inhomogeneity.

After using Eqs. (7.30) and (7.26) in Eq. (7.25), the effective stiffness tensor can be obtained in the following closed form:

$$\mathbf{C}^H = 3K^H \mathrm{I}^P + 2G^H \mathrm{I}^S, \tag{7.31}$$

where

$$K^H = K^{(0)}\left[1+\frac{\phi(K^{(1)}-K^{(0)})}{K^{(0)}+(1-\phi)S_P(K^{(1)}-K^{(0)})}\right] \tag{7.32}$$

is the effective bulk modulus, and

$$G^H = G^{(0)}\left[1+\frac{\phi(G^{(1)}-G^{(0)})}{G^{(0)}+(1-\phi)S_S(G^{(1)}-G^{(0)})}\right] \tag{7.33}$$

is the effective shear modulus. In reaching Eqs. (7.31)–(7.33), use has been made of

$$\left(\alpha\,\mathrm{I}^{\mathrm{P}}+\beta\,\mathrm{I}^{\mathrm{S}}\right)^{-1}=\frac{1}{\alpha}\,\mathrm{I}^{\mathrm{P}}+\frac{1}{\beta}\,\mathrm{I}^{\mathrm{S}}, \tag{7.34}$$

where α and β are two arbitrary non-zero scalars (see Appendix A).

The effective Young's modulus can be readily obtained in term of K^H and G^H given in Eq. (7.32) and Eq. (7.33) as (e.g., Sadd, 2009)

$$E^H=\frac{9K^HG^H}{3K^H+G^H}\ . \tag{7.35}$$

For all of the examples included below in this chapter, the Young's modulus of the inhomogeneity material is taken to be 20 times that of the matrix, i.e., $E^{(1)}/E^{(0)}=20$. The Poisson's ratio, ν, for both the matrix and the inhomogeneity materials is taken to be 0.3. The length scale parameter for the matrix material, $L^{(0)}$, is 17.6 μm.

Figure 7.2 shows the effective Young's modulus, E^H, of the two-phase composite with spherical inhomogeneities varying with the volume fraction of the inhomogeneity material, ϕ. The values of E^H based on the SSGET are calculated using Eqs. (7.27), (7.32), (7.33) and (7.35), for the composites with four different inhomogeneity sizes: $R = L$, $R = 2L$, $R = 3L$ and $R = 10L$. For comparison, the values of the effective Young's modulus based on classical elasticity are also displayed in Fig. 7.2, which are computed using Eqs. (7.29b),

(7.32) (7.33) and (7.35).

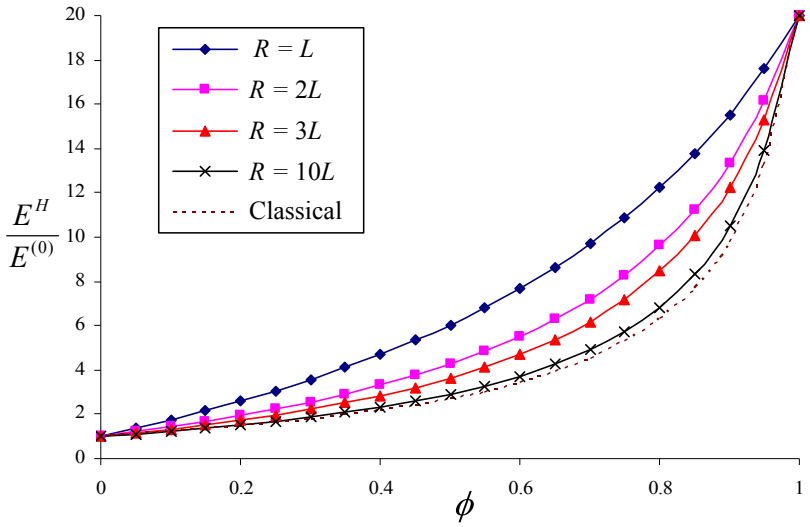

Fig. 7.2. Effective Young's modulus of a composite with spherical inhomogeneities.

From Fig. 7.2, it is observed that E^H based on the SSGET depends not only on the volume fraction of the inhomogeneity phase, but also on the inhomogeneity size R. Also, it is seen that the values of E^H based on the SSGET are much larger than those based on classical elasticity when R is small (with $R = L = 17.6$ μm here). This agrees with the experimental observations (Kouzeli and Mortensen, 2002): the smaller the inhomogeneity size is, the stiffer the composite material is. As R increases, the curves for E^H with the strain gradient effect become closer to that (the dashed curve) based on classical elasticity, which indicates that the strain gradient effect decreases as the inhomogeneity size increases. When the inhomogeneity size R is much larger than L (e.g., $R = 10L = 176$ μm here), the values of E^H approach the classical values, indicating that the strain gradient effect becomes insignificant and therefore may be ignored. The same trend is observed for the effective shear modulus of this composite containing spherical inhomogeneities.

The effective in-plane Young's modulus, E_{11}^{H}, of a composite with cylindrical inhomogeneities (fibers) of infinite length is shown in Fig. 7.3, where a is the fiber radius. The central lines of all the cylindrical fibers are aligned with x_3-axis. The values of E_{11}^{H} based on the SSGET are calculated using Eqs. (7.25), (7.19) and (4.29), while the values of its counterpart based on classical elasticity are obtained from Eqs. (7.25), (7.19) and (4.15a–c). Both the volume fraction dependence and the fiber size dependence can be seen from Fig. 7.3. As the radius a of the cylindrical fiber increases, the distance between the curves for E_{11}^{H} based on the SSGET and that for its classical counterpart decreases, which indicates that the gradient effect is diminishing. A comparison between Figs. 7.2 and 7.3 shows that the size effect is stronger for the composite containing spherical inhomogeneities than that filled with cylindrical inhomogeneities.

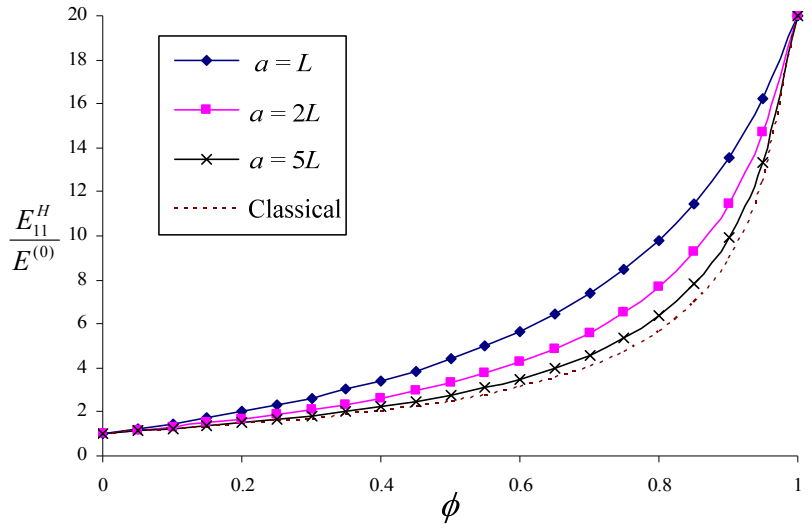

Fig.7.3. In-plane Young's Modulus of a composite with cylindrical inhomogeneities.

On the other hand, the size effect is not observed for the out-of-plane effective

Young's modulus E_{33}^H for the composite with cylindrical inhomogeneities. Both E_{33}^H based on the SSGET and its counterpart base on classical elasticity are linearly dependent on the volume fraction ϕ.

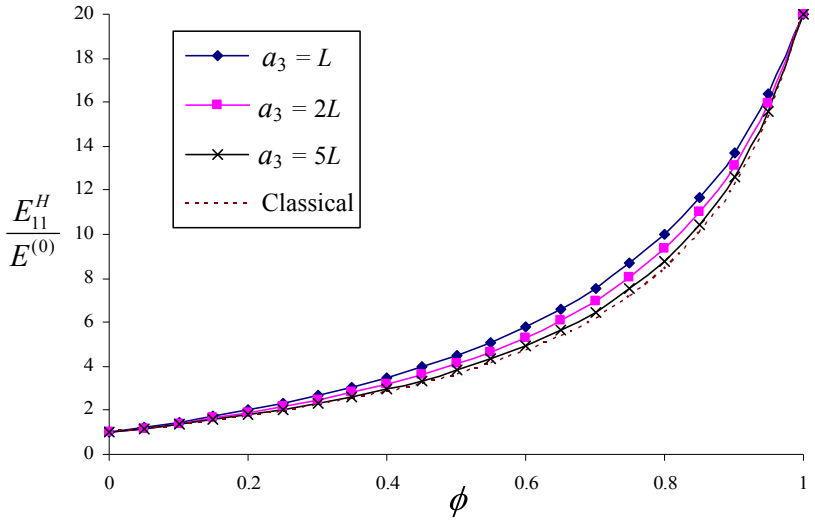

Fig. 7.4. Effective E_{11}^H of a composite with ellipsoidal inhomogeneities.

The effective Young's moduli are displayed in Figs. 7.4 and 7.5 for composites containing ellipsoidal inhomogeneities with three distinct semi-axes satisfying $a_1 : a_2 : a_3 = 3 : 2 : 1$. The a_3-axis of each of the ellipsoidal inhomogeneities is aligned with the x_3-axis in the chosen Cartesian coordinate system. E_{11}^H plotted in Fig. 7.4 is the effective Young's modulus in the x_1-direction, while E_{33}^H shown in Fig. 7.5 is the effective Young's modulus in the x_3-direction. Both E_{11}^H and E_{33}^H are obtained from the orthotropic effective stiffness tensor $\mathbf{C}^H$, calculated using Eqs. (7.25), (7.19) and (5.33). The size effect is clearly seen from Figs. 7.4 and 7.5 for both E_{11}^H and E_{33}^H: the smaller a_3 is, the larger the effective Young's modulus is. The size effect is more significant on E_{33}^H than on E_{11}^H, as indicated in

Figs. 7.4 and 7.5. This can be explained by the fact that the ellipsoidal inhomogeneities have the smallest dimension along the x_3-axis.

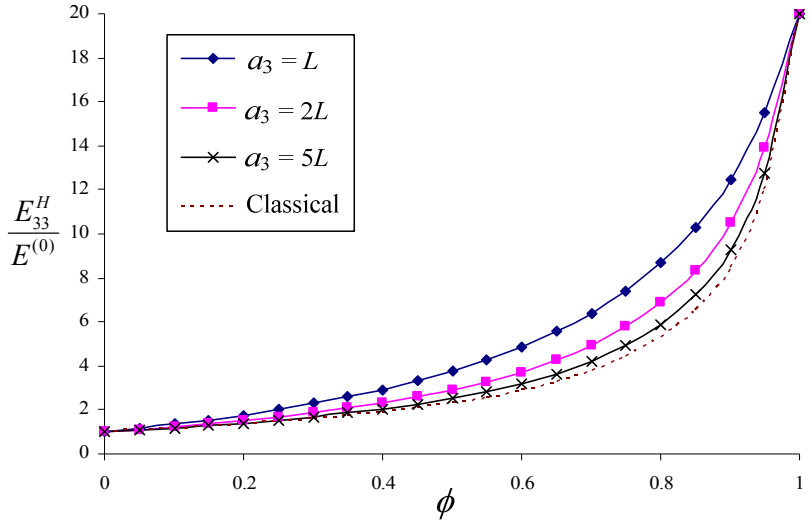

Fig. 7.5. Effective E_{33}^H of a composite with ellipsoidal inhomogeneities.

7.5. Summary

A homogenization method is developed in this chapter for predicting the effective elastic properties of a heterogeneous material using the SSGET. The overall behavior of the heterogeneous material is modeled as a homogeneous strain-gradient medium which is characterized by the SSGET. The effective elastic properties of the heterogeneous material are found to be dependent not only on the volume fractions, shapes and material properties of the inhomogeneities but also on the inhomogeneity sizes, unlike what is predicted by the homogenization methods based on classical elasticity. The effective elastic stiffness tensor is analytically obtained by using the Mori-Tanaka and Eshelby's equivalent inclusion methods.

To quantitatively illustrate the effective elastic properties of the composite material, sample numerical results are presented, which show that the inhomogeneity size has a strong influence on the effective Young's moduli when the inhomogeneity size is small (at the micron scale). The composite becomes stiffer when the inhomogeneities become smaller. It is also found that the inhomogeneity size effect on the effective Young's moduli becomes insignificant and may be neglected for composites filled by large inhomogeneities.

CHAPTER VIII

SUMMARY

The Eshelby inclusion problem of an inclusion embedded in an infinite homogeneous isotropic elastic material and prescribed with an eigenstrain and an eigenstrain gradient is solved analytically by using a simplified strain gradient elasticity theory (SSGET). This is accomplished by first deriving the three-dimensional Green's function in the SSGET in terms of elementary functions using Fourier transforms. The fourth-order Eshelby tensor is then obtained in a general form for an inclusion of arbitrary shape. The newly derived Eshelby tensor consists of two parts: a classical part depending only on Poisson's ratio, and a gradient part depending on the length scale parameter additionally. The accompanying fifth-order Eshelby-like tensor relating the prescribed eigenstrain gradient to the disturbed strain is also obtained analytically. When the strain gradient effect is not considered, the new Eshelby tensor reduces to that based on classical elasticity, and the Eshelby-like tensor vanishes.

The expressions of the Eshelby tensor for the special cases of a spherical inclusion and a cylindrical inclusion of infinite length are explicitly obtained by employing the general form of the newly derived Eshelby tensor. The numerical results quantitatively show that the components of the non-classical Eshelby tensor for either the spherical or the cylindrical inclusion vary with both the position and the inclusion size, unlike their counterparts in classical elasticity. For both the spherical and cylindrical inclusion problems, it is found that when the inclusion radius is small the contribution of the gradient part is significantly large and thus should not be ignored. For homogenization applications, the volume average of the non-classical Eshelby tensor over the spherical inclusion or the

cylindrical inclusion is derived in a closed form. It is observed that the components of the volume-averaged Eshelby tensor change with the inclusion size: the smaller the inclusion radius is, the smaller the component values are. Also, the values of these components are seen to approach from below those of their classical counterparts when the inclusion size becomes sufficiently large.

Moreover, the more general and complex ellipsoidal inclusion problem is analytically solved. By applying the general form of the Eshelby tensor in the SSGET, the Eshelby tensor for an ellipsoidal inclusion is obtained in analytical expressions for both of the regions inside and outside the inclusion in terms of two line integrals and two surface integrals over a unit sphere. The Eshelby tensor for the ellipsoidal inclusion problem includes those for the spherical and cylindrical inclusion problems based on the SSGET as two limiting cases. The volume-averaged Eshelby tensor over the ellipsoidal inclusion is also analytically obtained. Numerical results quantitatively show both the inclusion size dependence and the position dependence exhibited by the components of the Eshelby tensor derived. The same trend as that in the spherical and cylindrical inclusion problems is found here: the smaller the ellipsoidal inclusion is, the smaller the values of the components of the Eshelby tensor and its volume average are.

In order to incorporate the boundary effect, in addition to the particle size effect, a solution for the Eshelby-type inclusion problem of a finite homogeneous isotropic elastic body containing an inclusion is derived in a general form by using the SSGET. An extended Betti's reciprocal theorem and an extended Somigliana's identity based on the SSGET are proposed and utilized to solve the finite-domain inclusion problem. The solution for the disturbed displacement field is expressed in terms of the Green's function for an infinite three-dimensional elastic body in the SSGET. It contains a volume integral term and a

surface integral term. The former is the same as that for the infinite-domain inclusion problem based on the SSGET, while the latter represents the boundary effect. The solution reduces to that of the infinite-domain inclusion problem when the boundary effect is not considered. The problem of a spherical inclusion embedded concentrically in a finite spherical elastic body is analytically solved by applying the general solution, with the Eshelby tensor and its volume average obtained in closed forms. This Eshelby tensor depends on the position, inclusion size, matrix size, and material length scale parameter and, as a result, can capture the inclusion size and boundary effects, unlike existing ones. It reduces to the Eshelby tensor based on classical elasticity for the spherical inclusion in an infinite matrix if both the strain gradient and boundary effects are suppressed. Numerical results reveal that the inclusion size effect can be quite large when the inclusion is very small and that the boundary effect can dominate when the inclusion volume fraction is very high. However, the inclusion size effect is diminishing as the inclusion becomes large enough, and the boundary effect is vanishing as the inclusion volume fraction gets sufficiently low.

Finally, a homogenization method based on the SSGET is developed to predict the effective elastic properties of a heterogeneous (composite) material. The overall elastic behavior of the heterogeneous material is characterized by a homogeneous elastic medium that obeys the SSGET. An effective elastic stiffness tensor and an effective material length scale parameter are obtained for the heterogeneous material by applying the Mori-Tanaka and Eshelby's equivalent inclusion methods. Numerical results show that both of them are dependent not only on the volume fractions and shapes of the inhomogeneities but also on the inhomogeneity sizes, unlike what is predicted by existing homogenization methods based on classical elasticity. It is illustrated through numerical results for a two-phase

composite that the inhomogeneity size has a strong influence on the effective Young's moduli when the inhomogeneity size is small (at the micron scale). The composite becomes stiffer when the inhomogeneities get smaller. However the inhomogeneity size effect on the effective Young's moduli becomes insignificant and may be neglected for a composite filled with large inhomogeneities.

REFERENCES

Aifantis, E.C., 1999. Strain gradient interpretation of size effects. Int. J. Frac. 95, 299–314.

Aifantis, E.C., 2003. Update on a class of gradient theories. Mech. Mater. 35, 259–280.

Altan, B.S., Aifantis, E.C., 1992. On the structure of the mode III crack-tip in gradient elasticity. Scripta Met. 26, 319–324.

Altan, B.S., Aifantis, E.C., 1997. On some aspects in the special theory of gradient elasticity. J. Mech. Behavior Mater. 8 (3), 231–282.

Arfken, G.B., Weber, H.-J., 2005. Mathematical Methods for Physicists, 6th ed. Elsevier, San Diego.

Ashby, M.F., 1970. The deformation of plastically non-homogeneous materials. Phil. Mag. 21, 399–424.

Bigoni, D., Drugan, W.J., 2007. Analytical derivation of Cosserat moduli via homogenization of heterogeneous elastic materials. ASME J. Appl. Mech. 74, 741–753.

Cheng, Z.-Q., He, L.-H., 1995. Micropolar elastic fields due to a spherical inclusion. Int. J. Eng. Sci. 33, 389–397.

Cheng, Z.-Q., He, L.-H., 1997. Micropolar elastic fields due to a circular cylindrical inclusion. Int. J. Eng. Sci. 35, 659–668.

Eshelby, J.D., 1957. The determination of the elastic field of an ellipsoidal inclusion, and related problems. Proc. R. Soc. Lond. A 241, 376–396.

Eshelby, J.D., 1959. The elastic field outside an ellipsoidal inclusion. Proc. R. Soc. Lond. A 252, 561–569.

Evans, A.G., Hutchinson, J.W., 2009. A critical assessment of theories of strain gradient plasticity. Acta Mater. 57, 1675–1688.

Fleck, N.A. , Hutchinson, J.W., 1997. Strain gradient plasticity. Adv. Appl. Mech. 33, 295–361.

Fleck, N.A., Muller, G.M., Ashby, M.F. , Hutchinson, J.W., 1994. Strain gradient plasticity: theory and experiment. Acta Metall. Mater. 42, 475–487.

Forest, S., 1998. Mechanics of generalized continua: construction by homogenization. J. Phys. IV France 8, 39–47.

Gao, H., Huang, Y., Nix, W.D., Hutchinson, J.W., 1999. Mechanism-based strain gradient plasticity – I. Theory. J. Mech. Phys. Solids 47, 1239–1263.

Gao, X.-L., Ma, H. M., 2010a. Strain gradient solution for Eshelby's ellipsoidal inclusion problem. Proc. Royal Soc. A (published online in March 2010) (doi:10.1098/rspa.2009.0631)

Gao, X.-L., Ma, H. M., 2010b. Solution of Eshelby's inclusion problem with a bounded domain and Eshelby's tensor for a spherical inclusion in a finite spherical matrix based on a simplified strain gradient elasticity theory. J. Mech. Phys. Solids (published online in February 2010). (doi:10.1016/j.jmps.2010.01.006)

Gao, X.-L., Ma, H.M., 2009. Green's function and Eshelby's tensor based on a simplified strain gradient elasticity theory. Acta Mech. 207, 163–181.

Gao, X.-L., Park, S.K., 2007. Variational formulation of a simplified strain gradient elasticity theory and its application to a pressurized thick-walled cylinder problem. Int. J. Solids Struct. 44, 7486–7499.

Gao, X.-L., 2008. Analytical solution for the stress field around a hard spherical particle in a metal matrix composite incorporating size and finite volume effects. Math.

Mech. Solids 13, 357–372.

Gao, X.-L., Park, S. K., Ma, H.M., 2009. Analytical solution for a pressurized thick-walled spherical shell based on a simplified strain gradient elasticity theory. Math. Mech. Solids 14, 747–758.

Georgiadis, H.G., Vardoulakis, I., Velgaki, E.G., 2004. Dispersive Rayleigh-wave propagation in microstructured solids characterized by dipolar gradient elasticity. J. Elasticity 74, 17–45.

Giannakopoulos, A.E., Stamoulis, K., 2007. Structural analysis of gradient elastic components. Int. J. Solids Struct. 44, 3440–3451.

Gourgiotis, P.A., Georgiadis, H.G., 2009. Plane-strain crack problems in microstructured solids governed by dipolar gradient elasticity, J. Mech. Phys. Solids 57. 1898–1920.

Gradshteyn, I.S., Ryzhik, I.M., 2007. Table of Integrals, Series, and Products, Alan Jeffrey and Daniel Zwillinger (Eds.), 7th ed. Academic Press, Boston.

Green, A.E., Rivlin, R.S., 1964a. Simple force and stress multipoles. Arch. Rat. Mech. Anal. 16, 325–353.

Green, A.E., Rivlin, R.S., 1964b. Multipolar continuum mechanics. Arch. Rat. Mech. Anal. 17, 113–147.

Hashin, Z., 1983. Analysis of composite materials—a survey. J. Appl. Mech. 50, 481–505.

Hill, R., 1963. Elastic properties of reinforced solids: some theoretical principles. J. Mech. Phys. Solids 11, 357–372.

Ju, J. W., Sun, L. Z., 1999. A novel formulation for the exterior-point Eshelby's tensor of an ellipsoidal inclusion. ASME J Appl. Mech. 66, 570–574.

Kakunai, S., Masaki, J., Kuroda, R., Iwata, K., Nagata, R., 1985. Measurement of apparent Young's modulus in the bending of cantilever beam by heterodyne holographic interferometry. Exp. Mech. 25, 408–412.

Kinoshita, N., Mura, T., 1984. Eigenstrain problems in a finite elastic body. SIAM J. Appl. Math. 44, 524–535.

Kiris, A., Inan, E., 2006. Eshelby tensors for a spherical inclusion in microstretch elastic fields. Int. J. Solids Struct. 43, 4720–4738.

Koiter, W.T., 1964. Couple-stresses in the theory of elasticity: I and II. Proc. K. Ned. Akad. Wet. B67 (1), 17–44.

Kouzeli, M., Mortensen, A., 2002. Size dependent strengthening in particle reinforced aluminium. Acta Mater. 50, 39–51.

Kröner, E., 1963. On the physical reality of torque stresses in continuum mechanics. Int. J. Eng. Sci. 1, 261–278.

Lakes, R., 1995. Experimental methods for study of Cosserat elastic solids and other generalized elastic continua. In: Muhlhaus, H.(Ed.), Continuum Models for Materials with Micro-Structure. Wiley, New-York, pp.1–22.

Lam, D.C.C., Yang, F., Chong, A.C.M., Wang, J., Tong, P., 2003. Experiments and theory in strain gradient elasticity. J. Mech. Phys. Solids 51, 1477–1508.

Lazar, M., Maugin, G.A., 2005. Nonsingular stress and strain fields of dislocations and disclinations in first strain gradient elasticity. Int. J. Eng. Sci. 43, 1157–1184.

Lazar, M., Maugin, G.A., Aifantis, E.C., 2005. On dislocations in a special class of generalized elasticity. Phys. Stat. Sol. (b) 242, 2365–2390.

Lazopoulos, K.A., 2004. On the gradient strain elasticity theory of plates. Euro. J. Mech. A/Solids 23, 843–852.

Li, S., Wang, G., 2008. Introduction to Micromechanics and Nanomechanics, World Scientific, Singapore.

Li, S., Miskioglu, I., Altan, B.S., 2004. Solution to line loading of a semi-infinite solid in gradient elasticity. Int. J. Solids Struct. 41, 3395–3410.

Li, S., Sauer, R.A., Wang, G., 2007. The Eshelby tensors in a finite spherical domain – Part I: Theoretical formulations. ASME J. Appl. Mech. 74, 770–783.

Liu, L. P., 2008. Solutions to the Eshelby conjectures. Proc. Royal Soc. Lond. A 464, 573–594.

Lloyd, D.J., 1994. Particle reinforced aluminum and magnesium matrix composites. Int. Mater. Rev. 39, 1–23.

Luo, H.A., Weng, G.J., 1987. On Eshelby's inclusion problem in a three-phase spherically concentric solid, and a modification of Mori-Tanaka's method. Mech. Mater. 6, 347–361.

Luo, H.A., Weng, G.J., 1989. On Eshelby's S-tensor in a three-phase cylindrically concentric solid, and the elastic moduli of fiber-reinforced composites. Mech. Mater. 8, 77–88.

Ma, H.M., Gao, X.-L., 2010. Eshelby's tensors for plane strain and cylindrical inclusions based on a simplified strain gradient elasticity theory. Acta Mech. 211, 115–129.

Ma, H.S., Hu, G.K., 2006. Eshelby tensors for an ellipsoidal inclusion in a micropolar material. Int. J. Eng. Sci. 44, 595–605.

Ma, H.S., Hu, G.K., 2007. Eshelby tensors for an ellipsoidal inclusion in a microstretch material. Int. J. Solids Struct. 44, 3049–3061.

Magnus, W., Oberhettinger, F., Soni, R.P., 1966. Formulas and Theorems for the Special Functions of Mathematical Physics. Springer-Verlag, New York.

Maranganti, R., Sharma, P., 2007. A novel atomistic approach to determine strain-gradient elasticity constants: Tabulation and comparison for various metals, semiconductors, silica, polymers and the (Ir) relevance for nanotechnologies. J. Mech. Phy. Solids 55, 1823–1852.

Markenscoff, X., 1998. Inclusions with constant eigenstress. J. Mech. Phys. Solids 46, 2297–2301.

Michelitsch, T.M., Gao, H., Levin, V.M., 2003. Dynamic Eshelby tensor and potentials for ellipsoidal inclusions. Proc. R. Soc. Lond. A 459, 863–890.

Mindlin, R.D., Eshel, N.N., 1968. On first strain-gradient theories in linear elasticity. Int. J. Solids Struct. 4, 109–124.

Mindlin, R.D., 1964. Micro-structure in linear elasticity. Arch. Rat. Mech. Anal. 16, 51–78.

Mindlin, R.D., 1965. Second gradient of strain and surface-tension in linear elasticity. Int. J. Solids Struct. 1, 417–438.

Mori, T., Tanaka, K., 1973. Average stress in matrix and average elastic energy of materials with misfitting inclusions. Acta Metall. 21, 571–574.

Mura, T., 1987. Micromechanics of Defects in Solids, 2nd ed. Martinus Nijhoff, Dordrecht.

Nemat-Nasser, S., Hori, M., 1999. Micromechanics: Overall Properties of Heterogeneous Materials, 2nd ed. Elsevier Science, Amsterdam, The Netherlands.

Nix, W.D., Gao, H., 1998. Indentation size effects in crystalline materials: a law for strain gradient plasticity. J. Mech. Phys. Solids 46, 411–425.

Paris, F., Canas, J., 1997. Boundary Element Method: Fundamentals and Applications. Oxford Science Publications, Oxford.

Polyzos, D., Tsepoura, K.G., Tsinopoulos, S.V., Beskos, D.E., 2003. A boundary element method for solving 2-D and 3-D static gradient elastic problems Part I: Integral formulation. Comput. Methods Appl. Mech. Engrg. 192, 2845–2873.

Qu, J., Cherkaoui, M., 2006. Fundamentals of Micromechanics of Solids. Wiley, Hoboken, NJ.

Sadd, M.H., 2009. Elasticity: Theory, Applications, and Numerics, 2nd ed. Academic Press, Burlington, MA.

Shi, M.X., Huang, Y., Hwang, K.C., 2000. Fracture in a higher-order elastic continuum. J. Mech. Phys. Solids 48, 2513–2538.

Timoshenko, S.P., Goodier, J.N., 1970. Theory of Elasticity, 3rd ed. McGraw-Hill, New York.

Toupin, R.A., 1962. Elastic materials with couple-stresses. Arch. Rat. Mech. Anal. 11, 385–414.

Vollenberg, P.H.T., Heikens, D., 1989. Particle size dependence of the Young's modulus of filled polymers: 1. Preliminary experiments. Polymer 30, 1656–1662.

Vollenberg, P.H.T., de Haan, J.W., van de Ven, L.J.M., Heikens, D., 1989. Particle size dependence of the Young's modulus of filled polymers: 2. Annealing and solid-state nuclear magnetic resonance experiments. Polymer 30, 1663–1668.

Weng, G. J., 1984. Some elastic properties of reinforced solids, with special reference to isotropic ones containing spherical inclusions. Int. J. Eng. Sci. 22, 845–856.

Xun, F., Hu, G.K., Huang, Z.P., 2004. Effective in plane moduli of composites with a micropolar matrix and coated fibers. Int. J. Solids Struct. 41, 247–265.

Zhang, X., Sharma, P., 2005. Inclusions and inhomogeneities in strain gradient elasticity with couple stresses and related problems. Int. J. Solids Struct. 42, 3833–3851.

Zheng, Q.-S., Zhao, Z.-H., 2004. Green's function and Eshelby's fields in couple-stress elasticity. Int. J. Multiscale Comput. Eng. 2, 15–27.

APPENDIX A

Note that in reaching Eq. (2.13b) use has been made of the following identity:

$$\left(\alpha \mathrm{I}_{ij}^{P} + \beta \mathrm{I}_{ij}^{S}\right)^{-1} = \left(\frac{1}{\alpha}\mathrm{I}_{ij}^{P} + \frac{1}{\beta}\mathrm{I}_{ij}^{S}\right), \tag{A.1}$$

where α, β are two arbitrary non-zero scalars, $\mathrm{I}_{ij}^{S} = \xi_i^0 \xi_j^0$ are the components of a second-order spin tensor $\mathbf{I}^S = \boldsymbol{\xi}^0 \otimes \boldsymbol{\xi}^0$ (with $\boldsymbol{\xi}^0$ being a unit vector introduced in Eq. (2.12)), $\mathrm{I}_{ij}^{P} = \delta_{ij} - \xi_i^0 \xi_j^0$ are the components of the associated projection tensor $\mathbf{I}^P = \mathbf{I} - \mathbf{I}^S$, with $\mathbf{I} = \delta_{ij}\mathbf{e}_i \otimes \mathbf{e}_j$ being the second-order identity tensor. Eq. (A.1) can be easily proved by using the definition of an inverse matrix.

APPENDIX B

In this appendix, it is shown that the integration result given in Eq. (2.18) is true. That is,

$$\int_0^{2\pi} \xi_i^0 \xi_j^0 d\varphi = \pi\left[\delta_{ij} \sin^2\theta - x_i^0 x_j^0 (1 - 3\cos^2\theta)\right]. \tag{B.1}$$

[Proof] For the chosen spherical coordinate system (ξ, θ, φ) in the transformed space where the position vector $\boldsymbol{\xi} = \xi\boldsymbol{\xi}^0$ makes the angle θ with the position vector $\mathbf{x}$ (with the direction of $\mathbf{x}$ being where $\theta = 0$) in the physical space, one can write the unit vector in the $\boldsymbol{\xi}$ direction as

$$\boldsymbol{\xi}^0 = \mathbf{x}^0 \cos\theta + (\mathbf{y}^0 \cos\varphi + \mathbf{z}^0 \sin\varphi)\sin\theta, \tag{B.2}$$

where $\mathbf{x}^0$ is the unit vector along the $\mathbf{x}$ direction, and $\mathbf{y}^0$ and $\mathbf{z}^0$ are the unit vectors perpendicular to $\mathbf{x}^0$. In component form, Eq. (B.2) reads

$$\xi_i^0 = x_i^0 \cos\theta + (y_i^0 \cos\varphi + z_i^0 \sin\varphi)\sin\theta. \tag{B.3}$$

Then, it follows from Eq. (B.3) that

$$\begin{aligned} \xi_i^0 \xi_j^0 = {} & x_i^0 x_j^0 \cos^2\theta + x_i^0 y_j^0 \sin\theta\cos\theta\cos\varphi + x_i^0 z_j^0 \sin\theta\cos\theta\sin\varphi \\ & + y_i^0 x_j^0 \sin\theta\cos\theta\cos\varphi + y_i^0 y_j^0 \sin^2\theta\cos^2\varphi + y_i^0 z_j^0 \sin^2\theta\sin\varphi\cos\varphi \\ & + z_i^0 x_j^0 \sin\theta\cos\theta\sin\varphi + z_i^0 y_j^0 \sin^2\theta\sin\varphi\cos\varphi + z_i^0 z_j^0 \sin^2\theta\sin^2\varphi. \end{aligned} \tag{B.4}$$

Note that

$$\int_0^{2\pi} \cos\varphi d\varphi = 0,\ \int_0^{2\pi} \sin\varphi d\varphi = 0,\ \int_0^{2\pi} \sin\varphi\cos\varphi d\varphi = 0,\ \int_0^{2\pi} \cos^2\varphi d\varphi = \pi,\ \int_0^{2\pi} \sin^2\varphi d\varphi = \pi. \tag{B.5}$$

Integrating on both sides of Eq. (B.4), together with the use of Eq. (B.5), results in

$$\int_0^{2\pi} \xi_i^0 \xi_j^0 d\varphi = 2\pi x_i^0 x_j^0 \cos^2\theta + \pi y_i^0 y_j^0 \sin^2\theta + \pi z_i^0 z_j^0 \sin^2\theta. \tag{B.6}$$

Notice that

$$\begin{aligned} x_i^0 x_j^0 + y_i^0 y_j^0 + z_i^0 z_j^0 &= (\mathbf{x}^0 \cdot \mathbf{e}_i)(\mathbf{x}^0 \cdot \mathbf{e}_j) + (\mathbf{y}^0 \cdot \mathbf{e}_i)(\mathbf{y}^0 \cdot \mathbf{e}_j) + (\mathbf{z}^0 \cdot \mathbf{e}_i)(\mathbf{z}^0 \cdot \mathbf{e}_j) \\ &= \mathbf{e}_i \cdot (\mathbf{x}^0 \otimes \mathbf{x}^0)\mathbf{e}_j + \mathbf{e}_i \cdot (\mathbf{y}^0 \otimes \mathbf{y}^0)\mathbf{e}_j + \mathbf{e}_i \cdot (\mathbf{z}^0 \otimes \mathbf{z}^0)\mathbf{e}_j \\ &= \mathbf{e}_i \cdot [(\mathbf{x}^0 \otimes \mathbf{x}^0) + (\mathbf{y}^0 \otimes \mathbf{y}^0) + (\mathbf{z}^0 \otimes \mathbf{z}^0)]\mathbf{e}_j \\ &= \mathbf{e}_i \cdot \mathbf{I}\mathbf{e}_j = \delta_{ij}, \end{aligned} \tag{B.7}$$

where the fourth equality is based on the fact that the three orthogonal unit vectors $\mathbf{x}^0$, $\mathbf{y}^0$ and $\mathbf{z}^0$ form a set of base vectors in the 3-D physical space. Using Eq. (B.7) and the identity $\sin^2\theta = 1 - \cos^2\theta$ in Eq. (B.6) will immediately give Eq. (B.1).

APPENDIX C

In this appendix the following two identities, which are given in Eqs. (2.46a,b), are proven:

$$\Phi_{,ijkk} = 2\Lambda_{,ij}, \quad \Gamma_{,ijkk} = \frac{1}{L^2}\Gamma_{,ij}. \tag{C.1a,b}$$

The proof for Eq. (2.46c) can be found in Li and Wang (2008).

[Proof] From Eqs. (2.43a,b) it follows that

$$\begin{aligned}\Phi_{,kk}(\mathbf{x}) &= \frac{\partial^2}{\partial x_k \partial x_k}\int_\Omega |\mathbf{x}-\mathbf{y}|d\mathbf{y} = \frac{\partial^2}{\partial x_k \partial x_k}\int_\Omega \sqrt{(x_i-y_i)(x_i-y_i)}d\mathbf{y} = \int_\Omega \frac{\partial}{\partial x_k}\left(\frac{x_k-y_k}{\sqrt{(x_i-y_i)(x_i-y_i)}}\right)d\mathbf{y} \\ &= 2\int_\Omega \frac{d\mathbf{y}}{\sqrt{(x_i-y_i)(x_i-y_i)}} = 2\Lambda(\mathbf{x}).\end{aligned} \tag{C.2}$$

Differentiating both sides of Eq. (C.2) with respect to x_i and x_j sequentially will immediately give Eq. (C.1a), thereby proving Eq. (2.46a).

To prove Eq. (C.1b), note from Eq. (2.43c) that

$$\Gamma(\mathbf{x}) \equiv \left\langle \frac{e^{-|\mathbf{x}-\mathbf{y}|/L}}{|\mathbf{x}-\mathbf{y}|} \right\rangle = \left\langle \frac{e^{-r/L}}{r} \right\rangle \equiv \langle F(r) \rangle, \tag{C.3}$$

where $r \equiv |\mathbf{x}-\mathbf{y}|$, and $\langle \cdot \rangle$ denotes the volume integral over the inclusion region Ω. Differentiating (C.3) two times and four times respectively yields, with the help of the product and chain rules,

$$\frac{\partial^2 \Gamma(\mathbf{x})}{\partial x_i \partial x_j} = \langle (D_2F)(x_j-y_j)(x_i-y_i) + (D_1F)\delta_{ij} \rangle, \tag{C.4a}$$

$$\begin{aligned}\frac{\partial^4 \Gamma(\mathbf{x})}{\partial x_i \partial x_j \partial x_k \partial x_l} = \big\langle &(D_4F)(x_l-y_l)(x_k-y_k)(x_j-y_j)(x_i-y_i) + (D_3F)[\delta_{kl}(x_j-y_j)(x_i-y_i) \\ &+ \delta_{jl}(x_k-y_k)(x_i-y_i) + \delta_{il}(x_k-y_k)(x_j-y_j) + \delta_{jk}(x_l-y_l)(x_i-y_i) \\ &+ \delta_{ik}(x_l-y_l)(x_j-y_j) + \delta_{ij}(x_l-y_l)(x_k-y_k)] + (D_2F)(\delta_{il}\delta_{jk} + \delta_{ik}\delta_{jl} + \delta_{ij}\delta_{kl}) \big\rangle,\end{aligned} \tag{C.4b}$$

where

$$D_1F \equiv \frac{F'(r)}{r},\ D_2F \equiv \frac{1}{r}\frac{d(D_1F)}{d\,r} = \frac{1}{r^2}\left(F'' - \frac{F'}{r}\right),\ D_3F \equiv \frac{1}{r}\frac{d(D_2F)}{d\,r} = \frac{1}{r^3}\left(F''' - \frac{3F''}{r} + \frac{3F'}{r^2}\right),$$
$$D_4F \equiv \frac{1}{r}\frac{d(D_3F)}{d\,r} = \frac{1}{r^4}\left[F^{(4)} - \frac{6F'''}{r} + \frac{15F''}{r^2} - \frac{15F'}{r^3}\right], \tag{C.5}$$
$$F \equiv \frac{e^{-r/L}}{r},\quad F' = \frac{dF}{dr} = -\frac{1}{r^2}\left(1+\frac{r}{L}\right)e^{-r/L},\quad F'' = \frac{d^2F}{dr^2} = \left[\frac{1}{r^3}\left(2+\frac{r}{L}\right) + \frac{1}{L^2r}\left(1+\frac{L}{r}\right)\right]e^{-r/L},$$
$$F''' = \frac{d^3F}{dr^3} = -\left[\frac{1}{L^2r^2}\left(3+\frac{r}{L}\right) + \frac{6}{r^4}\left(1+\frac{r}{L}\right)\right]e^{-r/L},$$
$$F^{(4)} = \frac{d^4F}{dr^4} = \left[\frac{1}{L^3r^2}\left(4+\frac{r}{L}\right) + \frac{12}{Lr^4}\left(2+\frac{r}{L}\right) + \frac{24}{r^5}\right]e^{-r/L}.$$

It follows from Eqs. (C.4b) and (C.5) that

$$\nabla^2\Gamma_{,ij} = \frac{\partial^4\Gamma(\mathbf{x})}{\partial x_i \partial x_j \partial x_k \partial x_k} = \left\langle [(D_4F)r^2 + 7(D_3F)](x_j - y_j)(x_i - y_i) + [(D_3F)r^2 + 5(D_2F)]\delta_{ij} \right\rangle \tag{C.6}$$
$$= \left\langle \frac{1}{r^2L^2}\left(\frac{1}{rL^2} + \frac{3}{r^2L} + \frac{3}{r^3}\right)e^{-r/L}(x_j - y_j)(x_i - y_i) - \frac{1}{rL^2}\left(\frac{1}{rL} + \frac{1}{r^2}\right)e^{-r/L}\delta_{ij} \right\rangle,$$

and from Eqs. (C.4a) and (C.5) that

$$\frac{\partial^2\Gamma(\mathbf{x})}{\partial x_i \partial x_j} = \left\langle \frac{1}{r^2}\left(\frac{1}{rL^2} + \frac{3}{r^2L} + \frac{3}{r^3}\right)e^{-r/L}(x_j - y_j)(x_i - y_i) - \frac{1}{r}\left(\frac{1}{rL} + \frac{1}{r^2}\right)e^{-r/L}\delta_{ij} \right\rangle. \tag{C.7}$$

A comparison of Eqs. (C.6) and (C.7) immediately shows that Eq. (C1.b) is an identity, thereby completing the proof of Eq. (2.46b).

APPENDIX D

For the infinitely long cylindrical inclusion of the radius a, which occupies the domain Ω, the scalar-valued function $\Gamma(x)$ defined in Eq. (2.43c) becomes, in the cylindrical coordinate system (r, θ, y_3) originated from the symmetry axis (as the y_3-axis) of the inclusion,

$$\Gamma(x) = \int_0^{2\pi} \int_0^a r \left[\int_{-\infty}^{+\infty} \frac{e^{-\sqrt{R^2+(x_3-y_3)^2}/L}}{\sqrt{R^2+(x_3-y_3)^2}} dy_3 \right] dr d\theta, \tag{D.1}$$

where

$$R \equiv \sqrt{(x_1-y_1)^2+(x_2-y_2)^2}, \quad r \equiv \sqrt{y_1^2+y_2^2}, \quad \theta \equiv \tan^{-1}\frac{y_2}{y_1}. \tag{D.2a–c}$$

Note that

$$\int_{-\infty}^{+\infty} \frac{e^{-\sqrt{R^2+(x_3-y_3)^2}/L}}{\sqrt{R^2+(x_3-y_3)^2}} dy_3 = 2\int_0^{+\infty} \frac{e^{-\sqrt{R^2+t^2}/L}}{\sqrt{R^2+t^2}} dt \equiv 2K_0\left(\frac{R}{L}\right), \tag{D.3}$$

where K_0, as defined, is the modified Bessel function of the second kind of the zeroth order (e.g., Gradshteyn and Ryzhik, 2007). Eq. (D.2a) can be rewritten as

$$R = \sqrt{x^2 + r^2 - 2rx\cos\alpha}\,, \tag{D.4}$$

where $x = |\mathbf{x}| = \sqrt{x_1^2+x_2^2}$ (as defined earlier) and α is the angle between the vectors $\mathbf{x} = x_1\mathbf{e}_1+x_2\mathbf{e}_2$ and $\boldsymbol{R}_1 = y_1\mathbf{e}_1+y_2\mathbf{e}_2$ on the plane $y_3 = 0$. Clearly, $\alpha = \theta - c$, where c is the angle between the specified vector $\mathbf{x}$ and the y_1 axis and is a constant. Using the expression of R given in Eq. (D.4) in $K_0(\frac{R}{L})$ defined in Eq. (D.3) leads to (Magnus et al, 1966)

$$K_0\left(\frac{R}{L}\right) = \begin{cases} I_0\left(\frac{x}{L}\right)K_0\left(\frac{r}{L}\right) + 2\sum_{n=1}^{\infty} I_n\left(\frac{x}{L}\right)K_n\left(\frac{r}{L}\right)\cos(n\alpha) & (x<r) \\ I_0\left(\frac{r}{L}\right)K_0\left(\frac{x}{L}\right) + 2\sum_{n=1}^{\infty} I_n\left(\frac{r}{L}\right)K_n\left(\frac{x}{L}\right)\cos(n\alpha) & (x>r) \end{cases} \tag{D.5a,b}$$

where $I_n(\cdot)$ and $K_n(\cdot)$ (n = 0, 1, 2, …) are the modified Bessel functions of the indicated

arguments.

Using Eqs. (D.3) and (D.5a,b) in Eq. (D.1) then gives, for any point **x** located inside the inclusion (with $x < a$),

$$\begin{aligned}\Gamma(x) &= 2\left\{\int_0^x\int_0^{2\pi}\left[I_0\left(\frac{r}{L}\right)K_0\left(\frac{x}{L}\right)+2\sum_{n=1}^{\infty}I_n\left(\frac{r}{L}\right)K_n\left(\frac{x}{L}\right)\cos n(\theta-c)\right]rd\theta dr\right.\\ &\quad\left.+\int_x^a\int_0^{2\pi}\left[I_0\left(\frac{x}{L}\right)K_0\left(\frac{r}{L}\right)+2\sum_{n=1}^{\infty}I_n\left(\frac{x}{L}\right)K_n\left(\frac{r}{L}\right)\cos n(\theta-c)\right]rd\theta dr\right\}\\ &= 4\pi\left[\int_0^x I_0\left(\frac{r}{L}\right)K_0\left(\frac{x}{L}\right)rdr+\int_x^a I_0\left(\frac{x}{L}\right)K_0\left(\frac{r}{L}\right)rdr\right]\\ &= 4\pi Lx\left[I_1\left(\frac{x}{L}\right)K_0\left(\frac{x}{L}\right)+I_0\left(\frac{x}{L}\right)K_1\left(\frac{x}{L}\right)\right]-4\pi LaI_0\left(\frac{x}{L}\right)K_1\left(\frac{a}{L}\right)\\ &= 4\pi\left[L^2-LaI_0\left(\frac{x}{L}\right)K_1\left(\frac{a}{L}\right)\right],\end{aligned} \tag{D.6}$$

where use has been made of the following results:

$$\int_0^{2\pi}\cos[n(\theta-c)]d\theta=0,\quad \frac{d}{dr}[rI_1(r)]=rI_0(r),\quad \frac{d}{dr}[rK_1(r)]=-rK_0(r),$$

$$I_0(z)K_1(z)+I_1(z)K_0(z)=\frac{1}{z}. \tag{D.7a–d}$$

Note that Eq. (D.7a) is a result of direct integration, whereas Eqs. (D.7b–d) are obtained using the general formulas given in Magnus et al. (1966).

Similarly, substituting Eqs. (D.3) and (D.5b) into Eq. (D.1) yields, for any point **x** located outside the inclusion (with $x > a$ and thus $r < a < x$),

$$\begin{aligned}\Gamma(x) &= 2\int_0^a\int_0^{2\pi}\left[I_0\left(\frac{r}{L}\right)K_0\left(\frac{x}{L}\right)+2\sum_{n=1}^{\infty}I_n\left(\frac{r}{L}\right)K_n\left(\frac{x}{L}\right)\cos n(\theta-c)\right]rd\theta dr\\ &= 4\pi\int_0^a I_0\left(\frac{r}{L}\right)K_0\left(\frac{x}{L}\right)rdr=4\pi LaI_1\left(\frac{a}{L}\right)K_0\left(\frac{x}{L}\right),\end{aligned} \tag{D.8}$$

where use has been made of Eqs. (D.7a,b). The final results obtained in Eqs. (D.6) and (D.8) are exactly those listed in Eqs. (4.3a,b). They are also the same as those given in Cheng and He (1997) for a similar scalar-valued function involved in their analysis based

on a micropolar elasticity theory. However, in this appendix the more general case with $\alpha = \theta - c$ ($\neq \theta$) is considered and the derivation details are provided, which differ from what was presented in Cheng and He (1997).

APPENDIX E

In this appendix, the expressions of $\Gamma(\mathbf{x})$ for the ellipsoidal inclusion problem given in Eqs. (5.12) and (5.14) are derived.

Note that $\Gamma(\mathbf{x})$ in Eq. (2.43c) can be rewritten as

$$\Gamma(\mathbf{x}) = \int_{\Omega} \frac{e^{-\frac{r}{L}}}{r} d\mathbf{y}\,, \tag{E.1}$$

where $r \equiv |\mathbf{x} - \mathbf{y}|$. It can be shown using an inverse Fourier transform that

$$\frac{e^{-\frac{r}{L}}}{r} = \frac{1}{8\pi^3}\,\mathrm{Re}\left\{\int_{\Omega_\infty} \frac{4\pi L^2}{1+L^2\xi^2}\, \mathrm{e}^{i\,\boldsymbol{\xi}\bullet\mathbf{r}}\, d\boldsymbol{\xi}\right\}, \tag{E.2}$$

where **r** (= **x** –**y)** is the position vector of a point in the 3-D physical space, $\boldsymbol{\xi}$ is the position vector of the same point in the Fourier (transformed) space Ω_∞, i is the usual imaginary number with $i^2 = -1$. Using Eq. (E.2) in Eq. (E.1) then gives

$$\Gamma(\mathbf{x}) = \frac{L^2}{2\pi^2}\,\mathrm{Re}\left[\int_{\Omega} \mathrm{e}^{-i\,\boldsymbol{\xi}\bullet\mathbf{y}} \left(\int_{\Omega_\infty} \frac{1}{1+L^2\xi^2}\, \mathrm{e}^{i\,\boldsymbol{\xi}\bullet\mathbf{x}}\, d\boldsymbol{\xi}\right) d\mathbf{y}\right], \tag{E.3}$$

where Ω is the region occupied by the ellipsoidal inclusion. Consider the coordinate transformations:

$$Y_i = \frac{y_i}{a_I}, \quad \Xi_i = \frac{\xi_i a_I}{s\xi}, \tag{E.4}$$

where y_i, Y_i, ξ_i and Ξ_i are, respectively, the components of **y**, **Y**, $\boldsymbol{\xi}$ and $\boldsymbol{\Xi}$, $\xi = |\boldsymbol{\xi}|$, and

$$s = \frac{1}{\xi}\sqrt{(\xi_1 a_1)^2 + (\xi_2 a_2)^2 + (\xi_3 a_3)^2}\,. \tag{E.5}$$

Clearly, $\boldsymbol{\Xi}$, as defined in Eq. (E.4), is a unit vector. Then, it follows from Eq. (E.4) that

$$\Omega:\left(\frac{y_1}{a_1}\right)^2+\left(\frac{y_2}{a_2}\right)^2+\left(\frac{y_3}{a_3}\right)^2\le 1\Rightarrow|\mathbf{Y}|\le 1,\quad d\mathbf{y}=a_1a_2a_3d\mathbf{Y},\quad \boldsymbol{\xi}\bullet\mathbf{y}=\xi s\boldsymbol{\Xi}\bullet\mathbf{Y}. \tag{E.6}$$

The use of Eq. (E.6) leads to

$$\begin{aligned}\int_\Omega \mathrm{e}^{-i\,\boldsymbol{\xi}\bullet\mathbf{y}}\,d\mathbf{y} &= 2\pi a_1a_2a_3\int_0^1\int_0^\pi \mathrm{e}^{-i\,s\,\xi\,Y\cos\hat{\theta}}\sin\hat{\theta}\;d\hat{\theta}\;Y^2dY\\ &= -4\pi a_1a_2a_3\,\frac{1}{s^3\xi^3}\left[s\xi\cos(s\xi)-\sin(s\xi)\right],\end{aligned} \tag{E.7}$$

where the inclination angle $\hat{\theta}$ in the chosen spherical coordinate system (Y, $\hat{\theta}$, $\hat{\phi}$) is measured relative the direction of $\boldsymbol{\Xi}$. Substituting Eq. (E.7) into Eq. (E.3) then yields

$$\Gamma(\mathbf{x})=-\frac{2}{\pi}L^2a_1a_2a_3\int_{\Omega_\infty}\frac{s\xi\cos(s\xi)-\sin(s\xi)}{s^3\xi^3\left(1+L^2\xi^2\right)}\cos\left(\boldsymbol{\xi}\bullet\mathbf{x}\right)d\boldsymbol{\xi}. \tag{E.8}$$

To evaluate the integral in Eq. (E.8), consider the following coordinate transformations:

$$K_i=\xi_i a_I,\quad X_i=\frac{x_i}{a_I}, \tag{E.9a,b}$$

where K_i and x_i are, respectively, the components of **K** (with the magnitude K) and **x** (with the magnitude x). Also, a convenient spherical coordinate system (K, θ, φ) is chosen such that the angle between **K** and **X** (with the magnitude X) is θ, with the direction of **X** being the axis where $\theta = 0$. As a result,

$$K_1=K\sin\theta\cos\varphi,\quad K_2=K\sin\theta\sin\varphi,\quad K_3=K\cos\theta. \tag{E.10}$$

Using Eqs. (E.9a,b) and (E.10) then gives

$$K=\sqrt{K_iK_i}=s\xi,\quad m\equiv\frac{\boldsymbol{\xi}\bullet\mathrm{x}}{\xi}=\frac{\mathrm{K}\bullet\mathrm{X}}{\xi}=sX\cos\theta, \tag{E.11a,b}$$

$$s=\left[\left(\frac{\sin\theta\cos\varphi}{a_1}\right)^2+\left(\frac{\sin\theta\sin\varphi}{a_2}\right)^2+\left(\frac{\cos\theta}{a_3}\right)^2\right]^{-1/2}=s(\theta,\varphi), \tag{E.11c}$$

where use has also been made of Eq. (E.5) in reaching Eq. (E.11a) and the fact that

$\xi = \sqrt{\xi_i \xi_i}$ to obtain Eq. (E.11c). Finally, it follows from Eqs. (E.9a), (E.10) and (E.11a) that

$$\xi_1 = \frac{\xi}{a_1} s(\theta,\varphi)\sin\theta\cos\varphi, \quad \xi_2 = \frac{\xi}{a_2} s(\theta,\varphi)\sin\theta\sin\varphi, \quad \xi_3 = \frac{\xi}{a_3} s(\theta,\varphi)\cos\theta \tag{E.12}$$

as the coordinate transformation from the Cartesian system (ξ_1, ξ_2, ξ_3) to the curvilinear system (ξ, θ, φ). The Jacobian of this transformation can be readily obtained from Eq. (E.12) as

$$J = \frac{s^3}{a_1 a_2 a_3} \xi^2 \sin\theta, \tag{E.13}$$

which leads to the volume element relation:

$$d\boldsymbol{\xi} = \frac{s^3}{a_1 a_2 a_3} \xi^2 \sin\theta d\xi d\theta d\varphi\,. \tag{E.14}$$

With the help of the coordinate transformation in (E.12) and the associated volume element relation in (E.14), Eq. (E.8) becomes

$$\begin{aligned} \Gamma(\mathbf{x}) &= -\frac{2L^2}{\pi}\int_0^{2\pi}\int_0^{\pi}\int_0^{\infty} \frac{\left[s\xi\cos(s\xi)-\sin(s\xi)\right]\cos(m\xi)}{\xi\left(1+L^2\xi^2\right)} \sin\theta d\xi d\theta d\varphi \\ &\equiv -\frac{2L^2}{\pi}\int_0^{2\pi}\int_0^{\pi} F\sin\theta d\theta d\varphi, \end{aligned} \tag{E.15a}$$

where m and s are defined in Eqs. (E.11b,c), and

$$F \equiv \int_0^{\infty}\left[\frac{s\cos(s\xi)\cos(m\xi)}{(1+L^2\xi^2)} - \frac{\sin(s\xi)\cos(m\xi)}{\xi(1+L^2\xi^2)}\right] d\xi = F(\theta,\varphi). \tag{E.15b}$$

Note that (e.g., Gradshteyn and Ryzhik, 2007)

$$\int_0^{\infty}\frac{\cos(a\xi)\cos(b\xi)}{(1+\xi^2)}d\xi = \frac{\pi}{4}\left[e^{-|a-b|} + e^{-(a+b)}\right] \text{ for } a>0, \quad b>0; \tag{E.16a}$$

$$\int_0^{\infty}\frac{\sin(a\xi)\cos(b\xi)}{\xi(1+\xi^2)}d\xi = \begin{cases} \dfrac{\pi}{2}e^{-b}\sinh(a), & 0<a<b, \\ -\dfrac{\pi}{2}e^{-a}\cosh(b)+\dfrac{\pi}{2}, & 0<b<a. \end{cases} \tag{E.16b,c}$$

For the interior case with $\mathbf{x} \in \Omega$, there is $x_1^2/a_1^2 + x_2^2/a_2^2 + x_3^2/a_3^2 < 1$. This means

that $X_iX_i < 1$ (see Eq. (E.9b) or $X = |\mathbf{X}| < 1$, thereby giving $0 < m < s$ for $0 < \cos\theta < 1$ or $0 < -m < s$ for $-1 < \cos\theta < 0$ according to Eq. (E.11b) for any $\mathbf{x} \in \Omega$. It then follows from Eqs. (E.16a,c) that for the interior case with both $0 < m < s$ (or $0 < \theta < \pi/2$) and $0 < -m < s$ (or $\pi/2 < \theta < \pi$) there is

$$F = -\frac{\pi}{2} + \frac{\pi}{2}\left(1 + \frac{s}{L}\right)e^{-\frac{s}{L}} \cosh\left(\frac{m}{L}\right). \tag{E.17}$$

Using Eq. (E.17) in Eq. (E.15a) then results in

$$\Gamma(\mathbf{x}) = 4\pi L^2 - L^2 \int_0^{2\pi} \int_0^{\pi} \left(1 + \frac{s}{L}\right) e^{-\frac{s}{L}} \exp\left(-\frac{m}{L}\right) \sin\theta d\theta d\varphi \tag{E.18}$$

for the interior case with $\mathbf{x} \in \Omega$, where $m = sX\cos\theta$ from Eq. (E.11b), and $s = s(\theta, \varphi)$ is given in Eq. (E.11c). This completes the derivation of Eq. (5.12).

For the exterior case with $\mathbf{x} \notin \Omega$, there is $x_1^2 / a_1^2 + x_2^2 / a_2^2 + x_3^2 / a_3^2 > 1$ or $X > 1$, which makes the comparison between the values of m and s (satisfying $m = sX\cos\theta$ given in Eq. (E.11b)) more involved. In fact, the following four situations now need to be considered separately.

(1) $0 < s < m$ or $\cos\theta > 1/X > 0$ (see Eq. (E.11b)): Using Eqs. (E.16a,b) gives

$$F^{(1)} = \frac{\pi}{2} e^{-\frac{m}{L}} \left[\frac{s}{L}\cosh\left(\frac{s}{L}\right) - \sinh\left(\frac{s}{L}\right)\right]. \tag{E.19}$$

(2) $0 < m < s$ or $0 < \cos\theta < 1/X$ (see Eq. (E.11b)): Applying Eqs. (E.16a,c) yields

$$F^{(2)} = -\frac{\pi}{2} + \frac{\pi}{2}\left(1 + \frac{s}{L}\right)e^{-\frac{s}{L}} \cosh\left(\frac{m}{L}\right), \tag{E.20}$$

which is the same as F for the interior case given in Eq. (E.17).

(3) $0 < -m < s$ or $-1/|X| < \cos\theta < 0$ (see Eq. (E.11b)): The use of Eqs. (E.16a,c) leads to

$$F^{(3)} = -\frac{\pi}{2} + \frac{\pi}{2}\left(1+\frac{s}{L}\right)e^{-\frac{s}{L}}\cosh\left(\frac{m}{L}\right) = F^{(2)}. \tag{E.21}$$

(4) $0 < s < -m$ or $-1 < \cos\theta < -1/X$ (see Eq. (E.11b)): Utilizing (E.16a,b) results in

$$F^{(4)} = \frac{\pi}{2}e^{\frac{m}{L}}\left[\frac{s}{L}\cosh\left(\frac{s}{L}\right) - \sinh\left(\frac{s}{L}\right)\right]. \tag{E.22}$$

It then follows from Eqs. (E.15a) and (E.19)–(E.22) that

$$\Gamma(\mathbf{x}) = -\frac{2L^2}{\pi}\int_0^{2\pi}\left[\int_0^{\alpha} F^{(1)}\sin\theta\, d\theta + \int_{\alpha}^{\pi-\alpha} F^{(2)}\sin\theta\, d\theta + \int_{\pi-\alpha}^{\pi} F^{(4)}\sin\theta\, d\theta\right]d\varphi, \tag{E.23}$$

where $\alpha \equiv \cos^{-1}(1/X)$. Note that

$$\begin{aligned}
&\int_{\pi-\alpha}^{\pi} F^{(4)}\sin\theta d\theta = \int_{\alpha}^{0} F^{(4)}\Big|_{\theta=\pi-\beta}\sin\beta(-d\beta) = \int_0^{\alpha} F^{(1)}\sin\theta d\theta, \\
&\int_{\alpha}^{\pi-\alpha} F^{(2)}\sin\theta\, d\theta = \int_{\alpha}^{\pi/2} F^{(2)}\sin\theta\, d\theta + \int_{\pi/2}^{\pi-\alpha} F^{(2)}\sin\theta\, d\theta = 2\int_{\alpha}^{\pi/2} F^{(2)}\sin\theta\, d\theta,
\end{aligned} \tag{E.24}$$

where use has been made of the results $s(\pi-\theta, \varphi) = s(\theta, \varphi)$ and $m(\pi-\theta, \varphi) = -m(\theta, \varphi)$. Using Eq. (E.24) in Eq. (E.23) then yields

$$\Gamma(\mathbf{x}) = -\frac{4L^2}{\pi}\int_0^{2\pi}\left[\int_0^{\alpha} F^{(1)}\sin\theta\, d\theta + \int_{\alpha}^{\pi/2} F^{(2)}\sin\theta\, d\theta\right]d\varphi \tag{E.25}$$

for the exterior case with $\mathbf{x} \notin \Omega$, where $F^{(1)}$ and $F^{(2)}$ are given in Eqs. (E.19) and (E.20), respectively. This completes the derivation of Eq. (5.14).

APPENDIX F

In the appendix, the expressions of the transformation tensors $T_{ij}(\mathbf{x}-\mathbf{y})$ and $Q_{ij}(\mathbf{x}-\mathbf{y})$ given in Eqs. (6.12a,b) are derived.

From Eqs. (2.5a,c), (2.28) and (6.11a), it follows that

$$\tau_{ij}=\frac{1}{32\pi\mu(1-\nu)}\Big[\lambda(A_{,k}-B_{,mmk})\delta_{ij}+\mu(A_{,i}\delta_{jk}+A_{,j}\delta_{ik}-2B_{,ijk})\Big]e_k\,. \tag{F.1}$$

Using Eqs. (2.5b) and (2.7) in Eq. (6.4a) gives

$$t_i=\tau_{ij}n_j+L^2[-(\nabla^2\tau_{ij})n_j-\tau_{ij,pj}n_p+\tau_{ij,pl}n_pn_ln_j]+L^2\tau_{ij,p}(-n_{p,j}+n_{p,l}n_ln_j+n_pn_{l,l}n_j). \tag{F.2}$$

Substituting Eq. (F.1) into Eq. (F.2) results in

$$\begin{aligned}t_i=&\frac{1}{32\pi\mu(1-\nu)}\Big[\lambda(A-B_{,mm})_{,k}n_i+\mu(A_{,i}n_k+A_{,j}\delta_{ik}n_j-2B_{,ijk}n_j)\Big]e_k\\&+\frac{L^2}{32\pi\mu(1-\nu)}\Big\{-\lambda[\nabla^2(A-B_{,mm})_{,k}n_i+(A-B_{,mm})_{,ikp}n_p-(A-B_{,mm})_{,kpl}n_in_pn_l]\\&-\mu[\nabla^2(A_{,i}n_k)+\nabla^2(A_{,j}\delta_{ik}-2B_{,ijk})n_j+(A_{,ipk}+\nabla^2A_{,p}\delta_{ik}-2\nabla^2B_{,ikp})n_p\\&-A_{,ipl}n_kn_pn_l-(A\delta_{ik}-2B_{,ik})_{,jpl}n_pn_ln_j]\Big\}e_k+\frac{L^2}{32\pi\mu(1-\nu)}[\lambda(A-B_{,mm})_{,kp}\delta_{ij}\\&+\mu(A_{,ip}\delta_{jk}+A_{,jp}\delta_{ik}-2B_{,ijkp})](-n_{p,j}+n_{p,l}n_ln_j+n_pn_{l,l}n_j)e_k\,.\end{aligned} \tag{F.3}$$

Equation (F.3) can be rewritten as

$$t_i=T_{ik}e_k\,, \tag{F.4}$$

where

$$\begin{aligned}T_{ik}=&\frac{1}{32\pi\mu(1-\nu)}\Big[\lambda(A-B_{,mm})_{,k}n_i+\mu(A_{,i}n_k+A_{,j}\delta_{ik}n_j-2B_{,ijk}n_j)\Big]\\&+\frac{L^2}{32\pi\mu(1-\nu)}\Big\{-\lambda[\nabla^2(A-B_{,mm})_{,k}n_i+(A-B_{,mm})_{,ikp}n_p-(A-B_{,mm})_{,kpl}n_in_pn_l]\\&-\mu[\nabla^2(A_{,i}n_k)+\nabla^2(A_{,j}\delta_{ik}-2B_{,ijk})n_j+(A_{,ipk}+\nabla^2A_{,p}\delta_{ik}-2\nabla^2B_{,ikp})n_p\\&-A_{,ipl}n_kn_pn_l-(A\delta_{ik}-2B_{,ik})_{,jpl}n_pn_ln_j]\Big\}+\frac{L^2}{32\pi\mu(1-\nu)}[\lambda(A-B_{,mm})_{,kp}\delta_{ij}\\&+\mu(A_{,ip}\delta_{jk}+A_{,jp}\delta_{ik}-2B_{,ijkp})](-n_{p,j}+n_{p,l}n_ln_j+n_pn_{l,l}n_j),\end{aligned} \tag{F.5}$$

with $A=A(r)$ and $B=B(r)$ defined in Eqs. (2.29). The expression of the Cauchy traction

transformation tensor T_{ik} obtained in Eq. (F.5) is exactly what is given in Eq. (6.12a).

Next, using Eqs. (2.5b) and (F.1) in Eq. (6.4b) leads to

$$q_i = \frac{L^2}{32\pi\mu(1-\nu)}\left[\lambda(A - B_{,mm})_{,kp}\delta_{ij} + \mu(A_{,ip}\delta_{jk} + A_{,jp}\delta_{ik} - 2B_{,ijkp})\right]n_j n_p e_k \equiv Q_{ik}e_k, \qquad \text{(F.6)}$$

where

$$Q_{ik} = \frac{L^2}{32\pi\mu(1-\nu)}\left[\lambda(A - B_{,mm})_{,kp}\delta_{ij} + \mu(A_{,ip}\delta_{jk} + A_{,jp}\delta_{ik} - 2B_{,ijkp})\right]n_j n_p, \qquad \text{(F.7)}$$

with $A = A(r)$ and $B = B(r)$ defined in Eqs. (2.29). The expression of the double stress traction transformation tensors Q_{ik} obtained in Eq. (F.7) is exactly what is given in Eq. (6.12b). This completes the derivation of Eqs. (6.12a,b).

APPENDIX G

In this appendix, the following integral result (given in Eq. (6.45)) is proved:

$$\left\langle f(r)n_i \right\rangle = \int_{\partial\Omega} f(r)n_i dA = f_0(x)x_i \,, \tag{G.1}$$

where

$$r = \sqrt{x^2 + H^2 - 2xHt} \,, \quad f_0(x) = \frac{2\pi H^2}{x}\int_{-1}^{1} f(r)t dt \,. \tag{G.2a,b}$$

[Proof] To evaluate the surface integral in Eq. (G.1), a particular Cartesian coordinate system is chosen, in which the $\mathbf{e}_3$ axis is taken to be along the direction of position vector **x** (with $0 < |\mathbf{x}| < H$**)**, as shown in Fig. 6.3. The unit vector **n**, which represents the direction of position vector **y (**with $|\mathbf{y}| = H$**)** and coincides with the unit outward normal vector on the spherical surface, $\partial\Omega$, of the spherical elastic body having radius H, can then be expressed as

$$\mathbf{n} = \sin\theta\cos\varphi\,\mathbf{e}_1 + \sin\theta\sin\varphi\,\mathbf{e}_2 + \cos\theta\,\mathbf{e}_3 \,, \tag{G.3}$$

where $\varphi \in [0, 2\pi]$ is the azimuth angle relative to the $\mathbf{e}_1$ direction in the plane passing through the origin o and perpendicular to the $\mathbf{e}_3$ direction, and $\theta \in [0, \pi]$ is the inclination angle that equals the angle between **x** and **y**. Also, the distance between **x** and **y**, r, can be obtained from the cosine law as

$$r = |\mathbf{x} - \mathbf{y}| = \sqrt{x^2 + H^2 - 2xH\cos\theta} \,, \tag{G.4}$$

where $x = |\mathbf{x}|$ and $H = |\mathbf{y}|$.

Note that the surface integral of $f(r)\mathbf{n}$ over $\partial\Omega$ is given by

$$\langle f(r)\mathbf{n}\rangle \equiv \int_{\partial\Omega} f(r)\mathbf{n}\, dA = H^2 \int_0^{2\pi}\int_0^{\pi} f(r)\mathbf{n}\sin\theta\, d\theta d\varphi, \tag{G.5}$$

where use has been made of the surface element $dA = H^2 \sin\theta d\theta d\varphi$ on $\partial\Omega$. Using Eq. (G.3) in Eq. (G.5) leads to

$$\langle f(r)\mathrm{n}\rangle = 2\pi H^2 \int_0^{\pi} f(r)\cos\theta\sin\theta\, d\theta\, \mathrm{e}_3 . \tag{G.6}$$

Since $\mathbf{e}_3$ coincides with the direction of $\mathbf{x}$, Eq. (G.6) can be rewritten in the index form as

$$\langle f(r)n_i\rangle = \left[2\pi H^2 \int_{-1}^{1} f(r)t\, dt\right] x_i^0 , \tag{G.7}$$

where $x_i^0 = x_i / x$ is the ith component of the unit vector $\mathbf{x}^0$ = $\mathbf{x}/x$ (= $\mathbf{e}_3$), and t = $\cos\theta$. Equation (G.7) is exactly Eq. (G.1) or Eq. (6.45). This concludes the proof of Eq. (6.45).

APPENDIX H

In this appendix, the following integral result (given in Eq. (6.46)) is proven:

$$\left\langle f(r)n_i n_j n_k \right\rangle = f_1(x)\left(x_i\,\delta_{jk} + x_j\delta_{ik} + x_k\delta_{ij}\right) + f_2(x)x_i\,x_j x_k\,, \tag{H.1}$$

where

$$f_1(x) = \frac{\pi H^2}{x}\int_{-1}^{1} f(r)t(1-t^2)dt\,, \quad f_2(x) = \frac{\pi H^2}{x^3}\int_{-1}^{1} f(r)t(5t^2-3)dt\,. \tag{H.2}$$

[Proof] After rotating the Cartesian coordinate system with the base vectors $(\mathbf{e}_1, \mathbf{e}_2, \mathbf{e}_3)$ defined in Appendix G into a Cartesian coordinate system with the base vectors $(\hat{\mathbf{e}}_1, \hat{\mathbf{e}}_2, \hat{\mathbf{e}}_3)$ (see Fig. 6.3), the unit vector **n** becomes

$$\mathbf{n} = \sin\theta\cos\varphi\;R_{1i}\hat{\mathbf{e}}_i + \sin\theta\sin\varphi\;R_{2i}\hat{\mathbf{e}}_i + \cos\theta\;R_{3i}\hat{\mathbf{e}}_i\,, \tag{H.3a}$$

or, in the index form,

$$n_i = \sin\theta\cos\varphi R_{1i} + \sin\theta\sin\varphi\;R_{2i} + \cos\theta\;R_{3i}\,, \tag{H.3b}$$

where R_{ij} is the rotation tensor satisfying $\mathbf{e}_i = R_{ij}\hat{\mathbf{e}}_j$ and

$$R_{mi}R_{mj} = \delta_{ij}\,. \tag{H.4}$$

From Eq. (H.3b) it follows that

$$\begin{aligned}\int_0^{2\pi} n_i n_j n_k\,d\varphi = {} & 2\pi\cos^3\theta\;R_{3i}R_{3j}R_{3k} + \pi(\cos\theta - \cos^3\theta)\big[R_{3i}(R_{1j}R_{1k} + R_{2j}R_{2k}) \\ & + R_{3j}(R_{1i}R_{1k} + R_{2i}R_{2k}) + R_{3k}(R_{1i}R_{1j} + R_{2i}R_{2j})\big].\end{aligned} \tag{H.5}$$

Using Eq. (H.4) and the fact that the position vector **x** coincides with the $\mathbf{e}_3$ axis (i.e., $\mathbf{x}^0 = \mathbf{e}_3 = R_{3i}\hat{e}_i$ or $x_i^0 = R_{3i}$), Eq. (H.5) can be rewritten as

$$\int_0^{2\pi} n_i n_j n_k d\varphi = \pi(5\cos^3\theta - 3\cos\theta)\, x_i^0 x_j^0 x_k^0 + \pi\cos\theta\sin^2\theta(x_i^0\delta_{jk} + x_j^0\delta_{ik} + x_k^0\delta_{ij}). \quad \text{(H.6)}$$

The use of Eq. (H.6) leads to

$$H^2\int_0^{\pi}\int_0^{2\pi} f(r) n_i n_j n_k d\varphi \sin\theta\, d\theta = H^2\pi\Bigg[\int_0^{\pi} f(r)(5\cos^3\theta - 3\cos\theta)\sin\theta\, d\theta\, x_i^0 x_j^0 x_k^0 + \int_0^{\pi} f(r)\cos\theta\sin^3\theta\, d\theta\,(x_i^0\delta_{jk} + x_j^0\delta_{ik} + x_k^0\delta_{ij})\Bigg]. \quad \text{(H.7)}$$

With the surface element $dA = H^2\sin\theta d\theta d\varphi$ on $\partial\Omega$ and the unit vector component $x_i^0 = x_i / x$, Eq. (H.7) then becomes

$$\int_\Omega f(r) n_i n_j n_k dA = \frac{\pi H^2}{x}\int_0^{\pi} f(r)\cos\theta\sin^3\theta\, d\theta\,(x_i\delta_{jk} + x_j\delta_{ik} + x_k\delta_{ij}) + \frac{\pi H^2}{x^3}\int_0^{\pi} f(r)(5\cos^3\theta - 3\cos\theta)\sin\theta\, d\theta\, x_i x_j x_k. \quad \text{(H.8)}$$

Using $t = \cos\theta$ and Eq. (5.44) in Eq. (H.8) will immediately give Eq. (H.1) or Eq. (5.46). This concludes the proof of Eq. (5.46).

APPENDIX I

In this appendix, the following integral result (given in Eq. (7.4)) is proven:

$$U = \frac{1}{2\mathrm{Vol}(\Omega)}\int_{\Omega}(\tau_{ij}\varepsilon_{ij} + \mu_{ijk}\kappa_{ijk})dV = \frac{1}{2\mathrm{Vol}(\Omega)}\int_{\partial\Omega}(\sigma_{ij}u_i n_j + \mu_{ijk}\varepsilon_{ij}n_k)dA\,. \qquad \text{(I.1)}$$

From Eqs. (2.5c,d), it follows that

$$\int_{\Omega}(\tau_{ij}\varepsilon_{ij} + \mu_{ijk}\kappa_{ijk})dV = \int_{\Omega}(\tau_{ij}u_{i,j} + \mu_{ijk}u_{i,jk})dV\,. \qquad \text{(I.2)}$$

Using the divergence theorem and $\sigma_{ij,j} = \tau_{ij,j} - \mu_{ijk,kj} = 0$ (see Eq. (2.8), Eq. (I.2) becomes

$$\int_{\Omega}(\tau_{ij}\varepsilon_{ij} + \mu_{ijk}\kappa_{ijk})dV = \int_{\partial\Omega}(\tau_{ij}u_i n_j + \mu_{ijk}\varepsilon_{ij}n_k - \mu_{ijk,k}u_i n_j)dA\,. \qquad \text{(I.3)}$$

With the help of Eq. (2.8), Eq. (I.3) can be rewritten as

$$\int_{\Omega}(\tau_{ij}\varepsilon_{ij} + \mu_{ijk}\kappa_{ijk})dV = \int_{\partial\Omega}(\sigma_{ij}u_i n_j + \mu_{ijk}\varepsilon_{ij}n_k)dA\,, \qquad \text{(I.4)}$$

from which Eq. (I.1) or (7.4) is immediately proved. This completes the derivation of Eq. (I.1) or (7.4).

VITA

Hemei Ma was born and grew up in Heze, Shandong province, China. She enrolled in the Department of Engineering Mechanics, Tongji University, Shanghai, China in September 1999 and received her B.Sc. degree in July 2003. Upon graduation, she continued her graduate study at Tongji University and earned her M.Sc. degree in April 2006. She came to College Station, TX, USA, in August 2006 to pursue a Ph.D. degree in the Department of Mechanical Engineering, Texas A&M University. She received her Ph.D. in May 2010.

Hemei's permanent address is:

Texas A&M University

Department of Mechanical Engineering

3123 TAMU

College Station TX 77843-3123.

E-mail: ma-he-mei@hotmail.com.